Analytically tractable models of one-dimensional anomalous heat transport

A Thesis

Submitted to the

Tata Institute of Fundamental Research, Mumbai

for the degree of

Doctor of Philosophy

in

Physics

by

Aritra Kundu

International Center for Theoretical Sciences, Bengaluru

Tata Institute of Fundamental Research

Bengaluru

October 2018

Final Version Submitted in April 2019

Declaration

This thesis is a presentation of my original research work. Wherever contributions of others are involved, every effort is made to indicate this clearly, with due reference to the literature, and acknowledgement of collaborative research and discussions.

The work was done under the guidance of Prof. Abhishek Dhar, at the International Centre for Theoretical Sciences, Tata Institute of Fundamental Research, Bangalore.

Aritra Kundu.

Aritra Kundu

In my capacity as supervisor of the candidate's thesis, I certify that the above statements are true to the best of my knowledge.

Abhishek Dhar.

Prof. Abhishek Dhar
Date: 16-10-2018

Collaborators

- All of the work done in this thesis was advised by my thesis supervisor Prof. Abhishek Dhar.
- The work on hard particle gas was done with Prof. Sanjib Sabhapandit.
- The work presented in Chapter.4 was done in collaboration with Prof. Cédric Bernardin, Prof. Keiji Saito, Prof. Anupam Kundu
- The work presented in Chapter. 5 was done in collaboration with Priyanka and Prof. Anupam Kundu. Priyanka started the project and contributed in different aspects of numerical as well as analytical work.

List of publications

- *Equilibrium dynamical correlations in the Toda chain and other integrable models*, Aritra Kundu, Abhishek Dhar Phys. Rev. E 94 (6), 062130 , 2016 link
- *Anomalous heat equation in a system connected to thermal reservoirs*, Priyanka, Aritra Kundu, Abhishek Dhar, Anupam Kundu, Phys. Rev. E 98, 042105, link
- *Fractional diffusion equation description of an open anomalous heat conduction set-up*, Aritra Kundu, Cédric Bernardin, Keji Saito, Anupam Kundu, Abhishek Dhar, J. Stat. Mech. 13205 (2019), link
- *Spatio-temporal correlations in hard particle gas in one-dimensions*, Aritra Kundu, Sanjib Sabhapandit, Abhishek Dhar, In preparation

Contents

To my parents

Acknowledgments

First and foremost, I would like to express my heart felt gratitude to my guide and mentor Prof. Abhishek Dhar. His guidance has been a perfect balance with inputs and discussion when necessary and giving me enough freedom to be exploratory on my own. I have been inspired always by seeing his passion, dedication and energy to everything he does specially in science. He is the best supervisor that I could have found. I would also like to thank Prof. Anupam Kundu, who has been my mentor and collaborator in many of the projects during my PhD. I have learned a lot in academics as well as non-academics through enjoyable discussions with him. His office was always open for me to clear doubts and confusion.

I have been fortunate enough to work with Prof. Cédric Bernardin. The pleasant discussions with him are always enlightening, specially his unorthodox way of thinking about various problems. Apart from these, the two visits to his institute in Nice during my PhD are fond memories for me, with his very helpful and detailed guidance whenever I needed it. I am also very grateful to Prof. Keiji Saito, with whom I had similar enlightening conversations and discussions regarding our collaboration.

I would like to thank Pallab Basu and Samriddhi Sankar Ray along with Anupam Kundu, who have all taken the role of friend and guardian at various points in my journey during my PhD. I would like to also thank Prof. Visal Vasan, Prof. Subhro Bhattacharjee, Prof. Manas Kulkarni with whom I had very useful discussions regarding various aspects of physics and mathematics.

I thank Priyanka with whom I have collaborated in one of the project and for her every cheerful and enthusiastic moments.

Next in the lineup are my friends, who have all made my duration during PhD memorable. Firstly I would like to rejoice the memorable moments spend with Archak Purkayastha which spanned well outside physics including the conferences in abroad we traveled together over the years, the music, the short trips/treks etc.

I would like to thank Hemanta Kundu, Kasi Jaswin, Mayuri Chatterjee, Jyoti Banerjee, Abhirup Ghosh with whom I have shared various moments over the past few years and who stood by me

during my tough times.

I would like to thank Prof. Spenta Wadia for constructing such a wonderful institute as ICTS. I would like to thank Jeeva along with all other members of the amazing administrative staff at ICTS who made life much easier for all of us.

My PhD has been an enchanting journey – which would not have been possible without the help and sacrifice of my family. My words would not be enough to express my gratitude for them. I would like to thank Sramana Basu, my wife, who helped me navigate through the wavy journey of these five years. I would like to thank my sister Soumyabrataa for her constant support throughout and help.

Lastly but most importantly, I would like to express my respect to my parents Dhira Kundu and Sanatan Kundu, whose never-ending love and support throughout this journey is unfathomable. They believed in me at all times and has been my source of inspiration. I owe it to them for their many sacrifices over the years. I dedicate this thesis to them.

Part I

Introduction

The ability to reduce everything to simple fundamental laws does not imply the ability to start from those laws and reconstruct the universe.

P.W. Anderson, More is different, 1972

1

Introduction to heat transport

Thermodynamics gives a macroscopic description of matter in equilibrium and is an important ingredient for understanding diverse aspects in physics and has contributed enormously to the development of science and engineering in the last two century. The field of equilibrium statistical mechanics establishes a connection between the phenomenological macroscopic laws of thermodynamics and the microscopic description of matter. However, in many physical situations we encounter systems which are out of equilibrium and there is flow of mass, energy, charge etc across the system. Understanding the mechanisms of macroscopic transport in physical systems has been one of the interesting endeavors in physics. Transport is typically understood in terms of phenomenological equations, common examples of which include Ohm's law for electrical conduction and Fourier's law for heat conduction. However, it is not completely understood how the microscopic

dynamics, described for example by Newton's equations of motion for a classical system, would lead to macroscopic equations like Fourier's law, and this has been a puzzling and important question [1]. Enquiry into a microscopic derivation of these laws has given new results and insights over the past decades. In this thesis we will focus on the specific problem of the microscopic understanding of heat transport in one-dimensional systems.

1.1 Fourier law and its breakdown in one-dimensional systems

The phenomenological Fourier law has been highly successful in understanding diffusive heat transport behavior as seen in the vast majority of real materials. The law states that the local heat current $\bar{j}(\bar{r})$ at a point $\bar{r}$ is proportional to the local temperature gradient $\bar{\nabla}T(\bar{r})$, hence ($\bar{j} = -\kappa\bar{\nabla}T$), where the proportionality constant κ defines the thermal conductivity of the material. For a system in one dimension, Fourier's law along with the energy conservation equation, implies that temperature in a system evolves diffusively, and is governed by the heat diffusion equation

$$\partial_t T(x,t) = D\Delta T(x,t), \tag{1.1.1}$$

where $D = \kappa/c_v$, with c_v the specific heat capacity, κ is here assumed (for simplicity) to be temperature independent, and $\Delta = \partial_x^2$ is the Laplacian operator in one dimension.

However, a large number of numerical work as well as analytic studies over the last several decades indicate the breakdown of Fourier's law in classical one-dimensional systems [2, 3, 4]. These studies suggest that energy transport in these systems is not diffusive but instead is super-diffusive. This is referred to as anomalous transport and some of the important signatures are the following:

- Diverging system-size dependent thermal conductivity, $\kappa(N) \sim N^{\alpha}$, where N is the number of particles.
- Non-linear temperature profile in the non-equilibrium steady state which is present even for small temperature difference between the boundaries.
- Slow power-law decay (in time) of the equilibrium current auto-correlation function.
- Super-diffusive spreading of perturbations in equilibrium.

Besides numerical observations in many one-dimensional systems, the diverging thermal conductivity has now been observed experimentally in a few experiments on carbon-nanotubes [5, 6]

1.2 Set-ups used to investigate anomalous transport

For the microscopic study one typically considers a system of N particles, with positions $\{q_x\}$ and momenta $\{p_x\}$, $x = 1, 2, \ldots, N$, interacting with each other via a nearest neighbor potential $V(r_x)$ where $r_x = q_{x+1} - q_x$ is the local stretch. The system is described by a Hamiltonian

$$H = \sum_{x=1}^{N} \left[\frac{p_x^2}{2} + V(q_{x+1} - q_x) \right] , \tag{1.2.1}$$

where we have set to unity the masses of all the particles. The boundary conditions depend on the kind of transport set-up that we want to study and this will be discussed in the following sections. The dynamics in the bulk of the system is then given by the Hamiltonian equations of motion. In some cases (to be discussed later) one considers additional stochastic components in the bulk dynamics that respect the important conservation laws. We note that, associated with the above Hamiltonian, the total momentum $\sum_x p_x$ and the total energy H are conserved quantities. The total stretch (or volume), $\sum_x r_x$, is another trivial but important conserved quantity. Generically, one expects no other conserved quantities. However, for very special forms of the potential, a system can have N independent conserved quantities and such systems are called *Integrable*. One of the aims of this thesis will be to examine the role of integrability on energy transport. We briefly mention examples of some well-known integrable and non-integrable Hamiltonians, with momentum conservation, that have been studied in the context of heat transport.

Integrable systems:

- Harmonic chain: $V(r) = kr^2/2$
- Equal mass Hard particle gas (HPG): $V(r) = 0, \;\; r > 0, \;\; V(r) = \infty, \;\; r \leq 0.$
- Toda chain: $V(r) = (a/b)e^{-br}$.

Non-integrable systems:

- Fermi-Pasta-Ulam (FPU) chain: $V(r) = kr^2/2 + \alpha r^3/3 + \beta r^4/4$.
- Alternate mass hard particle gas: In this model, the interaction potential is the same as for the equal mass HPG defined above. However, instead of all particles with the same mass, one considers a chain of particles with alternate particles having different masses, say m_1 and m_2.

One of the approaches used to understand dynamics of non-integrable chains is to study the closely related exactly solvable integrable systems [7]. Understanding differences in heat transport properties in different kinds of integrable systems have been an important direction [8]. Integrable models are not only useful as starting points for the study of non-integrable systems that are in close proximity — they also provide some exact results which can be used to check the accuracy of numerical codes. Studies of non-integrable systems have mainly been restricted to numerical approaches, though recently much progress have been made using the phenomenological approach of nonlinear fluctuating hydrodynamics [9, 10, 11]. It is now well understood that momentum conservation causes singular advection of high wavelength modes and this leads to anomalous transport. However, there are exceptions where one finds anomalous transport despite momentum non-conservation [12].

There are two common set-ups to study thermal transport in a microscopic system, that are used to identify anomalous features in the transport properties.

1.2.1 Isolated system set-up

This is used to study the spatio-temporal decay of equilibrium correlations. In this set-up one usually considers a ring geometry [shown in Fig. 1.1(a)] with the N particles evolving with the Hamiltonian equations of motion

$$\dot{q}_x = p_x, \;\; \dot{p}_x = V'(q_{x+1} - q_x) - V'(q_x - q_{x-1}) \,, \quad x = 1, \ldots, N \,, \tag{1.2.2}$$

with the periodic boundary conditions $q_{N+x} = q_x + L$, where L is the total length of the lattice. We define the local stretch variable, $r_x = q_{x+1} - q_x$, and the local energy, $e_x = p_x^2/2 + V(r_x)$.

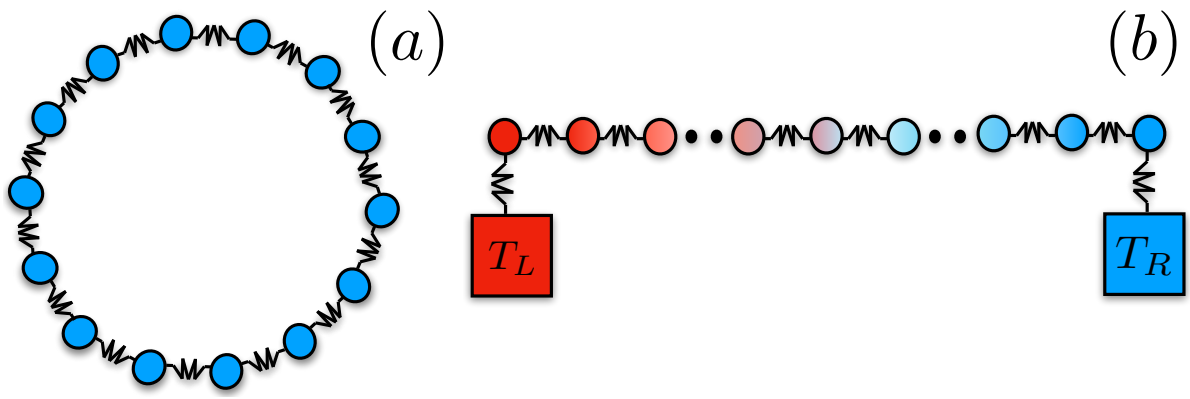

Figure 1.1: (a) Schematic showing the isolated periodic setup. (b) Schematic showing open setup connected to heat baths with different temperature at the ends.

The Hamiltonian dynamics exactly conserves the total energy, $\sum_{x=1}^{N} e_x$, the total momentum, $\sum_{x=1}^{N} p_x$, and the total stretch, $\sum_{x=1}^{N} r_x$. For non-integrable systems, these are typically the only conserved quantities and they constitute the slowly evolving hydrodynamic variables. In this set-up one then prepares the system in an appropriate equilibrium ensemble (at specified temperature T, pressure P and zero average momentum) and computes the equilibrium spatio-temporal correlations of the conserved variables. These equilibrium correlations provide information on transport properties of the system. The local energy satisfies a local continuity equation

$$\partial_t e_x + \partial_x j_x = 0\,, \quad \text{with} \quad j_x = \frac{1}{2}(p_{x+1} + p_x)V'(r_{x-1}), \tag{1.2.3}$$

which gives us the definition of the microscopic local current density. The total current operator is defined as $J = \sum_x j_x$.

Common signature indicating anomalous transport in the isolated set-up are:

- Super-diffusive spreading of spatio-temporal correlations of conserved quantities in equilibrium, for example

$$C_{ee}(x,t) = \langle e_x(t) e_0(0)\rangle - \langle e_x(0)\rangle\langle e_0(0)\rangle \sim \frac{1}{t^\gamma} f\left(\frac{x}{t^\gamma}\right),$$

  with $1/2 < \gamma < 1$ and the width of the energy spread growing as $\sigma^2(t) \sim t^\beta$, $2 > \beta > 1$. When $\gamma = 1/2$, the transport is diffusive while when $\gamma = 1$, the transport is ballistic. Another indicator which is commonly used in simulations are spatio-temporal spreading of

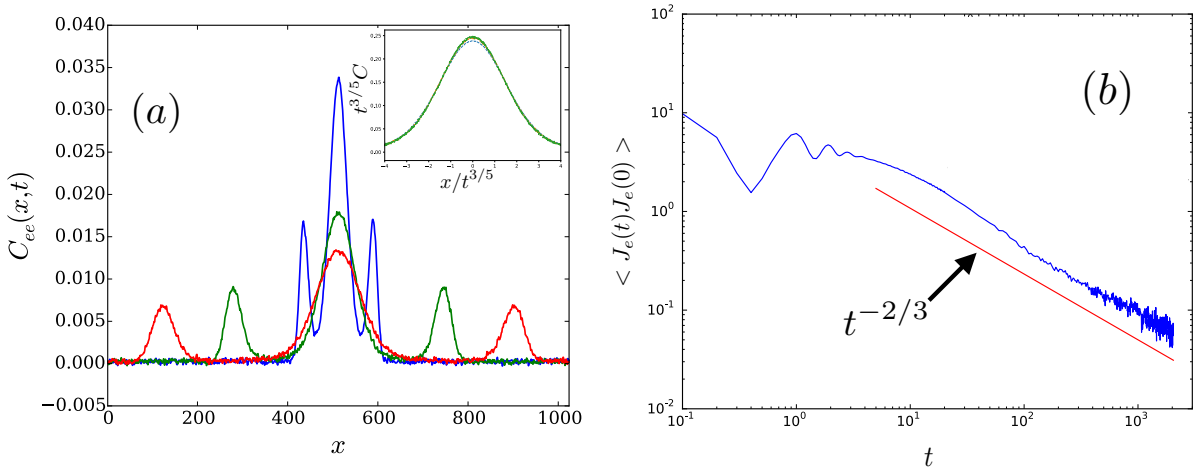

Figure 1.2: Equilibrium correlations in the Fermi-Pasta-Ulam chain: (a) Spread of energy correlations in equilibrium.The inset shows the anomalous scaling of the central peak at different times with $\gamma = 3/5$. (b) Slow decay of energy current correlations as $\langle J_e(t)J_e(0)\rangle \sim t^{-2/3}$.

an initial pulse. This spreading is related to the correlations of the conserved quantity when the strength of the initial pulse is small. A typical example of the energy spread is shown in Fig. 1.2(a).

- Secondly one finds a slow decay of total equilibrium energy current, $\langle J(t)J(0)\rangle \sim t^{(\delta-1)}$, $0 \leq \delta \leq 1$ [see Fig. 1.2(b)]. This slow decay of equilibrium current correlations leads to a diverging thermal conductivity, via the Green-Kubo formula [1, 3]

$$\kappa = \frac{1}{k_B T^2} \lim_{\tau\to\infty} \lim_{N\to\infty} \frac{1}{N} \int_0^\tau dt \langle J(t)J(0)\rangle. \tag{1.2.4}$$

One can heuristically argue that the upper limit in the time-integral above can be set to the system size N to give a size-dependent conductivity and this leads to the relation $\alpha = \delta$ (we recall that $\kappa(N) \sim N^\alpha$).

1.2.2 Open system set-up

In this case, the system of interacting particles is connected to heat baths which keep the two ends at fixed temperatures, as shown in Fig. 1.1(b) — this makes the system boundary driven. A standard way of modeling the baths is through adding Langevin-type terms to the equations of motion of

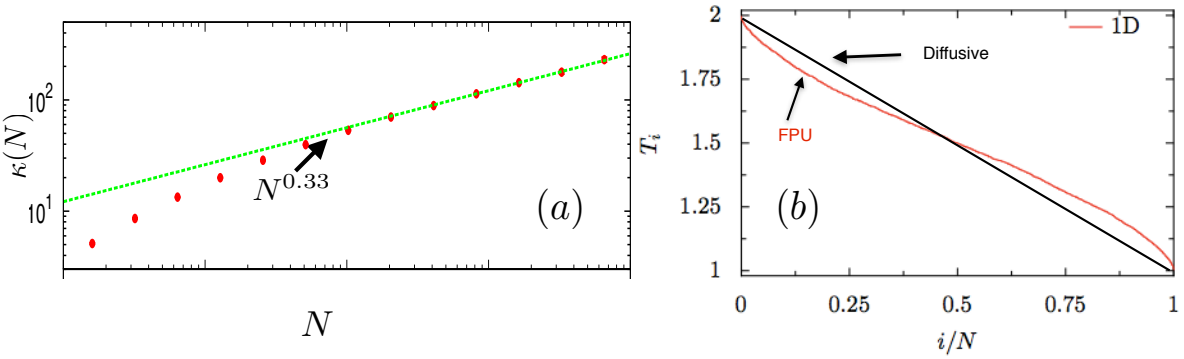

Figure 1.3: NESS properties of the Fermi-Pasta-Ulam chain: (a) Diverging thermal conductivity with system size. (b) Non-linear temperature profile for FPU-β chain. The black curve shows temperature profile for diffusive system. Image taken from [Dhar, 2008]

the boundary particles, so that the dynamical equations of motion are

$$\begin{aligned}
\dot{q}_x &= p_x, \;\; 1 \leq x \leq N \\
\dot{p}_1 &= V'(q_2 - q_1) - V'(q_1 - q_0) - \lambda p_1 + \sqrt{2\lambda T_L}\eta_L, \\
\dot{p}_x &= V'(q_{x+1} - q_x) - V'(q_x - q_{x-1}), \;\; 2 \leq x \leq N-1, \\
\dot{p}_N &= V'(q_{N+1} - q_N) - V'(q_N - q_{N-1}) - \lambda p_N + \sqrt{2\lambda T_R}\eta_R,
\end{aligned} \tag{1.2.5}$$

where $\eta_x, \; x = L, R$, are Gaussian white noise with $\langle \eta_x(t) \rangle = 0, \; \langle \eta_x(t)\eta_y(t') \rangle = \delta_{x,y}\delta(t-t')$. Two widely used boundary conditions (BC) are: fixed BC with $q_0 = q_{N+1} = 0$, and free BC with $q_0 = q_1$ and $q_{N+1} = q_N$. The system then evolves to a non-equilibrium steady state (NESS) characterized by a stationary temperature profile and a non-zero current flowing in the system. The microscopic local current operator is again given by Eq. (1.2.3) and the average NESS heat current $\langle j \rangle$ can be computed. The thermal conductivity would be obtained as $\kappa = N\langle j \rangle / \delta T$, where we consider a small temperature bias $\delta T = (T_L - T_R) > 0$, and take the limit of large N.

For systems with anomalous transport, one then finds that

- the conductivity diverges with system size as $\kappa \sim N^\alpha, \; 0 < \alpha \leq 1$. A typical example for FPU chain is shown in Fig. 1.3(a).
- the temperature profile is nonlinear even for arbitrarily small δT with singularities at the boundaries. A typical example is shown in Fig. 1.3(b). In contrast, for a diffusive system the steady state temperature profile is linear.

In the open system set-up, one finds that transport depends not only on the bulk properties but also on the choice of baths and boundaries and a general framework to understand transport in open systems is lacking.

1.3 Summary of previous work

Here we briefly discuss some of the previous work for understanding heat transport. More detailed references in the appropriate context are provided in the respective chapters.

Integrable systems: The problem of heat conduction in a classical integrable ordered 1D harmonic crystal was studied by Rieder, Lebowitz and Leib [13] and by Nakazawa [14] by finding the exact non-equilibrium covariance matrix in the Gaussian NESS, and later by Roy and Dhar [15] using the approach of non-equilibrium Green's functions. They were able to show that the bulk temperature profile was flat and given as the average of the two bath temperatures. The current in the steady state was shown to be independent of system size in the thermodynamic limit, which is expected since there is no mechanism for scattering of phonons, and transport is ballistic. In case of equilibrium correlations of conserved quantities, exact results for the correlations of velocity spatio-temporal correlations were obtained in the papers by Montroll and Mazur [16] for the harmonic chain and by Jepsen [17] for the hard particle gas. The energy current decay in the ordered Toda chain was studied by [18, 19].

Integrable systems typically have no scattering mechanism. Introducing new scattering processes in an integrable system manifests in many interesting phenomena. Some ways of introducing scattering mechanism and breaking integrability are by — (i) introducing disorder in the system, (ii) introducing an-harmonic interactions and (iii) introducing stochastic components in the dynamics, in addition to the Hamiltonian evolution. Next, we review some of the previous research in these directions for heat transport in one dimensional systems.

Disordered Harmonic chain: Heat conduction in harmonic chains with mass disorder are expected to be affected by the similar physics as of Anderson localization. Matsuda and Ishii [20] showed that all high frequency modes in a disordered harmonic chain were exponentially localized. The NESS of the disordered harmonic chain with different baths and boundary conditions were

studied by Connors and Lebowitz [21], who found $\kappa \gtrsim N^{-1/2}$, and by Rubin and Greer [22], who obtained $\kappa \gtrsim N^{1/2}$. The study by Casher and Lebowitz[23] shows that the system approaches a unique stationary state for a variety of baths. It was later proven rigorously that $\kappa \sim N^{-1/2}$ [24] for the Connors-Lebowitz model and $\kappa \sim N^{1/2}$ [25] for the Rubin-Greer model. It was shown by Dhar [26] that the conductivity in general depends strongly on boundary conditions and spectral properties of baths, and the previous results are special cases. One of the conclusions is thus that scattering by including disorder does not lead to normal heat transport.

Anharmonic chains: The case of equilibrium and non-equilibrium transport in non-integrable chains was studied by many authors before, here we give a very brief summary of the previous studies: The first study of heat conduction in anharmonic chain was explored in by Lepri [27, 28] where they studied the Fermi-Pasta-Ulam (FPU) model in both the open non-equilibrium setup and the isolated equilibrium set-up. In the non-equilibrium case they found that $\kappa \sim N^{0.37}$ and a highly nonlinear temperature profile for relatively small temperature differences, while the equilibrium current correlation showed a slow decay $\sim t^{-0.63}$. This clearly indicated anomalous transport with the conductivity divergence exponent $\alpha \sim 0.37$. A more recent study found $\alpha \sim 0.33$ [29]. Somewhat surprisingly, a study of the asymmetric $\alpha - \beta$ FPU chain and other asymmetric nonlinear potentials [30] found that in special parameter regimes, the system could exhibit normal transport. Subsequently it was pointed out by Das, Dhar, Narayan [31] and Wang, Li, Hanggi[32] that this could be attributed to finite size effects, and that in the large system, long time limit, one would always find anomalous behavior. The other extensively studied model of 1D heat transport is the alternate mass hard particle gas which was first studied by Casati [33] and then later by several other authors [34, 35, 36, 37, 38]. Here again one finds anomalous transport, with $\alpha \approx 0.33$, but the issue of slow convergence to the asymptotic behavior and possible finite size effects is there as has been pointed out in [38]. The conclusion from the numerical studies is therefore that one-dimensional anharmonic systems with momentum conservation exhibit anomalous transport with a divergent thermal conductivity $\kappa \sim N^{\alpha}$. It is also found that anharmonic chains with momentum conservation typically show non-linear temperature profiles which are characteristics of anomalous transport. The precise value of α, the question of universality classes and of finite-size effects, are some issues that are not clearly obtained from the numerical studies.

Analytical approaches for anharmonic chains:

Theoretical understanding of super-diffusive transport has been obtained using several approaches. Some of these include:

(a) Kinetic theory which describes thermal transport by considering the dynamics of a gas of phonons and treats the scattering between phonons by assuming that the non-linear effects are small and can be treated perturbatively [39, 40, 41, 42, 43].

(b) Non-linear fluctuating hydrodynamics (NLFH) [9, 10, 11, 44] which considers the evolution of the slow conserved fields at a coarse-grained level and, along with mode coupling theory, makes detailed predictions on the form of equilibrium spatio-temporal correlation functions of the conserved fields. In particular, it predicts the super-diffusive spreading of energy perturbations and the slow decay of energy current auto-correlation functions. For generic anharmonic systems with three conserved quantities (volume, momentum, energy), this theory predicts that there are two moving sound modes with a constant velocity and one stationary heat mode. Though this is not exhaustive, one expects two broad univerality classes :

- For symmetric potentials at zero pressure, NLFH predicts that the sound modes spread diffusively ($t^{1/2}$) and the heat mode spreads with Levy$-3/2$ characteristics. The current-correlation decay exponent is found to be $\delta = 1/2$.
- For asymmetric potentials the prediction is that the sound modes exhibit correlations as those in the Kardar-Parisi-Zhang (KPZ) ($t^{2/3}$) and the heat mode with that of Levy$-5/3$. The current-correlation decay exponent is obtained to $\delta = 1/3$.

There have been several extensive numerical studies of equilibrium correlations of the conserved quantities in the FPU system [45] and the hard-particle gas [46] to verify the predictions of NLFH. These studies find the expected heat mode and two sound modes in the equilibrium correlations. It was found that the scaling exponents for the spreading of these modes had a very good agreement with the predictions from NLFH theory. The scaling parameters and the scaling functions were in close agreement with the theoretical expectation in some parameter regimes but this was not the case in all parameter regimes studied. We note that Alder and

Wainwright [47, 48] numerically studied the slow decay of velocity autocorrelations in hard spheres which was understood in the framework of fluctuating hydrodynamics in [49].

(c) The study of specific exactly solvable stochastic models [50, 51, 52] gives a more rigorous hold on anomalous transport. Stochastic models were studied by [53] for uncoupled stochastic oscillators, where they showed that the model satisfied Fourier's law. Similar stochastic models [54, 55] has been used as a simple model version for understanding complex systems. In the models for anomalous transport, one considers harmonic chains whose Hamiltonian dynamics is perturbed by stochastic noise that breaks integrability of the system, but while maintaining the three important conservation laws. These models thus attempt to mimic nonlinear chains for which it is usually difficult to obtain any exact result. For these stochastic models, exact results have been obtained in the isolated system set-up, showing the slow decay of current correlations as well as the super-diffusive spreading of perturbations. It was also shown that these models lead to super-diffusive spreading of energy that is reminiscent of a Lévy walk and a fractional equation evolution. Some analytic results have also been obtained for the open system [56, 57, 58, 59]. The harmonic chain with stochastic flips of velocity, which does not conserve momentum, was studied by [60] and was shown to have diffusive transport. Another simplified model showing super-diffusive transport characterized by two conserved quantities was introduced by Bernardin and Stoltz [52]. In this thesis we study some questions related to these models.

1.4 Problems addressed in this thesis

In this thesis, we explore several analytically tractable models of anomalous transport — one involving transport properties of an integrable Hamiltonian system and the other on stochastic systems which are solvable in the sense that the dynamical equations for correlations form closed sets of equations at every order.

In the first part of the thesis (Chapter 2 and Chapter 3), we study transport in Hamiltonian integrable one-dimensional systems. We first study the equilibrium spatio-temporal correlations of conserved quantities in an interacting integrable system (Toda chain) in the *isolated set-up*. In special

limiting cases, the Toda chain reduces to either the Harmonic chain or the hard particle gas. In these cases, we find exact expressions for the spatio-temporal correlations of the three standard conserved quantities. We find that in general the correlations have the scaling form as $(1/t)f(x/t)$, which is a signature of ballistic transport. We then explore the differences in equilibrium spatio-temporal correlations between integrable Toda chain and the non-integrable truncated Toda chain. In contrast to the integrable system, the equilibrium correlations in the non-integrable systems have a slower spreading with a scaling form $(1/t^{\gamma})f(x/t^{\gamma})$, with $1/2 < \gamma < 1$. Despite these differences, we find that some of the tools from hydrodynamic theory used for non-integrable transport can be useful to study integrable transport. Next, we study the Toda system in an *open set-up*. It is believed that ballistic transport in this setup would manifest through a system-size independent current and a flat temperature profile across the system. This is consistent with our studies in the open Toda chain at various limits, which thus confirms ballistic transport.

In the second part of the thesis (Chapter 4 and Chapter 5), we study two exactly solvable stochastic models which show super-diffusive transport. These stochastic models, introduced to mimic the anomalous behavior of the non-integrable FPU-like models, have a linear Hamiltonian part with added stochastic noise which conserves energy, momentum and volume but otherwise destroys integrability [4, 52, 61]. For the case where transport in the system is diffusive, the heat equation provides an understanding of macroscopic description for the time-evolution of the temperature profile both in the open and closed system framework. We ask as to whether a similar equation exists for anomalous systems described by these stochastic models. The analytical tractability of these models arises from the fact that two-point correlations form closed set of equations.

Here we consider two such models in the open set-up — the Harmonic Chain with Momentum Exchange (HCME) and the Harmonic Chain with Volume Exchange (HCVE), and show that a non-local fractional diffusion equation emerges as a suitable replacement to the heat diffusion equation for describing super-diffusive energy transport in these models. The fractional equation in both the systems, is then solved to recover closed expressions for the temperature profile and current in NESS and is also used to describe the energy relaxation starting from arbitrary initial conditions. In the HCVE model, the evolution of correlation functions is also studied. All results are extensively verified with microscopic simulation of the system. In the case of HCME, we also consider

the question of writing a fractional equation with Langevin-type noise, to describe fluctuations in the system.

Part II

Transport and correlations in Integrable Systems

2

Equilibrium correlations in classically Integrable Toda chain

2.1 Introduction

There has been a lot of recent interest in equilibrium correlations of conserved quantities in one-dimensional Hamiltonian systems, in particular in the form of their spatio-temporal evolution. Remarkable predictions have been obtained for the form of spatio-temporal correlations in systems of one-dimensional fluids and anharmonic chains, using the framework of fluctuating hydrodynamics [9, 10, 11, 44]. For generic nonlinear systems with three conserved quantities (mass, momentum, energy), it has been predicted that there are two sound modes which exhibit correlations as those in the Kardar-Parisi-Zhang (KPZ) equation, and a single heat mode showing characteristics of a Levy walk. These predictions have been verified in many systems [45, 46, 62]. These studies of equilibrium fluctuations of conserved quantities have led to some progress in resolving the long standing puzzle of anomalous heat transport in one dimensional systems [2, 3, 4]. The general consensus now is that in one dimensional momentum conserving non-integrable systems, heat transport is anomalous, and the heat conductivity κ diverges with system size as $\kappa \sim N^{\alpha}$, with $0 \leq \alpha \leq 1$. The decay of equilibrium fluctuations shows similar anomalous features which lead to a understanding of the non-equilibrium state via linear response.

An important aspect, which affects transport and fluctuations in a many-body system, is the integrability of the Hamiltonian. In this chapter we are going to study transport in one-dimensional interacting integrable system and make comparisons with the non-integrable systems. In particu-

lar we study the well known Toda chain [63], first introduced in 1967 as example of an integrable one-dimensional (1D) system. The chain is characterized by non-linear interactions of exponential type between nearest neighbors. The exact solvability of the model was studied in [64, 65] where it was reported how to construct a full set of conserved quantities using the Lax pair formalism. The periodic lattice was studied in [66, 67] using the inverse scattering method. In the limit of large anharmonicity the chain is characterized by soliton solutions, which are stable wave packets localized in real space. For infinite chains the isolated soliton solution was found by Toda [63]. For periodic finite chains one can find exact solutions, the so-called cnoidal waves, which are periodic trains of solitons [63, 18]. The equilibrium thermodynamic properties such as specific heat, etc [68] can be studied by performing exact integrals with respect to Gibbs distribution. Although special exact classes of solutions are known for the Toda chain, finite temperature dynamical properties such as correlation functions are hard to access analytically. There have been some attempts to study finite temperature dynamical properties of Toda chain through non-interacting soliton gas analogy [69, 70, 71] and through taking classical limit of a quantum Toda chain [72]. The quantum Toda chain was solved using Bethe ansatz in [73, 74]. A review of various static and dynamic properties of the Toda chain can be found in [75].

Energy transport in the Toda chain was studied in [19], where the decay of current correlations and overlap of currents with other conserved quantities were studied in the context of Mazur inequalities. A careful numerical study was carried out in [18] looking at the decay of current correlations in finite systems prepared in canonical equilibrium. It was pointed out that the Mazur relations needed to be modified and that one needed to take projections of the current to not just the conserved quantities but also to their bilinear combinations. Among the other results in [18], the existence of special "cnoidal" solutions in the periodic Toda chain was noted and the effect of cubic and quartic perturbations on the decay of conserved quantities was studied.

To test the role of integrability in heat transport, it is interesting to study transport in perturbed integrable systems. The effect of solitons on the heat transport in Toda chain and its perturbations was studied in [76]. The diatomic alternate mass Toda chain which is non-integrable was studied in [77] where it was found that the thermal conductivity κ diverges with system size N as as $\kappa \sim N^{0.34}$. Heat transport in Toda chain perturbed with conservative noise was studied in

[78, 79] where again it was seen that the current decays with system size (anomalously). In [80] it was pointed out that the Fermi-Pasta-Ulam (FPU) chain can be studied as a perturbation of Toda chain and that they exhibit similar behavior at short times.

Another motivation for our study is from the context of recent studies on thermalization in integrable quantum systems. It has been shown that integrable quantum systems prepared in special initial conditions, relax to a state that can be described by a Generalized Gibbs Ensemble (GGE), i.e. thermal equilibrium state is described by a distribution $P = e^{-\sum_n \lambda_n I_n}/Z(\{\lambda_n\})$, where I_n are the conserved quantities of the system, λ_n are corresponding Lagrange multipliers and Z is the appropriate partition function [81]. On the other hand, typical states and also typical energy eigenstates are described by the usual Gibbs ensemble (with only temperature specified) [82, 83]. An interesting question then is to see how integrability shows up in the dynamics of the system when it is prepared in an initial thermal Gibbs state.

In this chapter we investigate the spatio-temporal equilibrium correlations of fluctuations of the three conserved quantities: stretch, momentum and energy in the Toda chain. The equilibrium state is chosen to correspond to the one with specified temperature (T) and pressure (P) with zero average momentum. Our main results are as follows:

- In all parameter regimes we find from numerical simulations that the correlations exhibit ballistic scaling, which means that all correlation functions have the form $C(x,t) = (1/t)f(x/t)$, where f is some scaling function (non-universal). In contrast, we show that with non-integrable perturbations of the Toda chain, correlation functions scale as $C(x,t) = (1/t^\alpha)f(x/t^\alpha)$, with $1/2 < \alpha < 1$, where f is universal scaling function.

- In two limiting cases, the Toda system reduces to the harmonic chain and the hard particle gas respectively. In these cases we are able to compute all correlation functions exactly. We show that there is excellent agreement between direct simulations of the Toda chain with these exact results.

- We follow the prescription used in the theory of fluctuating hydrodynamics of non-integrable anharmonic chains and carry out a transformation to the three "normal" modes corresponding to the three conserved quantities. We find that one can then again see a separation of the

heat and sound modes, but unlike the non-integrable case, here the cross correlations between different modes are non-vanishing even at long times.

- Finally we study the differences of non-equilibrium transport in open system connect to heat baths in integrable and non-integrable system. We find that integrable Toda chain cannot support a temperature gradient and the temperature profile is flat. However, the bulk temperature in different limits of Toda chain are different. We also find that the thermal conductivity diverges linearly with system size. When a non-integrable perturbation is added to the Toda chain, a non-linear temperature profile develops suggesting anomalous transport.

The plan of the chapter is as follows. In Sec. (2.2) we precisely define the Toda chain model and give a summary of some known exact results. In Sec. (2.3) we present analytical and numerical results for spatio-temporal correlations in two special limiting cases of the Toda system, namely the harmonic chain and the hard particle gas. The numerical results for spatio-temporal correlations of the three conserved quantities in the Toda chain are presented in Sec. (2.4). We also discuss the form of correlation functions of integrable Toda chain in the normal-mode basis and compare differences of spatio-temporal correlations in integrable and non-integrable systems. In Sec. (2.5) we discuss the non-equilibrium transport in open Toda system connected to heat baths and study the effect of non-integrable perturbation of Toda potential on the NESS profiles. We summarize the main findings of this chapter in Sec. (2.6).

2.2 Toda chain: Model, definitions and summary of some exact results

We first define the Toda model on a ring geometry. We consider N particles with position q_x, momentum p_x with $x = 1, \ldots, N$. We define a "stretch" variable $r_x = q_{x+1} - q_x$. The Toda Hamiltonian is given by

$$H = \sum_{x=1}^{N} \frac{p_x^2}{2} + V(r_x) \,, \qquad (2.2.1)$$
$$\text{where } V(r_x) = \frac{a}{b} e^{-b r_x} \,,$$

and we take periodic boundary conditions $q_{N+1} = \sum_{x=1}^{N} r_x = q_1 + L, q_0 = q_N - L$, where L is the length of the lattice. The equations of motion are

$$m\ddot{q}_x = -a[\, e^{-b(q_x - q_{x-1})} - e^{-b(q_{x+1} - q_x)}\,], \quad x = 1, \ldots, N\,. \tag{2.2.2}$$

2.2.1 Lax pairs and conservation laws in Toda chain

Toda chain is defined as

$$V(r_x) = \frac{a}{b} e^{-br_x} = Ce^{-br_x}. \tag{2.2.3}$$

Equations of motion are:

$$\dot{r}_x = p_{x+1} - p_x,\ \dot{p}_x = Cb(e^{-br_{x-1}} - e^{-br_x}),$$

With a change of variables $a_x = p_x/2$ and $d_x = \sqrt{V(r_x)}/2 = e^{-br_x/2}/2$ and using the notation $\tilde{a}_x = ba_x$ and $\tilde{d}_x = \sqrt{Cb^2}d_x$ the equations of motion (EOM) can be written as

$$\dot{\tilde{d}}_x = \tilde{d}_x(\tilde{a}_x - \tilde{a}_{x+1}),\ \dot{\tilde{a}}_x = 2(\tilde{d}^2_{x-1} - \tilde{d}^2_x). \tag{2.2.4}$$

These EOM can be cast in the form of $\frac{dL}{dt} = [L, A]$, where L and A are Lax pair matrices with elements

$$L_{ij} = \tilde{a}_x\delta_{xy} + \tilde{d}_x\delta_{x,y+1} + \tilde{d}_{x-1}\delta_{x,y-1},\ A_{ij} = \tilde{d}_x\delta_{x,y+1} - \tilde{d}_{x-1}\delta_{x,y-1}, \tag{2.2.5}$$

The Lax solution is written as $\frac{dL}{dt} = [L, A]$. It can be shown [64] that the which says eigenvalues of L are constant in time and so are any of their symmetric combinations. The conserved quantities are given as

$$I_m = \frac{2^m}{m} TrL^m. \tag{2.2.6}$$

The first few conserved quantities are,

$$
\begin{aligned}
I_1 &= \sum_{x=1}^{n} \tilde{p}_x = b \sum_{x=1}^{n} p_x, \\
I_2 &= \sum_{x=1}^{n} \frac{\tilde{p}_x^2}{2} + \tilde{V}(r_x) = \frac{b^2}{2}\left[\sum_{x=1}^{n} \frac{p_x^2}{2} + \frac{a}{b} V(r_x)\right], \\
I_3 &= \sum_{x=1}^{n} \frac{\tilde{p}_x^3}{3} + (\tilde{p}_x + \tilde{p}_{x+1})\tilde{V}(r_{x+1}) = \frac{b^3}{3}\left[\sum_{x=1}^{n} \frac{p_x^3}{3} + (p_x + p_{x+1})\frac{a}{b} V(r_{x+1})\right], \\
I_4 &= \frac{b^4}{4}\left[\sum_{x=1}^{n} \frac{p_x^4}{4} + (p_x^2 + p_x p_{x+1} + p_{x+1}^2)\frac{a}{b} V(r_{x+1}) + \frac{a^2}{2b^2} V(r_x)^2 + \frac{a^2}{b^2} V(r_x) V(r_{x+1})\right].
\end{aligned}
\tag{2.2.7}
$$

In addition we have a trivial but important conserved quantity $I_0 \equiv \sum_{x=1}^{N} r_x$, in the case of periodic boundaries. As we can see, the higher order conservation laws become more non-local in space.

Limiting cases: If one takes the limit $b \to 0, a \to \infty$ with $ab = \omega^2$ constant, then one gets a harmonic chain with spring constant ω^2. In addition there is a large linear term which can be canceled with an appropriate "pressure" term [adding a term Pr to the potential $V(r)$ with $P = a$]. On the other hand in the limit $b \to \infty$ the potential vanishes for $r > 0$ and is infinite at $r < 0$, thus mimicking a hard-particle gas. As we will see later, in these limiting cases, all dynamical correlations can be exactly computed. In both these cases, some equilibrium dynamical results were already known [17, 16, 84, 85] and even many exact properties of the non-equilibrium steady state are known [13, 15, 3].

Solitons and phonons: As noted in [18] the Toda chain on the ring has a family of the so-called "Cnoidal" wave solutions that are periodic in time and space, very similar to the normal modes of a harmonic chain. For harmonic lattice the overall amplitude of the normal modes is a free parameter and apart from this freedom, there are exactly N independent periodic solutions each specified by a wave-vector k and a corresponding frequency ω_k (independent of amplitudes). For the non-linear Toda lattice, one can again construct N solutions specified by wave-vectors k but there is a free "non-linearity" parameter depending on the amplitude A of the solution and in this case, the frequencies depend on A. The explicit solutions are stated in [18]. Here we note the observation made there, that for small amplitudes, the Cnoidal waves look like sinusoidal waves or phonons (the normal modes of a harmonic lattice) while for large amplitudes, they look like trains of solitons

(localized excitations).

In the hard particle gas limit, the dynamics consist of particles moving ballistically and exchanging velocities on collision. A velocity pulse would simply pass un-scattered through this system. Thus this limit is characterized by "non-interacting" solitons. So we see that the two limiting cases discussed above correspond to excitations being either phonon-like or soliton-like and for general parameters, we expect a mixture of these two.

2.2.2 Definitions for equilibrium spatio-temporal correlations

Specification of the equilibrium state and definition of correlation functions: The Toda chain has a large number of conserved quantities, and accordingly one can construct generalized ensembles which are invariant distributions. Such general ensembles are specified by a set of N Lagrange multipliers corresponding to the N conserved quantities. Here we restrict our discussion to the special case where the initial state is prepared such that only the conserved quantities energy, stretch and momentum are specified while all other Lagrange multipliers are set to zero. More specifically we prepare the system initially in a state described by the following canonical ensemble (with zero average momentum) and at specified temperature T and pressure P:

$$Prob(\{r_x, p_x\}) = \frac{e^{-\beta \sum_{x=1}^{N} \left[p_x^2/2 + V(r_x) + P r_x\right]}}{Z} \,, \tag{2.2.8}$$

where the partition function is simply given by $Z = [\int_{-\infty}^{\infty} dp \int_{-\infty}^{\infty} dr e^{-\beta(p^2/2 + V(r) + Pr)}]^N$.

Corresponding to the three global conserved quantities (I_0, I_1, I_2), we can define the local conserved fields $r_x(t), p_x(t), e_x(t) = p_x^2/2 + V(r_x)$. It is easy to see that they satisfy the continuity equations

$$\begin{aligned} \partial_t r_x &= p_{x+1} - p_x \\ \partial_t p_x &= V'(r_x) - V'(r_{x-1}) \\ \partial_t e_x &= p_{x+1} V'(r_x) - p_x V'(r_{x-1}) \,. \end{aligned} \tag{2.2.9}$$

Defining a local pressure variable $P = -V'(r)$, and the discrete derivative $\partial_x f(x) = f(x+1) -$

$f(x)$ we see that the above equations can be written in the following form

$$\begin{aligned}
\partial_t r_x(t) + \partial_x j_r(x,t) &= 0\,, \\
\partial_t p_x(t) + \partial_x j_p(x,t) &= 0\,, \\
\partial_t e_x(t) + \partial_x j_e(x,t) &= 0\,, \quad \text{where} \\
[j_r(x,t), j_p(x,t), j_e(x,t)] &= [-p_x(t), P_{x-1}(t), p_x(t)P_{x-1}(t)]
\end{aligned} \tag{2.2.10}$$

Next, we define the fluctuations of the fields from their equilibrium values as

$$u_1(x,t) = r_x(t) - \langle r \rangle,\ u_2(x,t) = p_x(t),\ u_3(x,t) = e_x(t) - \langle e \rangle\,, \tag{2.2.11}$$

where $\langle \ldots \rangle$ denote average over the initial equilibrium state. We will look at the following dynamic correlation functions:

$$C_{\alpha\nu}(x,t) = \langle u_\alpha(x,t) u_\nu(0,0) \rangle\,, \tag{2.2.12}$$

with $\alpha, \nu = 1, 2, 3$. The average is over initial conditions chosen from Eq. (2.2.8) and the dynamics in Eq. (2.2.2) [or equivalently the first two equations in Eq. (2.2.9)].

Sum rules: We note here [11, 4] that the correlation functions of conserved quantities satisfy the following exact sum rules (see appendix for derivation), in the limit $N \to \infty$

$$\sum_x C^{\alpha\beta}(x,t) = \sum_x C^{\alpha\beta}(x,0)\,, \tag{2.2.13}$$

$$\begin{aligned}
\frac{d}{dt} \sum_x x C^{\alpha\beta}(x,t) &= \langle J^\alpha(0) u^\beta(0,0) \rangle\,, \\
\frac{d^2}{dt^2} \sum_x x^2 C^{\alpha\beta}(x,t) &= 2 \langle J^\alpha(t) j^\beta(0,0) \rangle \\
\text{where } J(t) &= \sum_x j(x,t)\,.
\end{aligned} \tag{2.2.14}$$

These sum rules serve as useful check of numeric simulations. Further they provide useful information on transport properties. For example, the last of the above equation enables one to relate total current correlations to spreading of correlation functions of corresponding conserved quantities. One can then try to say something about non-equilibrium transport via linear response theory

[86, 87]. For the case of the integrable models studied here, we see ballistic scaling of correlations of all conserved currents, and this immediately implies that the corresponding total currents do not decay to zero in the infinite time limit.

2.3 Correlation functions in the special limiting cases of Toda lattice

Exact results for the correlations of velocity $\langle p_x(t)p_0(0)\rangle$ were obtained in the papers by Montroll and Mazur [16] for the harmonic chain and by Jepsen [17] for the hard particle gas. The dynamics of harmonic crystal being linear and the initial conditions taken from Gaussian distribution makes it simple to obtain exactly the full set of correlations $C_{\alpha\beta}(x,t)$. It turns out that for the hard-particle gas, one can use a recently developed formalism [84], to again compute the full set of correlation functions. Here we outline the computation for the harmonic case and summarize the results for the HPG (see next chapter for details).

2.3.1 Equilibrium correlations in Harmonic chain

The Hamiltonian for the harmonic chain is given by

$$H = \sum_{x=1}^{N} \frac{p_x^2}{2} + \frac{\omega^2 r_x^2}{2}\,, \tag{2.3.1}$$

where $r_x = q_{x+1} - q_x$ and we assume periodic boundary conditions $r_0 = r_N$ and $p_{N+1} = p_1$. The variables $\{r_x, p_x\}$ satisfy the equations of motion

$$\begin{aligned} \partial_t r_x &= p_{x+1} - p_x\,, \\ \partial_t p_x &= \omega^2(r_x - r_{x-1})\,. \end{aligned} \tag{2.3.2}$$

Defining Fourier transform variables $\tilde{r}_k = \sum_{x=1}^{N} e^{-ikx} r_x$, $\tilde{p}_k = \sum_{x=1}^{N} e^{-ikx} p_x$, these satisfy the equations

$$\partial_t \begin{pmatrix} \tilde{r}_k \\ \tilde{p}_k \end{pmatrix} = \hat{T} \begin{pmatrix} \tilde{r}_k \\ \tilde{p}_k \end{pmatrix}, \quad \text{where } \hat{T} = 2i\sin(k/2) \begin{pmatrix} 0 & e^{ik/2} \\ \omega^2 e^{-ik/2} & 0 \end{pmatrix}\,.$$

Let $\hat{S}$ be the matrix which diagonalizes $\hat{T}$, i.e, $\hat{S}^{-1}\hat{T}\hat{S} = i\Lambda$, where $\Lambda = diag(-\lambda, \lambda)$ with $\lambda = 2\omega \sin(k/2)$. Then the solution of the above equation is given by

$$\begin{aligned} \begin{pmatrix} \tilde{r}_k(t) \\ \tilde{p}_k(t) \end{pmatrix} &= \hat{S}e^{i\Lambda t}\hat{S}^{-1} \begin{pmatrix} \tilde{r}_k(0), \\ \tilde{p}_k(0) \end{pmatrix} \\ &= \begin{pmatrix} \cos(\lambda t) & \frac{ie^{ik/2}}{\omega}\sin(\lambda t) \\ i\omega e^{-ik/2}\sin(\lambda t) & \cos(\lambda t) \end{pmatrix} \begin{pmatrix} \tilde{r}_k(0) \\ \tilde{p}_k(0) \end{pmatrix}. \end{aligned} \tag{2.3.3}$$

The translational invariance of the problem means that the correlation matrix

$$C(x,t) = \begin{pmatrix} \langle r_x(t) r_0(0) \rangle & \langle r_x(t) p_0(0) \rangle \\ \langle p_x(t) r_0(0) \rangle & \langle p_x(t) p_0(0) \rangle \end{pmatrix}, \tag{2.3.4}$$

is given by

$$C(x,t) = \frac{1}{N}\sum_k \tilde{C}(k,t)e^{ikx}, \tag{2.3.5}$$

$$\text{where } \tilde{C}(k,t) = \begin{pmatrix} \langle \tilde{r}_k(t)\tilde{r}_{-k}(0) \rangle & \langle \tilde{r}_k(t)\tilde{p}_{-k}(0) \rangle \\ \langle \tilde{p}_k(t)\tilde{r}_{-k}(0) \rangle & \langle \tilde{p}_k(t)\tilde{p}_{-k}(0) \rangle \end{pmatrix}. \tag{2.3.6}$$

Using the solution in Eq. (2.3.3) and the fact that (since the initial distribution is taken from a Gibbs ensemble with temperature T)

$$\tilde{C}(k,0) = \begin{pmatrix} \langle \tilde{r}_k(0)\tilde{r}_{-k}(0) \rangle & \langle \tilde{r}_k(0)\tilde{p}_{-k}(0) \rangle \\ \langle \tilde{p}_k(0)\tilde{r}_{-k}(0) \rangle & \langle \tilde{p}_k(0)\tilde{p}_{-k}(0) \rangle \end{pmatrix} = \begin{pmatrix} T/\omega^2 & 0 \\ 0 & T \end{pmatrix},$$

we get

$$\tilde{C}(k,t) = T \begin{pmatrix} \cos(\lambda t)/\omega^2 & \frac{ie^{ik/2}}{\omega}\sin(\lambda t) \\ \frac{ie^{-ik/2}}{\omega}\sin(\lambda t) & \cos(\lambda t) \end{pmatrix}.$$

Doing inverse Fourier transform gives $C(x,t)$ [Eq. (2.3.5)]. After straightforward manipulations and going to large N limit we get the following explicit correlation matrix:

$$\begin{aligned} C_{rr}(x,t) &= T\mathcal{J}_{2|x|}(2\omega t)/\omega^2, \\ C_{rp}(x,t) &= T(-\frac{\mathcal{J}_{2|x|-1}(2\omega t)}{\omega}\Theta(-x) + \frac{\mathcal{J}_{2|x|+1}(2\omega t)}{\omega}\Theta(x)), \\ C_{pr}(x,t) &= T(-\frac{\mathcal{J}_{2|x|+1}(2\omega t)}{\omega}\Theta(-x) + \frac{\mathcal{J}_{2|x|-1}(2\omega t)}{\omega}\Theta(x)), \\ C_{pp}(x,t) &= T\mathcal{J}_{2|x|}(2\omega t), \end{aligned} \tag{2.3.7}$$

where $\mathcal{J}_n(z)$ is the Bessel function of first kind and $\Theta(x)$ is the Heaviside theta function. Since the process is Gaussian, the energy correlation is derived using expressing higher order moments in terms of two-point correlation functions, thus $C_{ee}(x,t) = [C_{rr}^2(x,t) + C_{rp}^2(x,t) + C_{pr}^2(x,t) + C_{pp}^2(x,t)]/2$.

2.3.2 Equilibrium Correlations in Hard particle gas

The explicit correlations for the hard particle gas is derived in the next chapter (Chapter 3). Here we summarize the results. For the HPG, the equilibrium Gibbs distribution means that initial velocities of all particles are chosen from the Maxwell distribution with variance $\bar{v}^2 = T$, while the positions of the N particles are chosen from a uniform distribution within a finite region of length L. In the thermodynamic limit with $N, L \to \infty$ with finite density $\rho = N/L$, the correlations in the bulk of the system are given by:

$$\begin{aligned} C_{rr}(x,t) &= \frac{1}{\rho^3\sigma_t}\frac{e^{-\frac{1}{2}(\frac{x}{\rho\sigma_t})^2}}{\sqrt{2\pi}}, \\ C_{pp}(x,t) &= \frac{\bar{v}^2}{\rho\sigma_t}\left(\frac{x}{\rho\sigma_t}\right)^2\frac{e^{-\frac{1}{2}(\frac{x}{\rho\sigma_t})^2}}{\sqrt{2\pi}}, \\ C_{ee}(x,t) &= \frac{\bar{v}^4}{4\rho\sigma_t}\left[\left(\frac{x}{\rho\sigma_t}\right)^4 - 2\left(\frac{x}{\rho\sigma_t}\right)^2 + 1\right]\frac{e^{-\frac{1}{2}(\frac{x}{\rho\sigma_t})^2}}{\sqrt{2\pi}}, \end{aligned} \tag{2.3.8}$$

where $\sigma_t = \bar{v}t$.

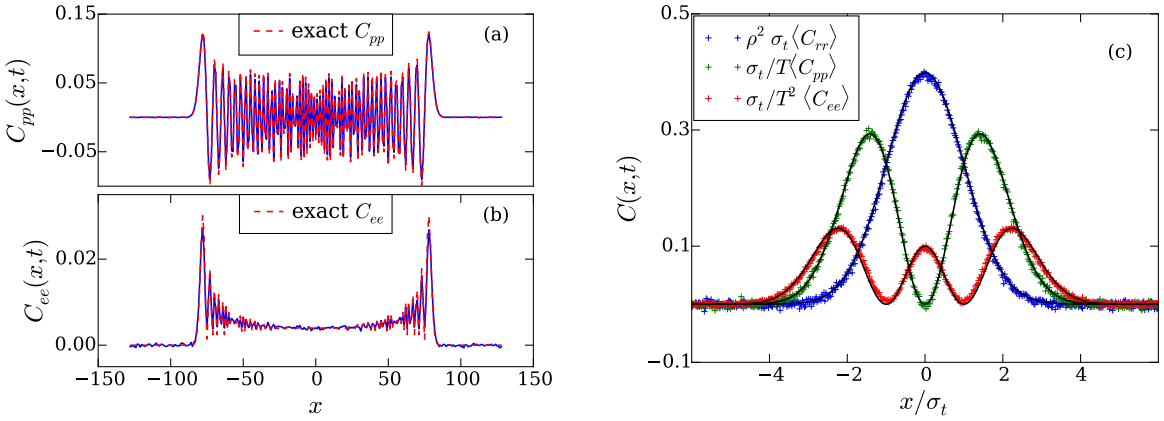

Figure 2.1: (a,b) Toda chain with parameters $a = 20.0, b = 0.05, P = 20.0, T = 1.0, N = 256$ at time $t = 80$. This corresponds to the harmonic limit. The simulations of the Toda are compared with the exact harmonic chain correlation functions (red dashed lines) as given in text. Here $\omega^2 = 1$, hence $C_{rr} = C_{pp}$. (c) Toda chain with parameters $a = 0.1, b = 10.0, P = 0.1, T = 1.0, N = 1024$ corresponding to hard-particle limit, at time $t = 400$. The solid black lines are the values of exact correlation function , as given in text (with $\sigma_t = \rho\bar{v}t$).

2.4 Equilibrium correlations of Toda chain

We now first present results from direct simulations on the form of these different correlation functions. In our simulations we explore different parameter regimes and in the two limiting cases, compare our results with the exact results of the previous section.

2.4.1 Numerical results for correlations of conserved quantities

Numerical details: The Toda-chain is simulated by numerically evaluating Eq. (2.2.2) using the velocity-Verlet algorithm. We choose a small time-step ($dt \leq 0.01$) in the simulations which keeps the total energy and momentum constant to a high accuracy (relative error less than 10^{-6} for energy and 10^{-4} in I_3). To capture the equilibrium correlations, we prepare the system in an initial state in a canonical (T, P) ensemble by drawing random numbers p, r for each particle from the distribution $e^{-\beta(p^2/2+V(r)+Pr)}/Z$ through inverse transform sampling. For the partition function to be bounded, we require that pressure is non-zero for Toda Lattice. The full set of spatio-temporal correlation functions, defined in Eq. (2.2.12) are computed by taking averages over $10^6 - 10^7$ initial conditions.

We present numerical results and discuss their scaling in three different parameter regimes. These correspond to the harmonic and hard particle limits and an intermediate regime. In the former

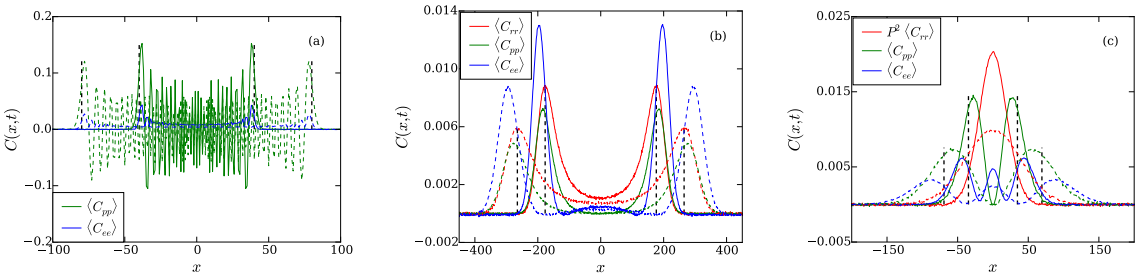

Figure 2.2: Diagonal correlation functions Eq. (2.2.12) for Toda lattice for two different times (dashed line indicates later time). The black dashed line show position of sound velocity as predicted from Eq. (2.4.3) at the two times (a) Harmonic Limit at time $t = 80, 120$ [parameters of Fig. 2.1(a)]. (b) Toda chain with parameter $a = 1, b = 1, P = 1, T = 1, N = 1024$ at time $t = 200, 300$. (c) Hard-Particle limit [parameters of Fig. 2.1(c)] at time $t = 200, 400$.

cases, comparisons are made with the exact results stated in the previous section. For the three conserved quantities we will use the notation $r \leftrightarrow 1,\ p \leftrightarrow 2,\ e \leftrightarrow 3$.

Case I: $a = 20, b = 0.05, P = 20.0, T = 1.0$ — In this limit, the Toda lattice is expected to show similar characteristics of the harmonic lattice. In Fig. 2.1(a) and 2.1(b) we show results for the diagonal correlations C_{rr}, C_{ee} in the Toda lattice respectively and compare them with exact harmonic chain results as given in Eqs. (2.3.8). We find an excellent agreement. For our parameters, the effective spring constant $\omega^2 = 1$ and hence $C_{rr} = C_{pp}$. The correlations are extended and oscillatory. In Fig. 2.2(a), the momentum and energy spatio-temporal correlations are shown for two different times illustrating how they spread with time. The speed of sound here is $c \approx 1$. In Fig. 2.3(a) and 2.3(b), we plot the same data after scaling the x and y axes by factors of $1/t$ and t respectively (ballistic scaling). We see a good collapse in the bulk with some deviations near the sound peaks, which occur near the edge.

Case II: $a = 1.0, b = 1.0, P = 1.0, T = 1.0$ — This corresponds to the intermediate regime and we no longer see the oscillations in the correlations. In Fig. 2.2(b), the momentum and energy correlations are shown for two different times. The speed of sound here is $c = 0.8833\ldots$. The stretch and momentum correlations only have peaks at the edges, while the energy correlation has an additional small peak in the middle. In Fig. 2.3(b) we see that there is a very good ballistic scaling of the correlation functions.

Case III: $a = 0.1, b = 10.0, P = 0.1, T = 1.0$ — This corresponds to the hard particle gas limit and again we see no oscillations. In Fig. 2.1(c) the results for correlation functions from direct simulations of the Toda chain are compared with the exact results for the hard particle gas in Eq. (3.3.5).

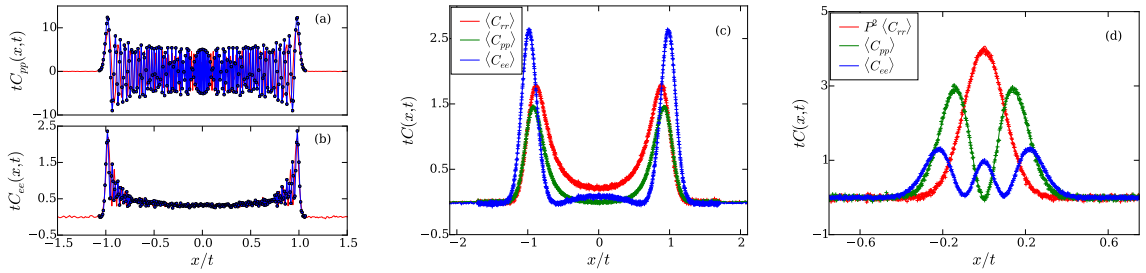

Figure 2.3: The diagonal correlation functions Eq. (2.2.12) for Toda lattice in various limits for two different times are plotted with ballistic scaling. (a) and (b) shows collapse momentum and energy correlations respectively in harmonic limit with parameters that of Fig. 2.2(a). Although the scaling is good in the bulk, the edges show significant deviations. (c) shows ballistic scaling for Toda with parameters as that of Fig. 2.2(b). In (d) we show ballistic scaling in the hard particle limit with parameters as in Fig. 2.2(c).

We again see excellent agreement with the numerical data. We now see that the nature of correlations are very different. The stretch correlation has a single peak at the center and energy correlation has a relatively large central peak. In Fig. 2.2(c) the correlations are shown at two different times. The speed of sound is $c = 0.1709\ldots$ while Fig. 2.3(c) shows the expected ballistic scaling.

2.4.2 Normal mode description of correlations

In the usual hydrodynamic theory of anharmonic chains [11], it is convenient to go to a description in terms of "normal" hydrodynamic modes of the system. The normal modes, which we will denote by (ϕ_+, ϕ_0, ϕ_-) consist of linear combinations of the original field (u_1, u_2, u_3) chosen in such a way that the correlation matrix becomes approximately diagonal at long times, i.e, the cross correlations between different modes become negligible at long times. At the level of linearized hydrodynamics, for the diagonal elements of the correlation matrix, well-separated peaks for each mode is seen. Specifically one finds (at the linear level) a single diffusively spreading heat mode and two propagating sound modes moving with speeds $\pm c$. While it is not obvious what such a normal mode transformation will achieve for our integrable system, we nevertheless proceed to construct such a transformation (using the three variable description) and analyze the correlations in this basis.

We briefly review the construction of the normal mode transformation, starting with the microscopic continuity equations given by Eq. (2.2.10). The conserved currents j_α are then expanded

about their equilibrium value up to linear order in the fields leading to the linear equations

$$\partial_t u_\alpha(x,t) + \partial_x(A^{\alpha\beta}u_\beta(x,t)) = 0, \tag{2.4.1}$$

where

$$A = \begin{pmatrix} 0 & -1 & 0 \\ \partial_l P & 0 & \partial_e P \\ 0 & P & 0 \end{pmatrix}.$$

The partial derivatives above are computed using the equilibrium equation of state $P = P(l,e)$ where $l = \langle r \rangle, e = \langle e \rangle$. The diagonalization of the matrix A leads to the form $RAR^{-1} = diag(-c,0,c)$, where the matrix R is completely fixed by the normalization condition $RC(t=0)R^T = 1$, with C the correlation matrix. We refer the reader to [11] for explicit expressions. The constant c corresponds to the sound velocity and can be computed explicitly from equilibrium correlation functions through the formula [11]

$$c^2 = \frac{1}{\Gamma}\left(\frac{1}{2\beta^2} + \langle V + Py; V + Py\rangle\right), \tag{2.4.2}$$

with $\Gamma = \beta(\langle y;y\rangle\langle V;V\rangle - \langle y;V\rangle^2) + \frac{\langle y;y\rangle}{2\beta}$, and where $\langle A;B\rangle = \langle AB\rangle - \langle A\rangle\langle B\rangle$. For the Toda potential one can simplify Eq.(2.4.2) to get the form

$$c^2 = \frac{b^2}{\beta}\frac{\left(2z^2\psi^{(1)}(z) - 2z + 1\right)}{\left[(2z+1)\psi^{(1)}(z) - 2\right]}, \tag{2.4.3}$$

where $z = \frac{\beta P}{b}$ and $\psi^{(1)}(z)$ is Polygamma function which is defined as $\psi^{(1)}(z) = \frac{d^2}{dz^2}\log(\Gamma(z))$ and $\Gamma(z)$ is the standard Gamma-function. It is interesting to note that for the special case with $P = b$, the above formula is very close to one derived in [70].

For small b and $P = a$, Eq. (2.4.3) can be expanded to give the expected speed of sound in a harmonic chain $c = \sqrt{ab}$. In the other limit, when $b \to \infty$ and the external pressure is P the above formula gives the hard particle limit $c = \sqrt{3\beta}P$. These two limits can also be obtained in the high temperature (corresponding to large b) and low temperature limits (small b) by expanding with respect to z, leading to the same expressions for speed of sound to the leading order.

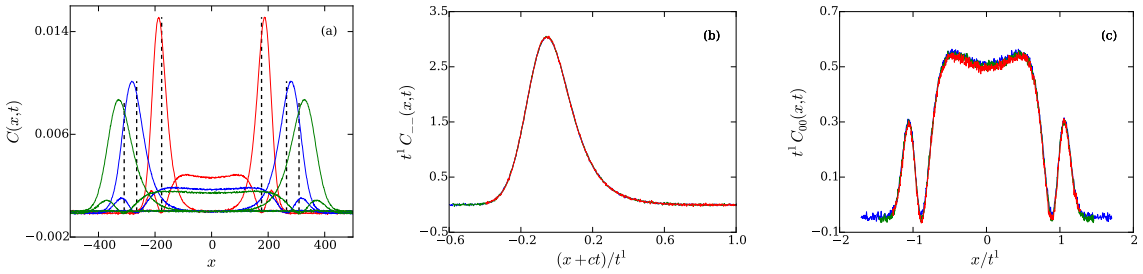

Figure 2.4: Normal mode representation- Case I with parameters $a = 1, b = 1, P = 1, T = 1$ and $N = 1024$. (a) Heat and sound modes plotted together at times $t = 200$ (red), $t = 300$ (blue) and $t = 350$ (green). The two sound modes move to left and to the right with velocities $\mp c$ (vertical dashed lines indicate the distance ct). (b) The sound modes at the three times are scaled ballistically and we see a good collapse even at small times. (c) The heat modes are scaled ballistically.

The normal mode transformation is then defined by $\phi_s = \sum_\alpha R_{s,\alpha} u_\alpha$, for $s = +, 0, -$. We can then compute correlations for these normal modes

$$C_{rs} = \langle \phi_r(x,t)\phi_s(0,0)\rangle \,, \tag{2.4.4}$$

for $r, s = +, 0, -$. As we will see this normal mode transformation separates the two sound modes $s = +, -$ moving with velocity $\pm c$ respectively and the heat mode $s = 0$. All the modes continue to show ballistic scaling. We now show numerical data of the correlations in normal modes for the Toda chain in various parameter regimes.

Case I: $a = 1.0, b = 1.0, P = 1.0, T = 1.0$ — In Fig. 2.4(a) we show the sound and heat modes plotted together at three different times $t = 200, 300, 350$. The speed of sound is $c = 0.883\ldots$. The scaled right moving sound modes and the scaled heat modes are plotted in Fig. 2.4(b) and Fig. 2.4(c) respectively. The scaling collapse is very good even for short times. The sound mode is broad and asymmetric. The heat mode on the other hand has a broad central peak and also significant side peaks. The amplitude of heat mode is much less than that of sound mode, which implies less scattering. In Figs. 2.4(b) and 2.4(c) we show the ballistic scaling of the right moving sound mode and the heat mode. Note that the shift by ct for the sound mode is not really necessary to see scaling collapse for the ballistic case. Typically we find that the off-diagonal correlations are of same magnitude as that of the diagonal correlations.

Case II: $a = 1.0, b = 1.0, T = 5.0, P = 1.0$ — In Fig. 2.5(a) we show the three normal modes correlations plotted together. The speed of sound in this case is $0.6232\ldots$. At high temperatures the dynamics is controlled by solitons, which are moving slower than their phonon counterparts. At

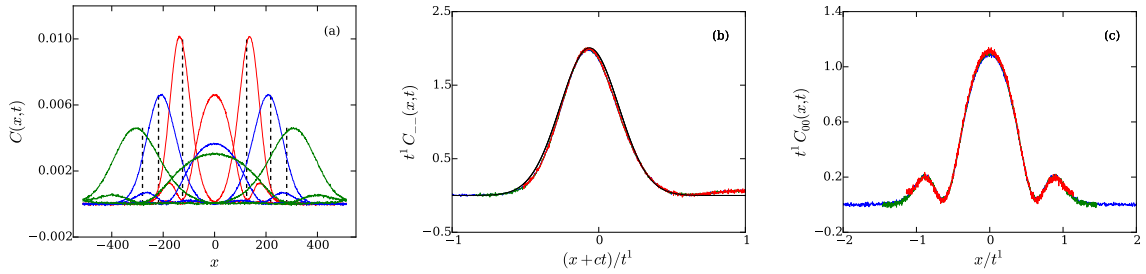

Figure 2.5: Normal mode representation - Case II with parameters parameters $a = 1.0, b = 1.0, P = 1.0, T = 5.0$ and $N = 1024$. (a) Heat and sound modes plotted together , at times $t = 200$ (red), $t = 300$ (blue) and $t = 450$ (green). The two sound modes move to the left and to the right with speed c (vertical dashed lines indicate the position ct). (b) This shows the ballistic scaling of the sound modes at the three different times. These are now almost Gaussian (shown by black solid line with standard deviation $\sigma = 0.1982\ldots$). (c) This shows the ballistically scaled heat mode. The amplitude of the heat and sound modes are now comparable.

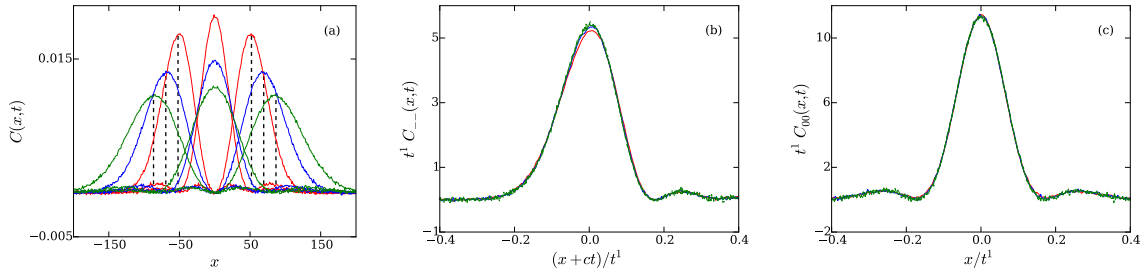

Figure 2.6: Normal mode representation - Case III with parameters $a = 0.1, b = 10.0, P = 0.1, T = 1.0$ and $N = 1024$, corresponding to the large anharmonicity limit. (a) This shows the heat and the two sound modes at times $t = 300$ (red), $t = 400$ (blue) and $t = 500$ (green). The distances $x = \pm ct$ are marked with vertical dashed lines. (b) This shows the ballistic scaling of the sound modes. (c) This shows ballistic scaling of the heat mode.

this temperature the phonon-soliton interaction is negligible and the sound mode is symmetric and fits well to a Gaussian with $\sigma = 0.1982$, while the heat mode has faster decay. Another feature is that at high temperatures the diagonal correlations are at least an order of magnitude larger than the cross-correlations. In Figs. 2.5(b) and 2.5(c) we show the ballistic scaling of the left moving sound mode and the heat mode.

Case III: $a = 0.1, b = 10.0, T = 1.0, P = 1.0$ — In Fig. 2.6(a) we show the three normal modes correlations plotted together, in a parameter regime corresponding to the hard particle limit. The speed of sound is 0.17093. The heat and sound modes now have single peaks but these are broad and with significant overlap at all times. Also note that the heat mode is larger in amplitude than the two sound modes unlike the other cases. In Figs. 2.6(b) and 2.6(c) we show the ballistic scaling

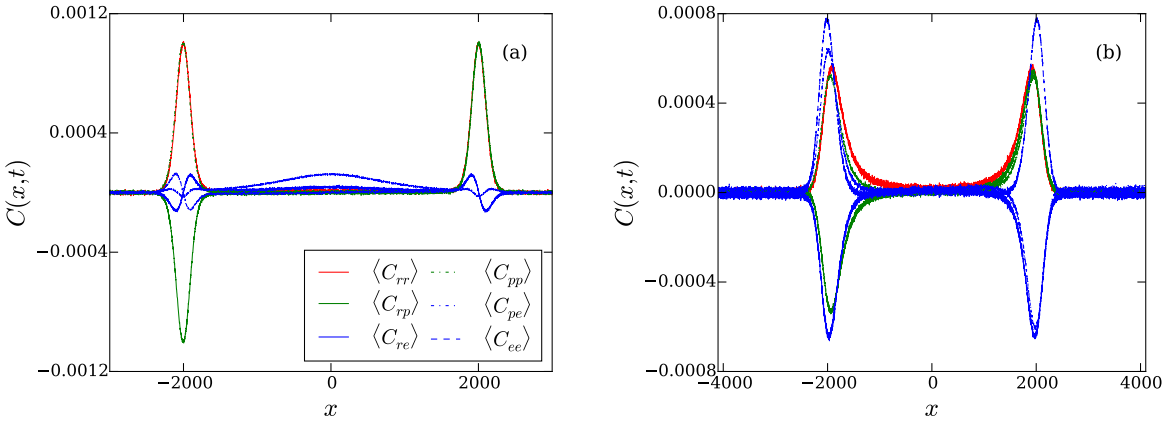

Figure 2.7: Figure shows all correlation functions between the three locally conserved quantities (r, p, e) for (a) truncated Toda chain [potential given by Eq. (2.4.5)] and parameters $P = 0, T = 0.5, N = 8192$ at time $t = 2000$. (b) Toda chain with $a = 1, b = 1, P = 1$ and all other parameters the same as in (a).

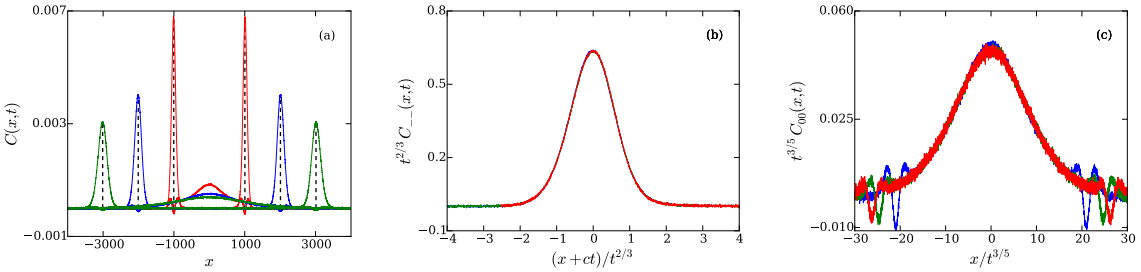

Figure 2.8: (a) Sound and Heat modes for truncated Toda chain (Eq. (2.4.5)) with parameters $P = 0.0, T = 0.5, N = 8192$ at times $t = 2000$ (red) $t = 3000$ (blue) and $t = 3500$ (green). The black dashed line show the positions $\pm ct$ and coincide with the peaks of the sound modes. (b) This shows the expected KPZ-scaling of the sound modes, with exponent $2/3$ as per hydrodynamics prediction. (c) This shows the heat mode scaling with the the expected Levy exponent $3/5$.

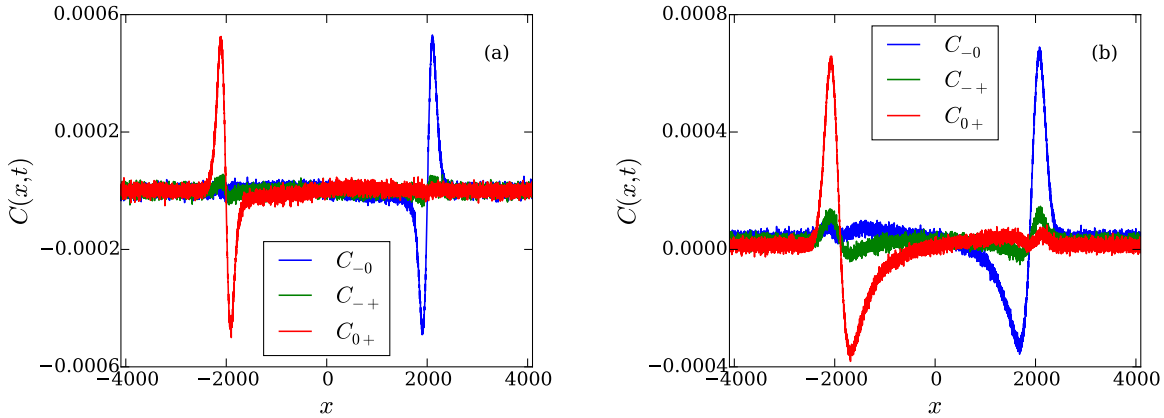

Figure 2.9: This shows the cross correlations between the normal modes at $t = 2000$ which are smaller than their respective diagonal correlations for (a) Truncated Toda chain with parameters as given in Fig. 2.7(a). (b) Toda chain with same parameters as Fig. 2.7 (b).

of the right moving sound mode and the heat mode.

2.4.3 Equilibrium correlations in truncated Toda chain

To see the huge effect of integrability on the form of correlations, we show results from a simulation with a potential corresponding to a truncated Toda potential with parameters P, T chosen to be close to the actual Toda simulations. Note that truncation leads to an FPU potential and is expected to destroy integrability. For the parameters $a = b = 1$, the truncated Toda potential to quartic order is given by

$$V_{tr}(r) = \frac{r^2}{2} - \frac{r^3}{6} + \frac{r^4}{24}\,, \tag{2.4.5}$$

and we set $P = 0.0, T = 0.5$ to match the equilibrium properties of the corresponding integrable Toda chain with parameters $a = 1, b = 1, P = 1, T = 0.5$. With this parameters, the speed of sound in truncated Toda chain is $c = 1.004...$ and for Toda chain is $c = 0.938...$ which is about a 6% difference.

In Fig. 2.7 we show a comparison of the correlation functions of Toda chain with the corresponding truncated Toda chain. We see that they show significant qualitative differences. In particular for the truncated Toda (FPU) chain, the correlation functions show localized and well-separated peaks, while in the Toda chain, they are broad and overlapping. The cross correlations are of similar order in both cases and we will now see how this changes when we transform to normal mode basis. The normal mode representation more clearly shows the difference between the Toda results and the FPU.

Finally we show that the normal mode representation also brings out clearly the striking differences between integrable and non-integrable models. In Figs. 2.8(a) and 2.8(b) we plot the normal mode correlations for the truncated Toda chain whose correlations (in usual variables) were presented in Fig. 2.7(a). We see the striking differences between these and the corresponding plots for the Toda chain in Figs. (2.4,2.5,2.6). In particular we see that for the non-integrable case, the sound modes show the KPZ scaling form $C_{++}(x,t) = f_+((x+ct)/(\lambda_s t^{2/3}))/(\lambda_s t)^{2/3}$, while the heat modes show Levy-$5/3$ scaling $C_{00} = f_0(x/(\lambda_h t^{3/5}))/(\lambda_h t)^{3/5}$, where $f_{+,0}$ and $\lambda_{s,h}$ are appropriate scaling functions and scaling factors. The cross correlation between the three normal modes in the truncated Toda lattice is shown in Fig. 2.9(a) and for Toda chain in Fig. 2.9(b). In this case

we see that for both the Toda chain and its truncated version, the off-diagonal correlations between heat and sound modes are much smaller than the diagonal correlations. The main difference between the two cases is that in the truncated Toda chain, the modes are localized around sound peak, while for integrable Toda chain they have a broad spreading.

2.5 Non-equilibrium transport in Toda chain connected to heat baths

In a non-equilibrium setup, we attach two heat-bath in different temperature (T_L and T_R) at the two ends of the lattice and let the system evolve sufficiently to equilibrium. The equations of motion are taken to be those in Eq. (2.2.1) with the Toda inter-particle potential $V(r) = (a/b)e^{-br}$,

$$\begin{aligned}
\dot{p}_1 &= -ae^{-b(q_2-q_1)} + ae^{-b(q_1-q_0)} - \lambda p_1 + \sqrt{2\lambda T_L}\eta_L, \\
\dot{p}_x &= -ae^{-b(q_{x+1}-q_x)} + ae^{-b(q_x-q_{x-1})}, \ 2 \leq x \leq N-1, \\
\dot{p}_N &= -ae^{-b(q_{N+1}-q_N)} + ae^{-b(q_N-q_{N-1})} - \lambda p_N + \sqrt{2\lambda T_R}\eta_R,
\end{aligned} \tag{2.5.1}$$

and we choose fixed boundary conditions $q_0 = 0$ and $q_{N+1} = L$ and with η is the Gaussian white noise with zero mean and unit variance. The non-equilibrium driving at the boundaries gives rise to a non-zero current in the system which leads to a temperature profile interpolating between the boundary temperatures. The local temperature given as $\langle v^2 \rangle$ is measured, along with current in the NESS of the system by averaging over time for around 10^6 data points (each data point is taken after time intervals 10). From Eq. (1.2.3), we get the current on the bond x to $x+1$ as

$$j_x = \frac{1}{2}(p_x + p_{x+1})V'(q_{x+1} - q_x). \tag{2.5.2}$$

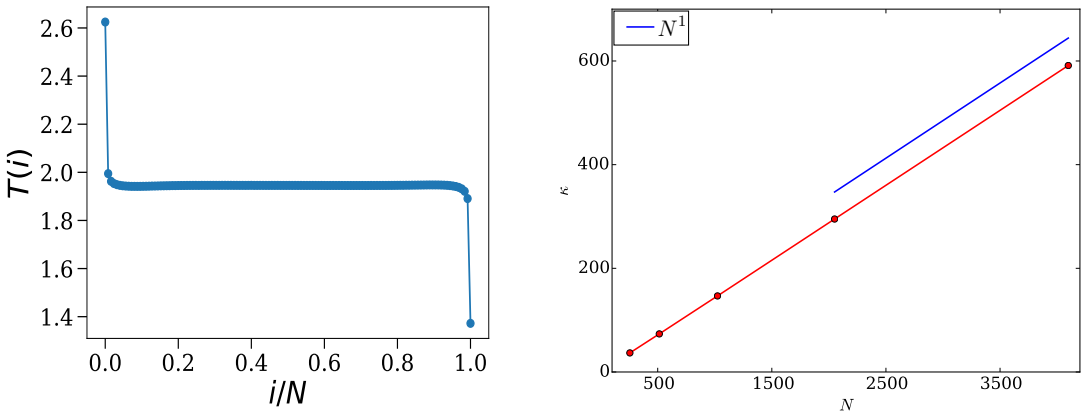

Figure 2.10: Non-equilibrium simulations of the Toda chain: (a) Temperature profile for Toda chain of size $N = 128$ with $T_L = 3$ and $T_R = 1$ and parameters $a = b = 1$ (b) Ballistic scaling of conductivity, κ, with system size N. The parameters for Toda chain are $a = 1, b = 1, \rho = 1$ with fixed boundary conditions. In all our simulations the bath dissipation constant $\lambda = 1$.

For small temperature differences, the thermal conductivity is given in terms of current in the system as

$$\kappa = \frac{N\langle j\rangle}{|T_L - T_R|}, \tag{2.5.3}$$

where $\langle j\rangle = \sum_{x=1}^{N-1}\langle j_x\rangle/(N-1)$. As expected we find [see Fig. (2.10)] that in the NESS, the temperature profile is flat and the thermal conductivity increases linearly with system size ($\kappa \sim N$). These are consistent with ballistic transport in integrable system. Note that in contrast, in a diffusive system, the temperature profile would be linear and thermal conductivity κ would be independent of system size, while for an anomalous system the temperature profile is non-linear and $\kappa \sim N^\alpha$ with $\alpha < 1$. An interesting question is to explore the dependence on the value of the bulk temperature (say T_{av}) on the system parameters. We first note a simple scaling relation for the temperature. The Langevin equations of motion, Eq. (2.5.2), have the following scaling symmetry: the transformations $x \to sx, b \to b/s, a \to sa, T \to s^2T$ and $L \to sL$ leaves the equations invariant. Using this we can write the following exact scaling relation for the temperature in the Toda lattice:

$$T(sa, b/s, s^2T_L, s^2T_R, \rho/s)/s^2 = T(a, b, T_L, T_R, \rho), \tag{2.5.4}$$

and a similar expression for current. This shows that the temperature, density and non-linearity parameters play a role interchangeably in determining the effective anharmonicity in the system. In

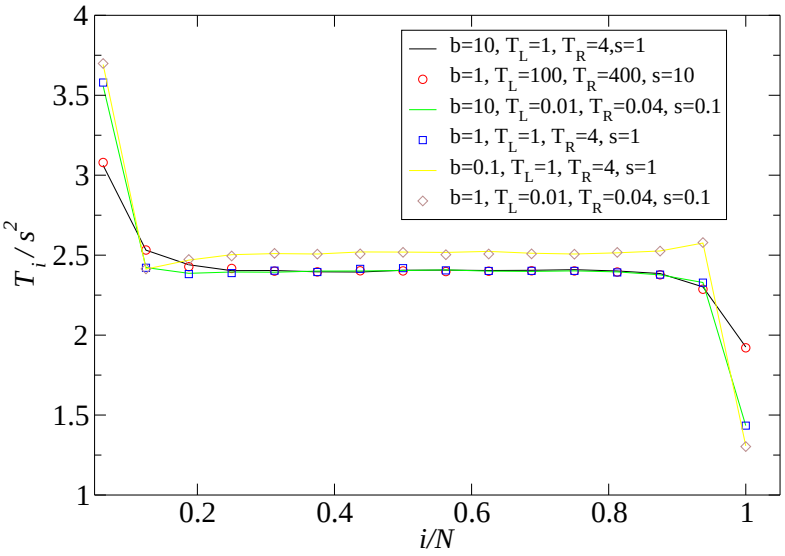

Figure 2.11: Test of scaling for different b and T as stated in Eq. (2.5.4) with fixed boundary conditions. We simulate the left hand side of the equation for various values of s. In all simulations the system size is $N = 16$, $T_L = 4$, $T_R = 1$, dissipation constant $\lambda = 1$ and $a = 1/b$. In the NESS, the average temperature in hard particle gas limit is almost $T_{av} = 2.4 \neq \sqrt{T_L T_R}$ while in the harmonic limit we find $T_{av} = 2.5 = (T_L + T_R)/2$.

Fig. (2.11) we test this scaling relation in the hard-particle gas and harmonic chain limits. It is known exactly that for the harmonic chain attached to Langevian baths T_{av} is given by $(T_R + T_L)/2$ while for the hard particle gas attached to Maxwell baths, it is given by $\sqrt{T_L T_R}$. The case of hard particle gas with Langevian baths has not been studied before. In our simulation results in Fig. (2.11), we find that for the Toda chain in the harmonic limit, we do get $T_{av} = (T_R + T_L)/2$, while in the hard particle gas limit we do not obtain the expected value $\sqrt{T_L T_R}$. Emperically we find that $T_{av} \approx \sqrt{T_1 T_N}$ where T_1, T_N are the temperatures of the boundary particles.

Energy transport in quartic perturbation of Toda chain: Next, we add a small quartic perturbation to the Toda chain which again breaks the integrable structure (in a different way than the truncated Toda). The quartic perturbation to Toda lattice is defined by taking the interaction potential to be

$$V(r) = \frac{a}{b} e^{-br} + \delta \frac{r^4}{4}. \tag{2.5.5}$$

The perturbed Toda is non-integrable and has three conservation laws with momentum conservation, hence we expect it to have anomalous transport. Here we study the effects of perturbing Toda chain on the non-equilibrium temperature profile and current. One must note that the Toda potential is a highly non-linear system and breaking its integrability is very different from breaking of integrability by adding perturbation in the linear harmonic chain. This makes it interesting to study

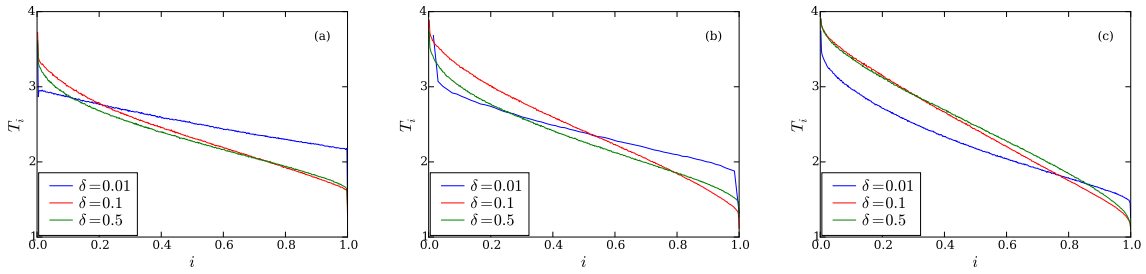

Figure 2.12: Non-Equilibrium simulations of Toda Lattice in different limits and perturbations. The left bath is kept at temperature $T_L = 4$ and right bath is at temperature $T_R = 1$. All simulations are for system size $N = 512, \rho = 1$. (a) perturbations in the Harmonic Limit $a = 10, b = 0.1$. Surprisingly, for small perturbation, the profile is almost linear. (b) perturbations on Toda parameters $a = 1.0, b = 1.0$ and (c) perturbations on Hard particle limit $a = 0.1, b = 10$. We see as we go to hard-particle limit, a greater temperature gradient is set up for same perturbation.

the crossover of transport from ballistic to anomalous.

The perturbations to exponential interaction is of interest as it can help understand the effects of non-linearity in heat transport. It has been suggested before that FPU chain can be viewed as a perturbation of Toda chain [80]. In the hard-particle limit, the lattice is governed by solitons, which are space localized. Any small perturbation in space affects the stability of the solitons and hence they break. In the harmonic limit the dynamics is governed by phonons localized in Fourier space. On small perturbations in real space, the large wavelength modes will be less affected. Here we study the non-equilibrium properties of the perturbed Toda chain. Further, to study the robustness of Toda lattice to quartic perturbations, we study the temperature profile in the harmonic chain and hard particle gas limits, with perturbations of the same strength.

In all the simulations, the density of the chain is kept fixed at $\rho = 1$. In harmonic limit, the parameters are $a = 10, b = 0.1$ and in hard-particle limit the parameters are $a = 0.1, b = 10$. Three different perturbations ($\delta = 0.01, 0.1, 0.5$) are applied and the resulting temperature gradient and heat current is studied. Fig. (2.12) shows that with the same perturbation strength, a greater temperature gradient is set up in case of high anharmonicity. The temperature profile also shows unexpected behavior as the perturbation is increased. In harmonic limit, $b = 0.1$, a quadratic perturbation of $\delta = 0.01, 0.1, 0.5$ shows increase in temperature gradient as expected. Interestingly, for small perturbation, the profile is almost linear. In case of HPG limit surprisingly, a perturbation of $\delta = 0.5$ creates a lesser temperature gradient than a perturbation of $\delta = 0.1$.

2.6 Conclusion

We have studied the spatio-temporal equilibrium correlation functions of the fluctuations of three conserved quantities (stretch, momentum and energy) in the Toda chain. We found analytical expressions of these correlations in two different limits of the Toda chain, namely harmonic chain and hard particle gas and verified them in direct molecular dynamics simulations. The two limits can be argued to correspond to either phonon dominated dynamics or soliton dominated dynamics.

For generic parameter regimes, our numerical data shows that the Toda correlations always exhibit ballistic scaling. We pointed out that this form is completely different from the correlations seen in a truncated Toda potential, which exhibits the universal scaling forms predicted by nonlinear fluctuating hydrodynamics of generic anharmonic chains. We carried out the transformation to normal modes following the approach of hydrodynamics (for the three variables) and found that this is still useful in separating the multiple peaks seen in correlation functions of the conserved variables in an integrable system. Also, an explicit formula for the speed of sound is obtained. Unlike non-integrable systems, the normal modes have peaks with large width (i.e. the width of the peaks scale linearly with time). Precise conditions and proofs are necessary for ballistic scaling of space-time correlations in classical integrable systems and remains an open interesting problem. The question is also of interest in the context of integrable quantum systems. We have further studied the transport in Toda chain connected to heat baths. The ballistic transport in this system implies that the thermal conductivity diverges linearly with the system size and the temperature profile is flat in all parameter regimes. However the precise value of the constant bulk temperature profile is the average of two boundary temperatures only in the harmonic limit, while it is different in other cases, including the hard-particle limit. We systematically study and comment on the temperature profile for various cases. Finally, we studied the effect of non-integrable perturbations on the temperarature profile and find that they immediately lead to non-flat temperature profiles.

2.7 Appendix

2.7.1 Sum Rules

Here we outline the proofs of the sum rules mentioned in Sec. (2.2). The zeroth sum rule says that for a conserved quantity, the total correlations of the system remain constant in time, i.e,

$$\sum_x C^{\alpha\beta}(x,t) = \sum_x C^{\alpha\beta}(x,0)\,. \tag{2.7.1}$$

Recall that we are interested in correlations of the fluctuations around equilibrium values $u_\alpha(x,t) = I_\alpha(x,t) - \langle I_\alpha\rangle$. Let us also define the current fluctuations as $\Delta j_\alpha(x,t) = j_\alpha(x,t) - \langle j_\alpha\rangle$ and the total current $J^\alpha(t) = \sum_x j^\alpha(x,t)$. From the equations of motion we get

$$\partial_t u^\alpha(x,t) = \Delta j^\alpha_{x-1}(t) - \Delta j^\alpha_x(t)\,.$$

Multiplying both sides by $u^\beta(0,0)$ and averaging over the initial equilibrium distribution gives

$$\begin{aligned}\partial_t C^{\alpha\beta}(x,t) &= \langle \Delta j^\alpha_{x-1}(t) u^\beta(0,0)\rangle - \langle \Delta j^\alpha_x(t) u^\beta(0,0)\rangle \\ &= \langle \Delta j^\alpha_0(0) u^\beta_{1-x}(-t)\rangle - \langle \Delta j^\alpha_0(0) u^\beta_{-x}(-t)\rangle\,,\end{aligned} \tag{2.7.2}$$

where we used space and time-translational invariance. Summing over all sites we then get

$$\frac{d}{dt}\sum_x C^{\alpha\beta}(x,t) = \sum_x [\langle \Delta j^\alpha_0(0) u^\beta_{x-1}(-t)\rangle - \langle \Delta j^\alpha_0(0) u^\beta_x(-t)\rangle],$$

which vanishes, since $\sum u^\beta_x$ is a conserved quantity. Hence the result in Eq. (2.7.1) follows.

The other sum rules are on the moments of spatial correlation functions of conserved quantities.

The first and second sum rules respectively state

$$\begin{aligned}\frac{d}{dt}\sum_x xC^{\alpha\beta}(x,t) &= \sum_{x=-N/2}^{N/2-1}\langle\Delta j^\alpha(x,0)u^\beta(0,0)\rangle \\ &\quad - N\langle j^\alpha(-N/2,t)^\beta(0,0)\rangle\,, \\ &= \langle J^\alpha u^\beta\rangle \quad (N\to\infty) \qquad (2.7.3)\\ \frac{d^2}{dt^2}\sum_x x^2C^{\alpha\beta}(x,t) &= 2\sum_{-N/2}^{N/2-1} C_j^{\alpha\beta}(x,t), \\ &\quad + N\left[C_j^{\alpha\beta}(-\frac{N}{2},t) - C_j^{\alpha\beta}(\frac{N}{2}-1,t)\right], \\ &= 2\sum_x C_j^{\alpha\beta}(x,t) \quad (N\to\infty), \qquad (2.7.4)\end{aligned}$$

where $C_j^{\alpha\beta}(x,t) = \langle\Delta j^\alpha(x,t)\Delta j^\beta(0,0)\rangle$ and we note that Eq. (2.7.3) only involves an equilibrium equal time correlation.

The proof starts by following steps as those for Eq. (2.7.2) to get

$$\partial_t C^{\alpha\beta}(x,t) = \langle\Delta j^\alpha_{x-1}(0)u^\beta_0(-t)\rangle - \langle\Delta j^\alpha_x(0)u^\beta_0(-t)\rangle\,.$$

Multiplying the above equation by x, summing over all x, and after simplifications using the fact that $\sum_x u^\beta(x,t) = const$ gives Eq. (2.7.3). Taking another time derivative, and on using the continuity equations we get

$$\begin{aligned}\frac{d^2}{dt^2}C^{\alpha\beta}(x,t) &= -[\langle\Delta j^\alpha_{x-1}(0)[\Delta j^\beta_{-1}(-t) - \Delta j^\beta_0(-t)]\rangle \\ &\quad - \langle\Delta j^\alpha_x(0)[\Delta j^\beta_{-1}(-t) - \Delta j^\beta_0(-t)]\rangle] \\ &= \left[C_j^{\alpha\beta}(x+1,t) - 2C_j^{\alpha\beta}(x,t) + C_j^{\alpha\beta}(x-1,t)\right]\,.\end{aligned}$$

Multiplying the above equation by x^2, summing over all x, and after simplifications using the first sum-rule $\sum_x C^{\alpha\beta}(x,t) = const$ gives Eq. (2.7.4).

3

Velocity correlation functions in the Hard Particle Gas in thermal equilibrium

3.1 Introduction

The hard point particle gas (HPG) is a simple example of an interacting many particle system. As discussed in 1, the alternate mass HPG has been studied both in equilibrium and non-equilibrium setups, and exhibits anomalous transport. On the other hand the equal mass hard particle gas is integrable and shows ballistic transport, that is NESS current is independent of system size and equilibrium correlation functions have the scaling form $t^{-1}f(x/t)$. In the previous chapter, we also saw that the equal mass HPG is obtained as a special limiting case of the Toda model.

In the HPG model, particles undergo elastic two-particle collisions with nearest neighbor particles, while in between the collisions, they move freely with constant velocity. For the equal mass case, elastic collisions conserve energy and momentum and this means that colliding particles simply exchange their velocities. The initial order of the particles remains the same as the particles cannot cross each other. Using these properties it was shown by Jepsen [17] that one can effectively map this to a gas of non-interacting particles and many exact results, such as tagged particle equilibrium velocity correlations, could be obtained. In recent work [84, 85, 88], much simplification of this approach was used to obtain exact results on properties of tagged particle displacements.

In this chapter we show how one compute higher order velocity correlations , by following the methods in [84]. Specifically we considered a set of $2N+1$ particles of unit masses moving inside a 1D box of length $2L$. The ordered particles have positions and velocities given by $\{x_i, v_i\}$ for $i =$

$1, 2 \ldots, 2N+1$. We are interested in computing general spatio-temporal correlation functions of velocity defined as

$$\langle v_i^m(t); v_j^n(0)\rangle = \left[\langle v_i^m(t) v_j^n(0)\rangle - \langle v_i^m(t)\rangle\langle v_j^n(0)\rangle\right]/\bar{v}^{m+n},, \tag{3.1.1}$$

where m, n are positive integers and the average is over initial configurations chosen from the equilibrium Gibb's distribution at temperature T and density ρ, and we have defined $\bar{v}^2 = T$. The notation $\langle ; \rangle$ denotes only the connected part with the average part subtracted. We are interested in computing these correlations in the thermodynamic limit with $N \to \infty, L \to \infty$ keeping $\rho = (2N+1)/(2L)$ constant and with i, j taken to be particles in the bulk. Hence in all our computations, we will ignore collisions with the wall. In this limit, the correlation function depends only on the relative position of the two particles, $r = i - j$.

The chapter is organized as follows: In section Sec. [3.2] we define the system of equal mass hard particles and the transformation to the non-interacting system. We then outline the main idea of computing the two particle joint probability distribution for the equal mass HPG. We relate the joint positional distribution to study the velocity correlations of the system in the thermodynamic limit. We also verify the results from simulations of the microscopic system. In Sec. [3.3] we give a heuristic derivation of the first few velocity correlations and stretch correlations. Finally we conclude the chapter in Sec. [3.4].

3.2 Main steps of the calculation

We consider a gas of $2N+1$ particles that are initially distributed uniformly in the interval $[-L, L]$. The positions of the ordered particles are given by $\{x_i\}$ and the initial velocities $\{v_i\}$ are chosen from the Gibbs distribution at temperature T, $P(\{v_i\}) = \prod_i e^{-v_i^2/2T}/\sqrt{2\pi T}$. As mentioned in the introduction, since we are interested only in the thermodynamic limit and in bulk properties, we do not need to include a confining wall at the ends of the interval. The particles move freely with constant velocity between elastic collisions with the neighbors. Under a collision the particles simply exchange their velocities. This allows us to make a mapping from interacting system of particles [Fig. 3.1(a)], where the particles collide with each other, to a system of non-interacting par-

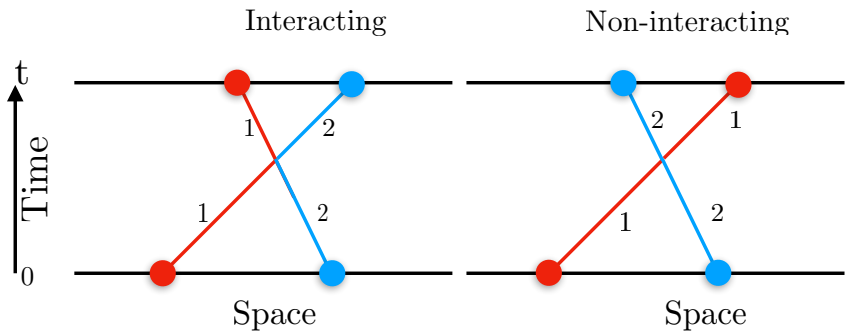

Figure 3.1: An interacting hard-point particles system can be constructed from a non-interacting system by exchanging tags (colors) when two trajectories cross.

ticles [Fig. 3.1 (b)] , where the particles evolve independently and pass through each other, and we exchange labels whenever particles cross. In fact this non-interacting picture allows one to evolve the system directly to any final time and the corresponding trajectory in the case where the particles are undergoing collisions can be obtained by relabeling the tags of the particles. The probability of obtaining the trajectories in the non-interacting picture is same as that of the interacting system. This mapping to the non-interacting gas was used by Jepsen [17] to obtain an exact solution for velocity-velocity autocorrelation functions in the hard-particle gas. A simpler approach was recently proposed in [84, 85, 89, 88] to obtain two particle distribution, tagged particle statistics and also a particular case of velocity correlations with $m = n = 1$ in Eq. (3.1.1).

In the non-interacting picture, a particle at x with velocity v travels to y at time t such that $y = x + vt$. It is useful to rewrite the non-interacting evolution as $y = x + \sigma_t v/\bar{v}$, where $\bar{v} = \sqrt{T}$ is the root-mean-square velocity of the particle and $\sigma_t = \bar{v}t$. For a particle with velocity chosen from the Maxwell distribution, the single particle propagator giving the probability of finding the particle at y at time t is then given by

$$\begin{aligned} G(y,t|x,0) &= \int_{-\infty}^{\infty} dv \delta(y - x - \sigma_t v/\bar{v}) \frac{e^{-v^2/2\bar{v}^2}}{\sqrt{2\pi\bar{v}^2}} \\ &= \frac{1}{\sqrt{2\pi\bar{v}^2 t}} e^{-\frac{(y-x)^2}{2\bar{v}^2 t^2}} = \frac{1}{\sigma_t} f\left(\frac{y-x}{\sigma_t}\right), \end{aligned} \tag{3.2.1}$$

where the function $f(x) = e^{-x^2/2}/\sqrt{2\pi}$, and we denote the m^{th} moment by $\delta_m = \int_{-\infty}^{\infty} x^m f(x) dx = [1 + (-1)^m](m-1)!!/2$ (where !! denotes the double factorial).

Our strategy is to compute the correlations of velocity via the two-time joint distribution function $P(x, j, 0, y, k, t)$ defined as the probability of the j^{th} particle being at x at time $t = 0$ and the

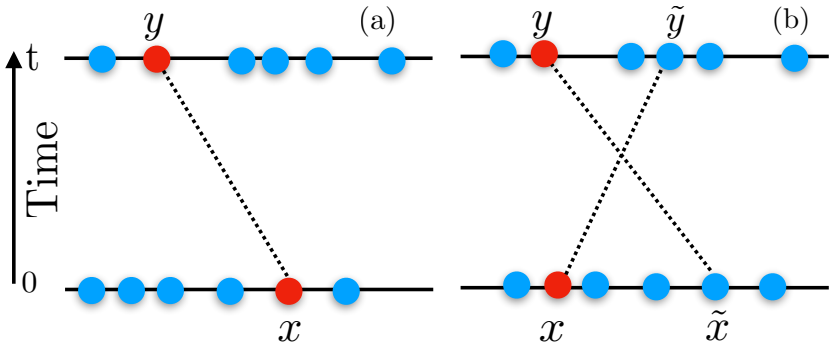

Figure 3.2: In the non-interacting picture, there are two possibilities: (a) the jth particle at time t = 0 becomes the kth particle at time t, (b) a second particle becomes the kth particle at time t.

k^{th} particle being at y at time t. Following [84], this joint PDF can be readily computed using the single particle propagator and through the mapping to non-interacting particles. In the next section we give the details.

3.2.1 Computation of the joint probability distribution of two particles

In terms of the non-interacting gas picture, the joint probability density, $P(x, j, 0, y, k, t)$, of the j^{th} particle being at x at time $t = 0$ and the k^{th} particle being at y at time t, has two independent contributions $P_1(x, j, 0, y, k, t)$ and $P_2(x, j, 0, y, k, t, \tilde{x}, \tilde{y})$. Both these quantities can be expressed in terms of the single particle propagator $G(y, t|x, 0)$ and another quantity which marks label of the particles at different times. These contributions are explained below

(i) In the non-interacting gas picture, $P_1(x, j, 0, y, k, t)$ is the probability that j^{th} particle, which is at x at time $t = 0$, becomes the k^{th} particle at y at time t [shown in Fig. 3.2(a)]. This is obtained by picking one of the non-interacting particles at random at time $t = 0$, with probability $\frac{2N+1}{2L}$, evolving with the propagator from $(x, 0)$ to (y, t) and multiplying by the probability that this is the jth particle at time $t = 0$ and the kth particle at time t. We thus get

$$P_1(x, j, 0, y, k, t) = \frac{2N + 1}{2L} G(y, t|x, 0) F_{1N}(x, j, y, k, t) \,, \tag{3.2.2}$$

where $F_{1N}(x, j, y, k, t)$ is the probability that there are $j - 1$ particles to the left of x at $t = 0$ and $k - 1$ particles to the left of y at time t. The explicit form of F_{1N} can be obtained

by combinatorial arguments [84] and is given in 3.5.1.

(ii) Similarly, for the non-interacting gas, $P_2(x, j, 0, y, k, t, \tilde{x}, \tilde{y})$ is the probability that the j^{th} particle at x at $t = 0$ becomes another particle at $\tilde{y}$ at time t and some other particle at $\tilde{x}$ at time $t = 0$ becomes the k^{th} particle at x at time t [shown in Fig. 3.2(b)]. In this case, two particles are chosen randomly at $t = 0$, with probability $\frac{(2N+1)(2N)}{(2L)^2}$, and are evolved with the propagator for the transition $(x, \tilde{x}, t = 0) \to (\tilde{y}, y, t)$. Finally we need to multiply this with the probability, $F_{2N}(x, j, y, k, \tilde{x}, \tilde{y}, t)$, that there are $j - 1$ particles to the left of x at $t = 0$ and $k - 1$ particles to the left of y at time t, *given* that there is a particle at $\tilde{x}$ at $t = 0$ and a particle at $\tilde{y}$ at time t. Combining these, we get

$$P_2(x, j, 0, y, k, t, \tilde{x}, \tilde{y}) = \frac{(2N + 1)(2N)}{(2L)^2} G(y, t|\tilde{x}, 0)G(\tilde{y}, t|x, 0)F_{2N}(x, j, y, k, \tilde{x}, \tilde{y}, t)\,. \tag{3.2.3}$$

The explicit form of F_{2N} can be obtained by combinatorial arguments [84] and is given in 3.5.1.

3.2.2 Relating velocity correlations to the joint positional distribution

The contribution to velocity correlations in the interacting system comes from two separate processes corresponding to the two joint probability distributions from the previous section. Hence we obtain

$$\mathcal{F}^{nm}(k, j, t) = \langle v_k^m(t) v_j^n(0)\rangle \bar{v}^{-(m+n)} = \underbrace{\langle v_k^m(t) v_j^n(0)\rangle_1/\bar{v}^{m+n}}_{\text{I}} + \underbrace{\langle v_k^m(t) v_j^n(0)\rangle_2/\bar{v}^{m+n}}_{\text{II}},$$

where I and II can be computed as follows.

(i) The first contribution comes when the j^{th} particle at x from time $t = 0$ becomes the k^{th} particle at y after time t. In the non-interacting picture, these two particles are correlated and have the same velocity, i.e. $\frac{v_k(t)}{\bar{v}} = \frac{v_j(0)}{\bar{v}} = \frac{y-x}{\sigma_t}$. Multiplying this with the appropriate probability $P_1(x, j, 0, y, k, t)$ and integrating over all possible initial and final positions, we get the first contri-

bution to velocity correlations

$$\begin{aligned} \mathrm{I} &= \int_{-\infty}^{\infty} dx \int_{-\infty}^{\infty} dy \left(\frac{y-x}{\sigma_t}\right)^{m+n} P_1(x,j,0,y,k,t), \\ &= \rho\sigma_t \int_{-\infty}^{\infty} \frac{dx}{\sigma_t} \int_{-\infty}^{\infty} \frac{dy}{\sigma_t} \left(\frac{y-x}{\sigma_t}\right)^{m+n} f\left(\frac{y-x}{\sigma_t}\right) F_{1N}(x,j,y,k). \end{aligned} \tag{3.2.4}$$

(ii) The second contribution is when the j^{th} particle at x with velocity $\frac{v_j(0)}{\bar{v}} = \frac{\tilde{y}-x}{\sigma_t}$ at $t = 0$ becomes another particle at $\tilde{y}$ time t and some other particle at $\tilde{x}$ with velocity $\frac{v_k(t)}{\bar{v}} = \frac{y-\tilde{x}}{\sigma_t}$ at time $t = 0$ becomes the k^{th} particle at y at time t. Multiplying this with the appropriate probability $P_2(x,j,0,y,k,t,\tilde{x},\tilde{y})$ and integrating over all position variables, we get

$$\begin{aligned} \mathrm{II} &= \int_{-\infty}^{\infty} dx \int_{-\infty}^{\infty} dy \int_{-\infty}^{\infty} d\tilde{x} \int_{-\infty}^{\infty} d\tilde{y} \left(\frac{\tilde{y}-x}{\sigma_t}\right)^{m} \left(\frac{y-\tilde{x}}{\sigma_t}\right)^{n} P_2(x,j,0,y,k,t,\tilde{x},\tilde{y}), \\ &= (\rho\sigma_t)^2 \int_{-\infty}^{\infty} \frac{dx}{\sigma_t} \int_{-\infty}^{\infty} \frac{dy}{\sigma_t} \int_{-\infty}^{\infty} \frac{d\tilde{x}}{\sigma_t} \int_{-\infty}^{\infty} \frac{d\tilde{y}}{\sigma_t} \left(\frac{\tilde{y}-x}{\sigma_t}\right)^{m} \left(\frac{y-\tilde{x}}{\sigma_t}\right)^{n} \\ &\qquad \times f\left(\frac{\tilde{y}-x}{\sigma_t}\right) f\left(\frac{y-\tilde{x}}{\sigma_t}\right) F_{2N}(x,j,y,\tilde{x},\tilde{y},k,t). \end{aligned} \tag{3.2.5}$$

In both cases we are already taking the thermodynamic limit, $N \to \infty,\ L \to \infty$ while keeping the average density $\rho = N/L$ constant.

3.2.3 Asymptotic results in the thermodynamic limit

Next we use the explicit forms of F_{1N}, F_{2N} given in 3.5.1. One can perform the integrals over $\tilde{x}, \tilde{y}$ in the second term II in Eq. (3.2.5). We also make a change of integration variables from x, y to the variables $z = (x-y)/\sigma_t$ and $\bar{z} = (x+y)/\sigma_t$, in Eq. (3.2.4) and Eq.(3.2.5). After some amount of

algebra we finally obtain the following expression for the velocity correlations:

$$\mathcal{F}^{nm}(r=k-j,0,t) = \mathrm{I} + \mathrm{II} = \tag{3.2.6}$$

$$\rho\sigma_t \int_{-\infty}^{\infty} dz \int_{-\infty}^{\infty} \frac{d\bar{z}}{2} \int_{-\pi/2}^{\pi/2} \frac{d\phi}{\pi} \int_{-\pi}^{\pi} \frac{d\theta}{2\pi} D(z,\theta,\phi) e^{-2N(1-\cos\phi)} e^{i\rho\sigma_t(-\bar{z}\sin\phi + z\sin\theta)} e^{(\phi r - \theta r)} e^{\rho\sigma_t 2Q(z)(1-\cos\theta)},$$

$$\text{where } Q(z) = z\int_0^z dw\, f(w) + \int_z^{\infty} dw\, w f(w), \tag{3.2.7}$$

$$D(z,\theta,\phi) = (\rho\sigma_t)^{-1} z^{m+n} f(z) + \Delta_1^m(z)\Delta_2^n(z)e^{-i\phi} + \Delta_1^n(z)\Delta_2^m(z)e^{i\phi} + \Delta_2^m(z)\Delta_2^n(z)e^{i\theta} + \Delta_1^m(z)\Delta_1^n(z)e^{-i\theta}, \tag{3.2.8}$$

and the Δs are related to moments of the propagator

$$\Delta_1^p(z) = \int_z^{\infty} d\omega\, \omega^p f(\omega),\ \Delta_2^p(z) = \int_{-\infty}^{z} d\omega\, \omega^p f(\omega), \tag{3.2.9}$$

$$\Delta_1^p(z) + \Delta_2^p(z) = \delta_p,\ \ \partial_z\Delta_1^p(z) = -\partial_z\Delta_2^p(z) = z^p f(z). \tag{3.2.10}$$

Since in Eq.3.2.6 the ϕ term comes with a factor of N, a saddle point analysis reveals that the major contribution comes from $\phi = 0$. We do a Taylor expansion around $\phi = 0$, up to second order, perform the resulting Gaussian in ϕ and then perform the resulting Gaussian integral in the variable $\bar{z}$. This then leads us to following simpler form

$$\mathcal{F}^{nm}(r,0,t) = \rho\sigma_t \int_{-\infty}^{\infty} dz \int_{-\pi}^{\pi} \frac{d\theta}{2\pi} D(z,\theta,0) e^{-\rho\sigma_t[2Q(z)(1-\cos\theta) - iz\sin\theta]} e^{-i\theta r}. \tag{3.2.11}$$

We define a new scaling variable $l = r/(\rho\sigma_t)$ and rewrite the above equation as

$$\mathcal{F}^{nm}(r=\rho\sigma_t l,0,t) = \rho\sigma_t \int_{-\infty}^{\infty} dz \int_{-\pi}^{\pi} \frac{d\theta}{2\pi} D(z,\theta,0) e^{-\rho\sigma_t I(z,\theta)}, \tag{3.2.12}$$

where, $I(z,\theta) = [2Q(z)(1-\cos\theta) - iz\sin\theta - i\theta l]$. Now we are interested in the large time (hence $v\sigma_t >> 1$) behaviour and so we again use saddle point methods. We find the minimum point z^*, θ^*, of the function $I(z,\theta)$ and expand both the functions I and D in Eq. (3.2.11) around

this minimum. We find that the minimum can be obtained by first minimizing with respect to θ which gives

$$\frac{\partial}{\partial\theta}[2Q(z)(1-\cos\theta) - iz\sin\theta + i\theta l]\Big|_{\theta=\theta^*} = 0, \tag{3.2.13}$$

whose solution is

$$e^{\pm i\theta^*} = \frac{\pm l + \sqrt{l^2 + 4Q^2(z) - z^2}}{2Q(z) \pm z}.. \tag{3.2.14}$$

Choosing the positive root, this then gives

$$I(z,\theta^*) = 2Q(z)(1-\cos\theta^*) - iz\sin\theta^* + i\theta^* l, \tag{3.2.15}$$

and after substituting θ^* from Eq. 3.2.14 we get

$$I(z,\theta^*) = 2Q(z) - \sqrt{l^2 + 4Q^2(z) - z^2} + l\ln\left[\frac{l + \sqrt{l^2 + 4Q^2(z) - z^2}}{2Q(z) + z}\right]. \tag{3.2.16}$$

We now note that $Q(z)$ is a positive function with a minimum at $z = l$, where $I(z = l, \theta^*) = 0$. Correspondingly from Eq.3.2.14 we then get $\theta^* = 0$. To study the contribution at large times, we expand Eq. (3.2.12) around the minimum point $z^* = l, \theta^* = 0$, using appropriate scaling variables. We set $z = l + w\sqrt{\epsilon}$ and $\theta = u\sqrt{\epsilon}$, where $\epsilon = 1/\rho\sigma_t$. We then obtain the expansion:

$$\begin{aligned}\frac{I(l + w\sqrt{\epsilon}, u\sqrt{\epsilon})}{\epsilon} &= (u^2 Q(l) - iuw) + C_1\epsilon^{1/2} + C_2\epsilon + \mathcal{O}(\epsilon^{3/2}), \\ \text{where } C_1 &= \left(u^2 w Q'(l) + \frac{1}{6}ilu^3\right), \quad C_2 = -\frac{1}{12}u^2\left(-6w^2Q''(l) + u^2Q(l) - 2iuw\right).\end{aligned} \tag{3.2.17}$$

Similarly $D(l + w\sqrt{\epsilon}, u\sqrt{\epsilon})$ can be expanded to give

$$\begin{aligned}D(l + w\sqrt{\epsilon}, u\sqrt{\epsilon}) \;=\; & \delta_m\delta_n + \sqrt{\epsilon}\left(iu\Delta_2^m(l)\right)\Delta_2^n(l) + iu\left(\delta^m - \Delta_2^m(l)\right)\left(\delta^n - \Delta_2^n(l)\right)\big) + \epsilon f(l) l^{m+n} \\ & -\frac{1}{2}u\epsilon\left(u\delta^m\left(\delta^n - \Delta_2^n(l)\right) - u\Delta_2^m(l)\left(\delta^n - 2\Delta_2^n(l)\right) - 2iwf(l)\left(l^n\delta^m + l^m\delta^n\right)\right) \\ & +\mathcal{O}(\epsilon^{3/2})\end{aligned} \tag{3.2.18}$$

We then expand the product $De^{-C_1\epsilon^{1/2}-C_2\epsilon}$ as a power series in $\epsilon^{1/2}$ — let use denote this expansion as EXP (this contains polynomials in u and w). Plugging all these into Eq. (3.2.12), we then get

$$\mathcal{F}^{nm}(r=\rho\sigma_t l,0,t)=\int_{-\infty}^{\infty}du\int_{-\infty}^{\infty}\frac{dw}{2\pi}e^{-u^2Q(l)-2iuw}\times\text{ EXP}. \tag{3.2.19}$$

Finally we perform Gaussian integrations over the variables u and w to get

$$\mathcal{F}^{nm}(r/\rho\sigma_t=l,0,t)=\delta_m\delta_n+(l^m-\delta_m)(l^n-\delta_n)f(l)/\rho\sigma_t+\mathcal{O}(\epsilon^{3/2}), \tag{3.2.20}$$

where δ_n is defined in Eq. (3.2.1). The scaled correlation function after subtracting off the mean is then finally given by

$$\rho\sigma_t\langle v^m(l=r/\rho\sigma_t,t);v^n(0,0)\rangle=(l^m-\delta_m)(l^n-\delta_n)f(l). \tag{3.2.21}$$

In the next section we will verify this result from simulations with the microscopic dynamics of the hard particle gas.

3.2.4 Numerical verification with Hamiltonian evolution of the hard-particle gas

We now present results from numerical simulations of the hard particle gas. In our simulations we considered a gas of N hard point particles moving on a ring of length L. The density of the gas is $\rho = N/L$ and we choose the initial condition from an equilibrium distribution at temperature T (*i.e* we distribute the particles uniformly in space and the velocity of each particle is independently chosen from the distribution $e^{-v^2/(2T)}/\sqrt{2\pi T}$. The mapping to the independent particle picture means that time-evolution of this system can be done very efficiently. Basically, starting from any given initial condition, we evolve the non-interacting gas up to time t. In order to get the actual positions, we can get the correct tag of the interacting particle by simply sorting their final positions and taking into account the effect of periodic boundaries. We then compute the correlations $\langle v^m(x,t);v^n(0,0)\rangle$ by taking averages over initial conditions. In our simulations we took

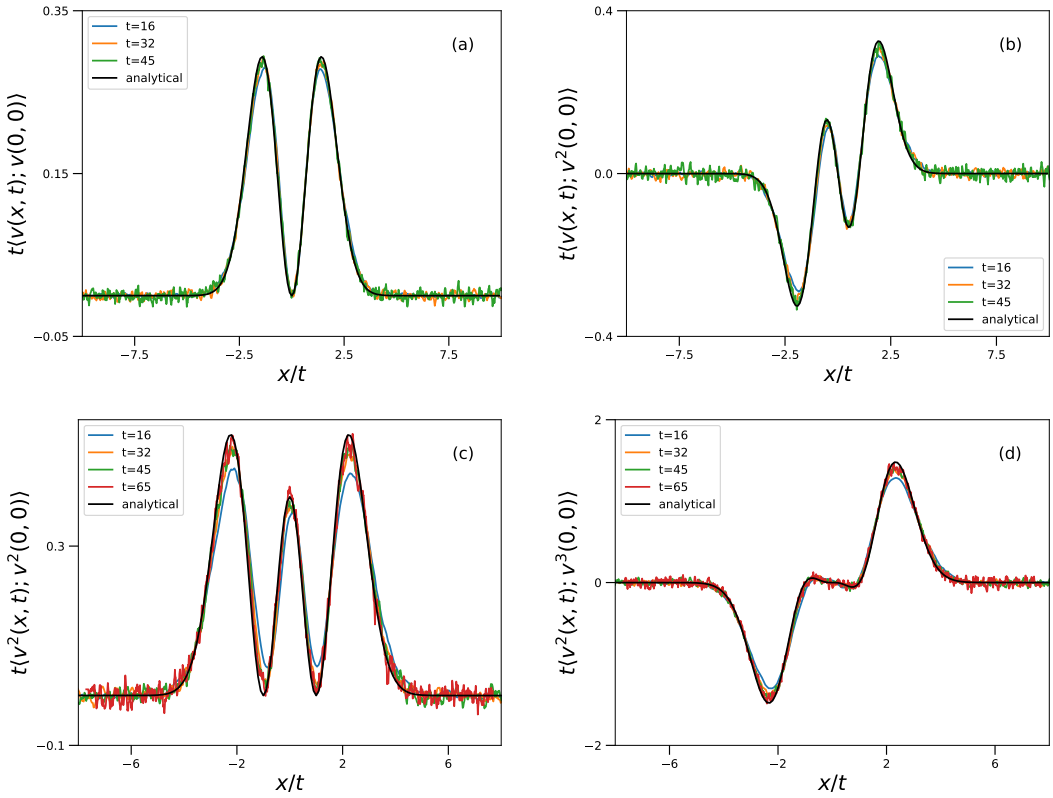

Figure 3.3: Scaled velocity correlation functions at different times, for various choices of m, n as obtained from simulations of the HPG. The black curves are from the analytical result as given by Eq. (3.2.20). The curves are for $t << L$. The parameters in the simulation are $N = 1001, L = 1000$ and temperature $T = 1$.

$N = 1001$ particles and took averages over 10^8 initial conditions. In Fig. (3.3) we plot the scaled correlation functions $t\langle v^m(x/t,t);v^n(0,0)\rangle$ (corresponding to ballistic scaling), obtained from the microscopic simulations and compare them with the corresponding theoretical predictions from Eq. (3.2.21). For several choices of m, n we find very good agreement between simulations and theory, even at relatively early times. At very short times there is a small deviation from the theory and this is expected, since the theory makes predictions for long time behaviour, well after the transient dynamics. On the other hand, finite size effects would show up at times $t \gtrsim \mathcal{O}(L)$. The peak of the correlation functions at time t, for odd values of m, n, is given by $x_p = \sqrt{m+n}\bar{v}t$. In contrast to this, the sound velocity for the HPG is given by $\sqrt{3}\bar{v}$. Using this, we estimate that finite size effects would show up in correlation functions of order $m + n$, at times approximately $t^* \sim \frac{L}{\bar{v}\sqrt{m+n}}$.

3.3 A heuristic argument and derivation of stretch and energy correlations

Here we present a heuristic approach which gives the asymptotic exact results of the previous section. These are then used to obtain the stretch and energy correlations of the HPG.

Since the initial velocities are chosen independently for each particle, the contribution to the correlation function $\langle v_r(t)v_0(0)\rangle$ is non-zero only when the velocity of the rth particle at time t is the same as that of the zero-th particle at time 0. The initial velocity distribution of each particle is chosen from a Maxwell distribution $f(v) = \frac{e^{-v^2/2\bar{v}^2}}{\sqrt{2\pi}\bar{v}}$, with $\bar{v}^2 = k_BT = 1/\beta$. The velocity correlation function is thus approximately given by

$$\begin{aligned}\langle v_x(t)v_0(0)\rangle &= \int dv v^2 \delta(x-\rho v t)\frac{f(v/\bar{v})}{\bar{v}} \\ &= \frac{\bar{v}^2}{\rho\sigma_t}\left(\frac{x}{\rho\sigma_t}\right)^2 \frac{e^{-\frac{1}{2}(\frac{x}{\rho\sigma_t})^2}}{\sqrt{2\pi}}\,, \end{aligned} \tag{3.3.1}$$

where $\sigma_t = \bar{v}t$. To compute the stretch correlations, we note that

$$\begin{aligned}\langle r_x(t)r_0(0)\rangle &= \langle [q_{x+1}(t)-q_x(t))(q_1(0)-q_0(0)]\rangle \\ &= -\left[\langle q_{x+1}(t)q_0(0)\rangle - 2\langle q_x(t)q_0(0)\rangle + \langle q_{x-1}(t)q_0(0)\rangle\right] \\ &= -\partial_x^2\langle (q_x(t)q_0(0)\rangle\,, \end{aligned} \tag{3.3.2}$$

where we have used the translation symmetry of the chain. Now taking two time derivatives gives

$$\begin{aligned}\partial_t\langle r_x(t)r_0(0)\rangle &= -\partial_x^2\langle (v_x(t)q_0(0)\rangle = -\partial_x^2\langle (v_x(0)q_0(-t)\rangle\,, \\ \partial_t^2\langle r_x(t)r_0(0)\rangle &= \partial_x^2\langle (v_x(0)v_0(-t)\rangle = -\partial_x^2\langle (v_x(t)v_0(0)\rangle,\end{aligned}$$

where we used time-translation invariance. Using this, the stretch correlation can be written in terms of velocity correlations as follows:

$$\langle r_x(t)r_0(0)\rangle = \int_0^t dt' \int_0^{t'} dt'' \partial_x^2\langle v_x(t)v_0(0)\rangle\,.$$

This finally gives (taking the continuous x limit):

$$\langle r_x(t) r_0(0)\rangle = \frac{1}{\rho^3 \sigma_t} \frac{e^{-\frac{1}{2}(\frac{x}{\rho\sigma_t})^2}}{\sqrt{2\pi}} \,. \tag{3.3.3}$$

For energy correlation, we need to compute

$$\begin{aligned}\langle e_x(t); e_0(0)\rangle &= \langle e_x(t) e_0(0)\rangle - \langle e_x(t)\rangle\langle e_0(0)\rangle \\ &= \frac{1}{4}\langle [v_x^2(t) - \langle v_x^2(0)\rangle][v_0^2(0) - \langle v_0^2(0)\rangle]\rangle \,.\end{aligned}$$

A similar computation as that leading to Eq. (3.3.1) now gives

$$\langle e_x(t); e_0(0)\rangle = \frac{\bar{v}^4}{\rho\sigma_t}\left[\left(\frac{x}{\rho\sigma_t}\right)^4 - 2\left(\frac{x}{\rho\sigma_t}\right)^2 + 1\right] f\left(\frac{x}{\rho\sigma_t}\right) \,. \tag{3.3.4}$$

To summarize, for the hard particle gas we consider initial velocities chosen from Maxwell distribution with variance $\bar{v}^2 = T$. The correlation functions are then given by

$$\begin{aligned} C_{rr}(x,t) &= \frac{1}{\rho^3\sigma_t}\frac{e^{-\frac{1}{2}(\frac{x}{\rho\sigma_t})^2}}{\sqrt{2\pi}} \\ C_{pp}(x,t) &= \frac{\bar{v}^2}{\rho\sigma_t}\left(\frac{x}{\rho\sigma_t}\right)^2 \frac{e^{-\frac{1}{2}(\frac{x}{\rho\sigma_t})^2}}{\sqrt{2\pi}} \\ C_{ee}(x,t) &= \frac{\bar{v}^4}{4\rho\sigma_t}\left[\left(\frac{x}{\rho\sigma_t}\right)^4 - 2\left(\frac{x}{\rho\sigma_t}\right)^2 + 1\right] \frac{e^{-\frac{1}{2}(\frac{x}{\rho\sigma_t})^2}}{\sqrt{2\pi}}. \end{aligned} \tag{3.3.5}$$

3.4 Conclusion

Using the mapping of the HPG to a non-interacting gas, we were able to compute exact long-time spatio-temporal correlation functions of arbitrary powers of velocities. We also discussed a heuristic derivation of these results and then used them to obtain correlations of stretch and energy in the HPG. Finally, we verified our analytic results, by performing simulations of the HPG using a very efficient numerical scheme, which again uses the mapping to non-interacting particles.

3.5 Appendix

3.5.1 Computation of F_{1N} and F_{2N}

The expressions for $F_{1N}(x, y, j, k, t)$ and $F_{2N}(x, y, \tilde{x}, \tilde{y}, j, k, t)$ were explicitly computed in [84], using combinatorial arguments. Here we give the explicit expressions:

$$F_{1N}(x, y, j, k, t) = \int_{-\pi/2}^{\pi/2} \frac{d\phi}{\pi} \int_{-\pi}^{\pi} \frac{d\theta}{2\pi} [H(x, y, \theta, \phi, t)]^{2N} e^{-i\phi(2N+2-k+j)} e^{-i\theta(k-j)}, \tag{3.5.1}$$

$$F_{2N}(x, y, \tilde{x}, \tilde{y}, j, k, t) = \int_{-\pi/2}^{\pi/2} \frac{d\phi}{\pi} \int_{-\pi}^{\pi} \frac{d\theta}{2\pi} [H(x, y, \theta, \phi, t)]^{2N-1} e^{-i\phi(2N+2-k+j)} e^{-i\theta(k-j)} e^{-i\phi\chi_1} e^{-i\theta\chi_2}, \tag{3.5.2}$$

where χ_1, χ_2 are defined as follows

1. $\tilde{x} < x$ and $\tilde{y} < y$, then $\chi_1 = 1$ and $\chi_2 = 0$,
2. $\tilde{x} < x$ and $\tilde{y} > y$, then $\chi_1 = 0$ and $\chi_2 = 1$,
3. $\tilde{x} > x$ and $\tilde{y} < y$, then $\chi_1 = 0$ and $\chi_2 = -1$,
4. $\tilde{x} > x$ and $\tilde{y} > y$, then $\chi_1 = -1$ and $\chi_2 = 0$.

The function $H(x, y, \theta, \phi, t)$ is defined as

$$\begin{aligned} H(x, y, \theta, \phi, t) &= p_{++}(x, y, t) e^{i\phi} + p_{--}(x, y, t) e^{-i\phi} + p_{+-}(x, y, t) e^{i\theta} + p_{-+}(x, y, t) e^{-i\theta}, \\ &= 1 - (1 - \cos\phi)(p_{++} + p_{--}) + i \sin\phi (p_{++} - p_{--}), \\ &\quad - (1 - \cos\theta)(p_{+-} + p_{-+}) + i \sin\theta (p_{+-} - p_{-+}), \end{aligned} \tag{3.5.3}$$

where $p_{-+}(x, y, t)$ is defined as the probability that a single non-interacting particle is to the left of x at time $t = 0$ and to the right of y at time t, and p_{+-}, p_{--} and p_{++} are defined similarly. Their

explicit forms are

$$p_{-+}(x,y,t) = \frac{1}{2L}\int_{-L}^{x} dx' \int_{y}^{L} dy'\, G(y',t|x',0), \tag{3.5.4}$$

$$p_{+-}(x,y,t) = \frac{1}{2L}\int_{y}^{L} dx' \int_{-L}^{x} dy'\, G(y',t|x',0), \tag{3.5.5}$$

$$p_{++}(x,y,t) = \frac{1}{2L}\int_{x}^{L} dx' \int_{y}^{L} dy'\, G(y',t|x',0), \tag{3.5.6}$$

$$p_{+-}(x,y,t) = \frac{1}{2L}\int_{-L}^{x} dx' \int_{-L}^{x} dy'\, G(y',t|x',0)\,. \tag{3.5.7}$$

We note that $p_{-+} + p_{+-} + p_{--} + p_{++} = 1$. We can explicitly find the expressions for $p_{\pm\pm}$ using the exact propagator Eq. (3.2.1). In the large N, L limit, expanding in $1/L$, we get

$$\begin{aligned}
p_{-+} &= \frac{\sigma_t}{2L}\left(-\frac{-z}{2} + Q(z)\right) + \mathcal{O}(1/L^2),\\
p_{+-} &= \frac{\sigma_t}{2L}\left(\frac{-z}{2} + Q(z)\right) + \mathcal{O}(1/L^2),\\
p_{++} &= \frac{1}{2} + \frac{\sigma_t}{2L}\left(-\frac{\bar{z}}{2} - Q(z)\right) + \mathcal{O}(1/L^2),\\
p_{--} &= \frac{1}{2} + \frac{\sigma_t}{2L}\left(\frac{\bar{z}}{2} - Q(z)\right) + \mathcal{O}(1/L^2),
\end{aligned} \tag{3.5.8}$$

where $z = (x-y)/\sigma_t$ and $\bar{z} = (x+y)/\sigma_t$ and

$$Q(z) = z\int_{0}^{z} dw\, f(w) + \int_{z}^{\infty} dw\, w f(w). \tag{3.5.9}$$

Now, substituting these asymptotic expressions of $p_{\pm\pm}$ in Eq. (3.5.3) for large N, keeping only the dominant terms, one finds

$$[H(x,y,\theta,\phi,t)]^{2N} = e^{-2N(1-\cos\phi)} e^{i\rho\sigma_t \bar{z}\sin\phi} e^{-2\rho\sigma_t Q(z)(1-\cos\theta)} e^{i\rho\sigma_t z\sin\theta}. \tag{3.5.10}$$

Part III

Non-local fractional equation description for open system transport in stochastic models

4

Harmonic chain with momentum exchange

4.1 Introduction

Energy transport across an extended system is a fundamental non-equilibrium phenomena which is often described by the phenomenological Fourier law. This law leads to the heat equation for the evolution of the temperature field $T(y,t)$, which in one dimension is given by

$$\partial_t T(y,t) = (\kappa/c)\partial_y^2 T(y,t), \tag{4.1.1}$$

where c is the specific heat capacity and κ the heat conductivity (assumed, for simplicity to be temperature independent). This equation plays a central role in understanding heat transport through macroscopic materials in several contexts.

One picture that has emerged from many studies is that, for systems with anomalous transport, the standard heat diffusion equation has to be replaced by a fractional diffusion equation [4, 52, 57, 58, 59, 61, 90]. A particular model of anomalous transport where some rigorous results have been obtained is that of the harmonic chain whose Hamiltonian dynamics is supplemented by a stochastic part that keeps the conservation laws (volume, energy, momentum) intact — we will refer this model as the harmonic chain momentum exchange (HCME) model. For the infinite HCME system, it was shown exactly that at equilibrium the energy current autocorrelation has a $\sim\ t^{-1/2}$ decay [50]. It was also shown that, in contrast to Eq. (4.1.1), the evolution of a localized energy perturbation $e(y,t)$, is described by a non-local fractional diffusion equation $\partial_t e(y,t) = -\bar{\kappa}(-\Delta)^{3/4} e(y,t)$, where $\bar{\kappa}$ is some constant which depends on microscopic parameters [61]. The fractional Laplacian operator $(-\Delta)^{3/4}$ in the infinite space is defined by its Fourier

spectrum: $|q|^{3/2}$ which for the normal Laplacian operator $-\Delta \equiv -\partial_y^2$ is q^2.

While most of the studies in HCME model consider evolution in infinite systems, it is also of interest to study transport across a finite system connected to two reservoirs of different temperatures at its two ends. For diffusive systems in this set-up, the heat equation continues to describe both non-equilibrium steady state (NESS) and time-dependent properties. However, for anomalous transport, it is a priori not clear how to write a corresponding evolution equation in a finite domain. Since we expect this evolution to be governed by a fractional Laplacian which is a non-local operator, it is difficult to guess its representation in a finite system from its representation in the infinite system. Note that in the finite system one has to include the effects of the boundary conditions which are important as the operator itself is non-local. Hence, extending its definition to a finite domain is a non-trivial problem. Several studies have addressed this problem of obtaining and studying fractional diffusion description in finite domain [91, 92, 93].

In this chapter we study heat transfer across the HCME model connected to two reservoirs at its two ends. It has been observed and proved that in this model, heat current scaling with system size is anomalous and the steady state temperature profile is inherently non-linear [4, 57? , 94]. In the present work we provide a fractional equation description of the anomalous heat transfer both in the stationary as well as in the non-stationary state. Using this fractional description we derive new results related to evolution of temperature profile, equilibrium current fluctuations and to two point correlations in NESS. Below we summarize the main results of our work along with the plan of the chapter:

- In Sec. (4.2) we first review previous studies on the HCME model and give the derivation of the finite domain fractional equation that follows essentially from these studies. These studies show that the macroscopic time evolution of two-point correlations is described by a set of coupled local linear PDEs [57, 58]. Starting from these PDEs, it can be shown that they naturally give rise to an evolution equation for the temperature profile $T(y,\tau)$

$$\partial_\tau T(y,\tau) = -\bar{\kappa}\, \mathbb{L} T(y,\tau),$$

governed by a fractional Laplacian $\mathbb{L}$ defined in a finite domain, where τ is a scaled time (see

later). The operator $\mathbb{L}$ is defined in the domain $0 \leq y \leq 1$ through it's action

$$\mathbb{L}\phi_n(y) = \lambda_n^{3/4}\phi_n(y)$$

on the complete Neumann basis $\langle y|\phi_n\rangle = \phi_n(y) = \sqrt{2}\cos(n\pi y)$ for $n \geq 1$ and $\langle y|\phi_0\rangle = \phi_0(y) = 1$ with $\lambda_n = (n\pi)^2$. Using this representation, we show in Sec. 4.3 that one can recover the exact results [57] for the steady state temperature and current profiles in the HCME.

- Next in Sec. (4.4) we discuss the time evolution of the temperature profile, starting from an arbitrary initial profile, to the long-time NESS profile. In order to solve the fractional diffusion equation with Dirichlet boundary conditions for arbitrary time we are required to find the eigenvalues and eigenvectors of the fractional operator $\mathbb{L}$ with Dirichlet boundary conditions. We describe an efficient procedure to compute this eigensystem. We also provide a detailed discussion of some properties of the eigensystem that distinguish them from the eigensystem of the normal Laplacian operator with the same boundary conditions.

- Inspired by the fluctuating equations for energy evolution in diffusive systems[60, 95], in Sec. (4.5) we extend the definition of the fractional equation to include fluctuations and noise in equilibrium such that fluctuation-dissipation relation holds locally. Using the fluctuating fractional equation description, we verify the validity of the equilibrium Green-Kubo relation in finite systems — in the process we encounter some interesting mathematical identities that we establish numerically.

- Finally we study the long-range correlations in NESS in Sec. (4.6), where we propose a conjecture on the relation between these correlations and the Inverse of the fractional operator $\mathbb{L}$.

4.2 Definition of Model and definition of the finite domain fractional operator

We consider the so-called harmonic chain momentum exchange model (HCME), which considers an added stochastic component in the usual Hamiltonian dynamics of a harmonic chain. The stochastic part is such that it preserves volume, momentum and energy conservation but the other conserved variables of the harmonic chain are no longer conserved. Thus the stochastic model restores ergodicity while preserving the important conservation laws. Here we are interested in the open system where the system is driven by two Langevin-type heat baths. Specifically we consider a system consisting of N particles and attached to two heat baths. The Hamiltonian plus heat bath part of the dynamics is described by the following equations

$$\begin{aligned}
\dot{q}_i &= p_i\,, \;\; \dot{p}_i = \omega^2(q_{i+1} - 2q_i + q_{i-1}), \;\; 1 < i < N, \\
\dot{p}_1 &= \omega^2(q_2 - 2q_1) - \lambda p_1 + \sqrt{2\lambda T_L}\eta_L, \\
\dot{p}_N &= \omega^2(q_{N-1} - 2q_N) - \lambda p_N + \sqrt{2\lambda T_R}\eta_R\,,
\end{aligned} \tag{4.2.1}$$

where $\{q_i, p_i\}, i = 1, 2 \ldots, N$, are the positions and momenta of the particles, T_L, T_R are the temperatures of the left and the right Langevin baths and η_L, η_R are Gaussian white noise terms. Additionally there is a stochastic element, such that the momenta of nearest neighbour particles are exchanged (*i.e* $p_{i+1} \leftrightarrow p_i$) at a rate γ. For this model the two point correlation functions satisfy a closed set of equations. Following [58] let us denote the possible correlation matrices by $\mathbf{U}_{i,j} = \langle q_i q_j \rangle$,$\mathbf{V}_{i,j} = \langle p_i p_j \rangle$, and $\mathbf{Z}_{i,j} = \langle q_i p_j \rangle$. One can show that the time evolution of these correlation functions is given by linear equations involving only these set of correlations, and source terms that arise from the boundary driving [58]. The correlation is defined as $\mathbf{z}^+_{i,j} = (\mathbf{Z}_{i,j} - \mathbf{Z}_{i-1,j} + \mathbf{Z}_{j,i} - \mathbf{Z}_{j-1,i})/2$. The most interesting physical observables involve the correlations $T_i = \mathbf{V}_{ii}$, which can be taken as the definition of local temperature and the energy current $J = \omega^2 \mathbf{z}^+_{i,i+1} + (\gamma/2)\,(\mathbf{V}_{i+1,i+1} - \mathbf{V}_{i,i})$. In the $N \to \infty$ limit, one observes that the fields T_i and $\mathbf{z}^+_{i,j}$ have the scaling forms $T_i(t) = T(i/N, t/N^{3/2})$ and $\mathbf{z}^+_{i,j} = \frac{1}{\sqrt{N}} C(|i-j|)/N^{1/2}, (i+j)/(2N), t/N^{3/2})$. In terms of the following scaling variables $x = |i-j|/N^{1/2}, y = (i+j)/(2N), \tau = t/N^{3/2}$, it has

been shown in [58] that the fields $T(y,\tau)$ and $C(x,y,\tau)$ satisfy the following coupled set of PDEs:

$$\begin{aligned}\gamma^2\partial_x^4 C(x,y,\tau) &= \omega^2\partial_y^2 C(x,y,\tau),\\ \partial_y T(y,\tau) &= -2\gamma\partial_x C(x,y,\tau)|_{x\to 0},\\ \partial_\tau T(y,\tau) &= \omega^2\partial_y C(x,y,\tau)|_{x\to 0},\end{aligned} \tag{4.2.2}$$

with boundary conditions $C(x,0,\tau) = C(x,1,\tau) = 0, C(\infty,y,\tau) = 0, \partial_x^3 C(0,y,\tau) = 0$ and $T(0,\tau) = T_L$ and $T(1,\tau) = T_R$ where, the domain of variables are $x \in [0,\infty)$ and $y \in [0,1]$ [note that in [58] $y \in (-1,1)$]. To study the time-evolution of the fields $C(x,y,\tau)$ and $T(y,\tau)$, one has to subtract the steady state solutions $C_{ss}(x,y)$ and $T_{ss}(y)$ of the above equations (whose explicit forms are given in [57]). The boundary conditions suggest that one expand the difference fields using the complete Dirichlet basis $\langle y|\alpha_n\rangle = \alpha_n(y) = \sqrt{2}\sin(n\pi y)$ for $n \geq 1$

$$C(x,y,\tau) - C_{ss}(x,y) = \sum_{n=1}^{\infty} \hat{C}_n(x,\tau)\alpha_n(y), \tag{4.2.3}$$

$$T(y,\tau) - T_{ss}(y) = f(y,\tau) = \sum_{n=1}^{\infty} \hat{f}_n(\tau)\alpha_n(y)\,. \tag{4.2.4}$$

Following [58] one then gets (see 4.8.2) the following matrix equation for the evolution of the components f_n:

$$\dot{\hat{f}}_n = -\,\bar{\kappa}\sum_{k=1}^{\infty}\mathbb{L}_{nk}\hat{f}_k, \quad n = 1,2,\ldots,\infty, \tag{4.2.5}$$

$$\text{where, } \mathbb{L}_{nk} = \left[\mathcal{T}\Lambda^{3/4}\mathcal{T}^\dagger\right]_{nk}, \tag{4.2.6}$$

with $\mathcal{T}_{nl} = \langle\alpha_n|\phi_l\rangle = \int_0^1 dy\alpha_n(y)\phi_l(y)$, where $\phi_m(y) = \sqrt{2}\cos(m\pi y)$ for $m > 0$, $\phi_0(y) = 1$ and $\Lambda_{ml} = \lambda_m\delta_{ml}$ is a diagonal matrix with $\lambda_n = (n\pi)^2$. The constant $\bar{\kappa} = \omega^{3/2}/(2\sqrt{2\gamma})$. Therefore, the function $f(x,\tau)$ with homogeneous boundaries $f(0,\tau) = f(1,\tau) = 0$ satisfies,

$$\partial_\tau f(y,\tau) = -\bar{\kappa}\mathbb{L}f(y,\tau). \tag{4.2.7}$$

From Eq. (4.2.6), one notices that $\mathbb{L}_{nk}$ can be written as

$$\mathbb{L}_{nk} = \langle\ \alpha_n\ |\mathbb{L}|\ \alpha_k\ \rangle = \langle\ \alpha_n\ |\left[\sum_{m=0}^{\infty} \lambda_m^{3/4}|\ \phi_m\ \rangle\langle\ \phi_m\ |\right]|\ \alpha_k\ \rangle,\ \ \forall\ n,k = 1,2,\ldots,\infty$$

which allows us to identify the action of the operator $\mathbb{L}$ acting on the set of basis functions ϕ_m (which satisfy Neumann boundary conditions):

$$\mathbb{L}|\ \phi_m\ \rangle = \lambda_m^{3/4}|\ \phi_m\ \rangle\ . \tag{4.2.8}$$

It is important to notice that the above representation of the operator $\mathbb{L}$ is not the "spectral fractional Laplacian with Dirichlet boundary conditions" which would consist to replace ϕ_n by α_n in (4.2.8). This definition has been mentioned in [4] and a more mathematically rigorous derivation has been obtained [93]. The above results imply that the temperature field $T(y,\tau)$ evolves according to the fractional equation

$$\partial_\tau T(y,\tau) = -\bar{\kappa}\mathbb{L}T(y,\tau) = -\mathbb{L}_{\bar{\kappa}}T(y,\tau)\ , \tag{4.2.9}$$

where we have defined $\mathbb{L}_{\bar{\kappa}} = \bar{\kappa}\mathbb{L}$ and the steady state is required to satisfy the condition $\mathbb{L}_{\bar{\kappa}}T_{ss}(y) = 0$. To describe the evolution of the temperature profile, one is specifically interested in finding the eigenvectors of the operator $\mathbb{L}$ which satisfy Dirichlet boundary conditions. This can be obtained by diagonalizing the infinite-dimensional matrix in Eq. (4.2.6). Let the eigenvector components of this matrix be denoted by $\psi_n^{(m)}$, corresponding to eigenvalue μ_n, so that $\sum_k \mathbb{L}_{mk}\psi_n^{(k)} = \mu_n\psi_n^{(m)}$. Then the eigenvector in the position basis is given by $\psi_n(y) = \sum_m \psi_n^{(m)}\alpha_m(y)$. In Sec. 4.4 we provide an alternate and more efficient method of computing eigenvalues and eigenvectors. This method involves finding roots of a transcendental equation and avoids diagonalization of infinite dimensional matrices. We also discuss various properties of the spectrum there. We now describe several results that follow for the steady state and the time evolution towards it.

4.3 Steady state results

Let us write the steady state temperature in the form

$$T_{ss}(y) = \overline{T} + \delta T\, \Theta(y), \tag{4.3.1}$$

where $\overline{T} = (T_L + T_R)/2$, $\delta T = T_L - T_R$ and the function $\theta(y)$ satisfies the boundary conditions, $\Theta(0) = 1/2, \Theta(1) = -1/2$. Then expanding $\Theta(y) = \sum_n \hat{\Theta}_n \phi_n(y)$, the stationarity condition $\mathbb{L}_{\bar{\kappa}}\Theta = 0$ along with Eq. (4.2.8) gives

$$\sum_n \lambda_n^{3/4} \hat{\Theta}_n \phi_n = 0. \tag{4.3.2}$$

Now we note the identities (see 4.8.3), which have to be understood in a distributional sense:

$$\sum_{n\ odd} \phi_n(y) = 0, \quad \sum_{n\ even} \phi_n(y) = -1/\sqrt{2}. \tag{4.3.3}$$

Using these and the boundary conditions $\Theta(0) = -\Theta(1) = \frac{1}{2}$ we finally get

$$\begin{aligned} \Theta(y) &= \sum_{n\ odd} \frac{c}{\lambda_m^{3/4}} \phi_m(y), \\ \text{with } c &= \frac{\pi^{3/2}}{[\sqrt{8}-1]\zeta(3/2)}, \end{aligned} \tag{4.3.4}$$

where $\zeta(s)$ is the Riemann-Zeta function. The temperature profile matches with the one presented in [4, 57, 94]:

$$T_{ss}(y) = \overline{T} + \delta T \frac{\pi^{3/2}}{[\sqrt{8}-1]\zeta(3/2)} \sum_{n\ odd} \frac{\phi_n(y)}{\lambda_n^{3/4}}. \tag{4.3.5}$$

A comparison of the above equation with the microscopic simulation of the system Eq. (4.2.1) in Fig. (4.1) shows a very good agreement. The systematic differences are due to finite size effects, as was already noted in [57]. We next consider the steady state current. First, we observe that the fractional Laplacian $\mathbb{L}_{\bar{\kappa}}$ can be expressed in the form of a divergence, namely in the form $\mathbb{L}_{\bar{\kappa}} = \bar{\kappa}\partial_y \mathbb{A}$

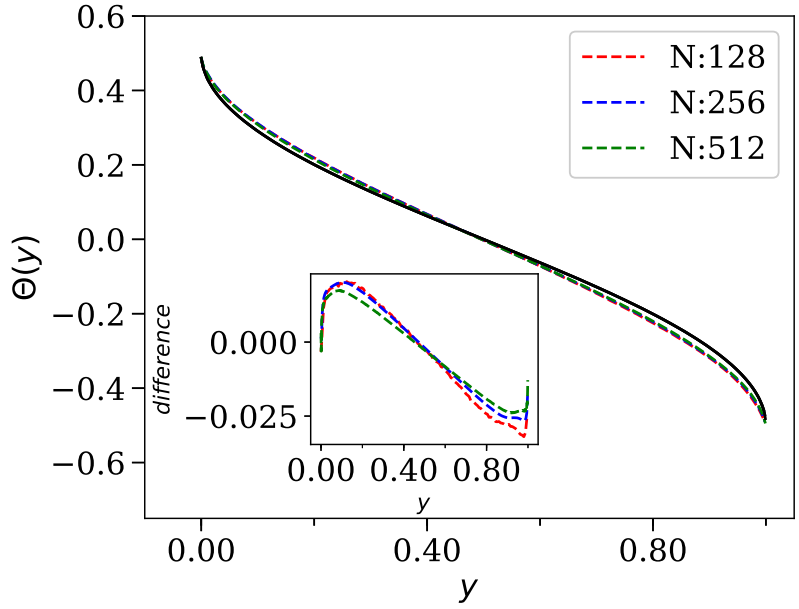

Figure 4.1: Temperature profile from Eq. (4.3.5)(solid black line) compared with direct numerical simulations of microscopic system for system sizes $N = 128, 256, 512$. In the inset the difference between Eq. (4.3.5) and numerical simulations is plotted for various system size.

where the operator $\mathbb{A}$ is defined through the following action on Neumann basis vectors

$$\mathbb{A}\phi_n(y) = \lambda_n^{1/4}\alpha_n(y)\,. \tag{4.3.6}$$

We then see that (4.2.9) is in the form of a continuity equation $\partial_\tau T(y,\tau) = -\partial_y j(y,\tau)$ with the non-local energy current defined as $j(y,\tau) = \bar{\kappa}\mathbb{A}T(y,\tau)$. Using this definition of the current and the steady state temperature profile in (4.3.5) we immediately get the steady state current as

$$\frac{j}{\delta T} = \frac{\bar{\kappa}\mathbb{A}T_{ss}(y)}{\delta T} = \frac{\bar{\kappa}c}{2\sqrt{2}}\,, \tag{4.3.7}$$

where we used the identity $\sum_{n\in\text{odd}} \alpha_n(y)/\lambda_n^{1/2} = 1/(2\sqrt{2})$ (4.8.3). Note that this gives us the scaled current while the actual current is given by $J = j/\sqrt{N}$, in agreement with results obtained in [57].

4.4 Time evolution of temperature profile

The fractional Laplacian equation (4.2.9) allow us to study the time evolution of the temperature profile, starting from given initial and boundary conditions, and the eventual approach to the

steady state at large times. Here we address the problem of describing the system's time evolution. As before, the temperature profile at any time τ in the form $T(y,\tau) = T_{ss}(y) + f(y,\tau)$, where again $f(y,\tau)$ satisfies Eq. (4.2.9) but with vanishing Dirichlet boundary conditions, $f(0,\tau) = f(1,\tau) = 0$. Let $\{\psi_n\}$ be the eigenvectors with corresponding eigenvalues $\mu_1 < \mu_2 < \mu_3 \ldots$ of $\mathbb{L}$, satisfying the equation

$$\mathbb{L}\psi_n(y) = \mu_n \psi_n(y) \tag{4.4.1}$$

and boundary conditions $\psi_n(0) = \psi_n(1) = 0$. It can be shown that the operator $\mathbb{L}$ has a non-degenerate and positive spectrum (see below). We can then immediately write the solution for $f(y,\tau)$ as

$$f(y,\tau) = \sum_{n=1} \hat{f}_n(0) e^{-\bar{\kappa}\mu_n \tau} \psi_n(y), \tag{4.4.2}$$
$$\text{where } \hat{f}_n(0) = \int_0^1 dy\, f(y,0)\psi_n(y),$$

are "fractional-Fourier coefficients" for the initial field $f(y,0)$. In the first section we outlined the procedure followed in [58] to find the Dirichlet eigenfunctions expanding the eigenfunctions ψ_n in the orthogonal basis of $\{\alpha_l\}_{l\geq 1}$ as $\psi_n(y) = \sum_{l\geq 1} \xi_{nl}\alpha_l(y)$. We show here that much simplification and better accuracy is achieved if one expands ψ_n directly in the Neumann basis $\{\phi_m\}_{m\geq 0}$.

$$\psi(y) = \sum_m \hat{\zeta}_m \phi_m(y). \tag{4.4.3}$$

From Eq. (4.4.1), and using the definition of $\mathbb{L}$ in Eq. (4.2.8), we have

$$\sum_{m\geq 0} (\mu - \lambda_m^{3/4}) \hat{\zeta}_m \phi_m(y) = 0. \tag{4.4.4}$$

There are two sets of solution for this equation. The first set is given by

$$\hat{\zeta}_0 = -\frac{b}{\sqrt{2}\mu},\ \hat{\zeta}_{2k} = \frac{b}{\lambda_{2k}^{3/4} - \mu},\ \ k \geq 1,\ \ \hat{\zeta}_{2k+1} = 0,\ \ k \geq 0\,, \tag{4.4.5}$$

where we have made use of the identity $\sum_{m=1}^{\infty}\phi_{2m}(x) = -1/\sqrt{2}$. The second solution set is given by

$$\hat{\zeta}_{2k+1} = \frac{b}{\lambda_{2k+1}^{3/4} - \mu}, \;\; k \geq 0, \;\; \hat{\zeta}_{2k} = 0, \;\; k \geq 0, \tag{4.4.6}$$

where we have used the identity $\sum_{m=0}^{\infty}\phi_{2m+1}(y) = 0$ (4.8.3). So far, b and μ are un-determined. We now use the Dirichlet boundary condition $\psi(0) = \hat{\zeta}_0 + \sqrt{2}\sum_{k\geq 1}\hat{\zeta}_{2k} + \sum_{k\geq 0}\hat{\zeta}_{2k+1} = 0$. From our first solution set Eq. (4.4.5) we then get the following equation satisfied by μ

$$\sum_{k\geq 1}\frac{1}{\lambda_{2k}^{3/4} - \mu} = \frac{1}{2\mu}\,. \tag{4.4.7}$$

Similarly, from the second solution set Eq. (4.4.6), we get

$$\sum_{k\geq 0}\frac{1}{\lambda_{2k+1}^{3/4} - \mu} = 0\,. \tag{4.4.8}$$

The solution of either of the above two equations gives us the required eigenvalue, while Eqs. (4.4.5)-(4.4.6) provide us with the corresponding eigenfunction, with the constant b fixed by normalization. We label the first set of solutions by $\mu_{2n+1}, \psi_{2n+1}, n \geq 0$ and the second set by μ_{2n}, ψ_{2n+2}, $n \geq 0$. From the structure of the eigenvalue equations it is clear that the roots are ordered set of numbers such that $\lambda_{2n}^{3/4} < \mu_{2n+1} < \lambda_{2n+2}^{3/4}$ and $\lambda_{2n-1}^{3/4} < \mu_{2n} < \lambda_{2n+1}^{3/4}$. Finally, introducing the notation, $\langle f|g\rangle = \int_0^1 dx' f(x')g(x')$, such that $\langle x|\psi_n\rangle = \int_0^1 dx\delta(x-x')\psi_n(x') = \psi_n(x)$, the eigenvectors can now be written explicitly as

$$|\,\psi_{2n+1}\,\rangle = D_{2n+1}\left(-\frac{1}{\sqrt{2}\mu_{2n+1}}|\,\phi_0\,\rangle + \sum_{m\geq 1}\frac{1}{\lambda_{2m}^{3/4} - \mu_{2n+1}}|\,\phi_{2m}\,\rangle\right), \tag{4.4.9}$$

$$|\,\psi_{2n+2}\,\rangle = D_{2n+2}\left(\sum_{m\geq 0}\frac{1}{\lambda_{2m+1}^{3/4} - \mu_{2n+2}}|\,\phi_{2m+1}\,\rangle\right), \tag{4.4.10}$$

where D_n, found from the normalizing condition $\langle\psi_n|\psi_n\rangle = 1$, is explicitly given as,

$$D_{2n+1} = \left[\frac{1}{2\mu_{2n+1}^2} + \sum_{m\geq 1}\frac{1}{(\lambda_{2m}^{3/4} - \mu_{2n+1})^2}\right]^{-1/2},$$
$$D_{2n+2} = \left[\sum_{m\geq 0}\frac{1}{(\lambda_{2m+1}^{3/4} - \mu_{2n+2})^2}\right]^{-1/2}. \tag{4.4.11}$$

Thus, as promised, we have managed to obtain a much efficient method for computing the Dirichlet spectrum of the fractional operator $\mathbb{L}$. The roots of the eigenvalue equations (4.4.7)-(4.4.8) are solved numerically using Newton-Raphson method scanning in between these intervals. This procedure gives a fast and efficient way to compute the eigenvector while avoiding diagonalizing infinite dimensional matrices. For large k, we have, $\mu_k \approx \lambda_k^{3/4}$.

This procedure can be generalized to a fractional operator defined through the equation

$$\mathbb{L}^{(\beta)}\phi_n(y) = \lambda_n^{\beta}\phi_n(y), \tag{4.4.12}$$

for arbitrary β. For diffusive case ($\beta = 1$) one can obtain exact results and recover the expected result $\mu_k^{(\beta=1)} = \pi^2 k^2$ and $\psi_k(y) = \alpha_k(y)$.

4.4.1 Properties of Dirichlet eigensystem of the fractional operator in bounded domain

The numerical values of the computed eigenvalues are plotted in Fig. (4.2) in log-log scale, where we find that for large n $\mu_n \approx (n\pi)^{3/2}$, while for smaller values n, there is a systematic deviation from the scaling due to the fact we are now working in a bounded domain. The first three eigenvalues (μ_n) are approximately $\mu_1 \approx 2.75, \mu_2 \approx 12.02, \mu_3 \approx 24.22$. The first eigenvalue we have $|\mu_1 - \pi^{3/2}|/\pi^{3/2} \approx 0.5046$ (see inset in Fig. (4.2)). This eigenvalue spectrum is expected to be identical to that in [58], upto a constant factor (see discussion in previous section). The first few numerically computed eigenvectors are shown in Fig. (4.3). The eigenvectors are similar to $\sin$ functions but have divergent derivatives near the left and right boundaries. In order to compare it with corresponding $\sin$ functions, we plot in Fig. (4.4) the overlap of integral between $\psi_n(y)$ and

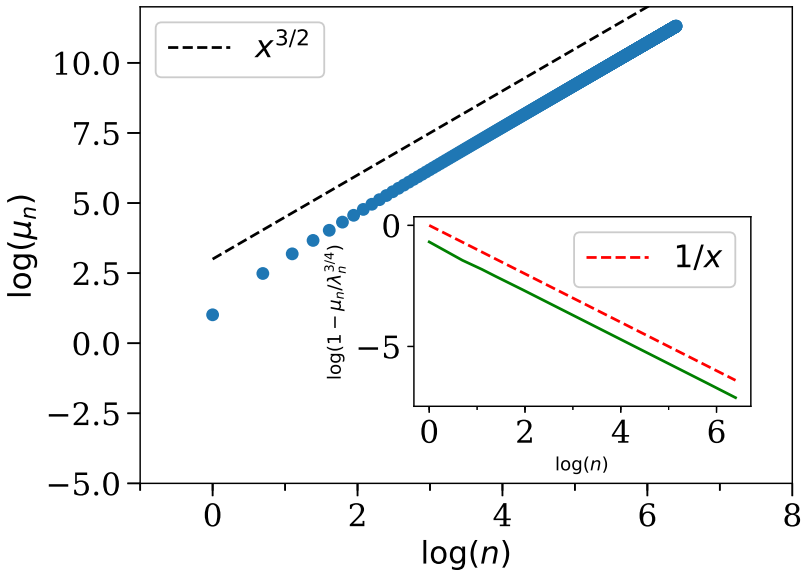

Figure 4.2: Eigenvalues computed from Eq. (4.4.7) and (4.4.8) plotted (blue dots) in log-log scale. Number of basis state used to approximate the function is 600. For large n, $\mu_n \sim (n\pi)^{3/2}$, i.e. the Dirichlet and Neumann eigenvalues are same. For small n there is a systematic difference between the two. A straight line of exponent $x^{3/2}$ (black dot) is plotted alongside. In the inset we plot, $\log(1 - \mu_n/\lambda_n^{3/4})$ vs $\log(n)$, which characterizes the difference between the Dirichlet and Neumann boundary eigenvalues. For large n the value of this function goes to zero with slope 1, suggesting he difference between the two decreases linearly with n. The red dashed line shows that it decays with an inverse power law of exponent 1.

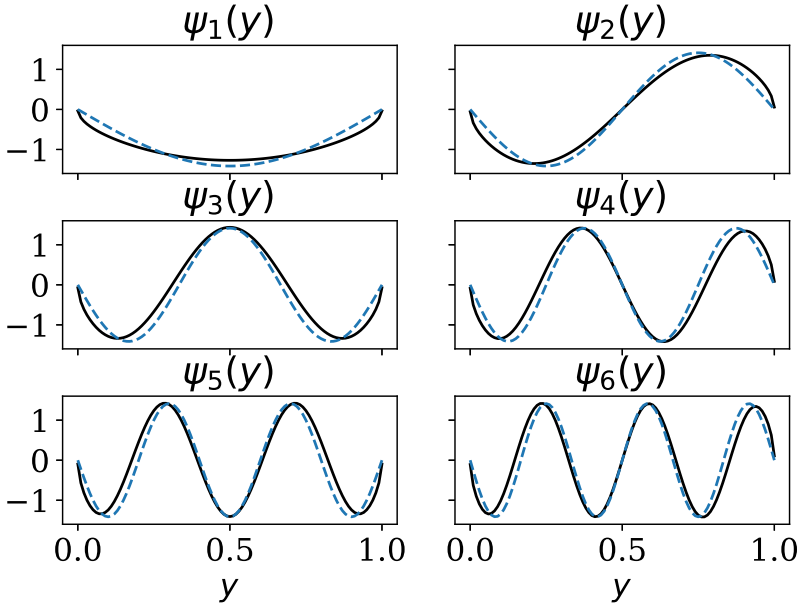

Figure 4.3: The first six eigenvectors of fractional operator, $\psi_n(y)$, (black) as compared to corresponding eigenfunctions of Laplacian i.e. $\sin$ functions (blue dotted). The eigenstates are different from corresponding $\sin$ functions near the boundaries even for large n. These eigenfunctions are computed by summing over 600 basis states.

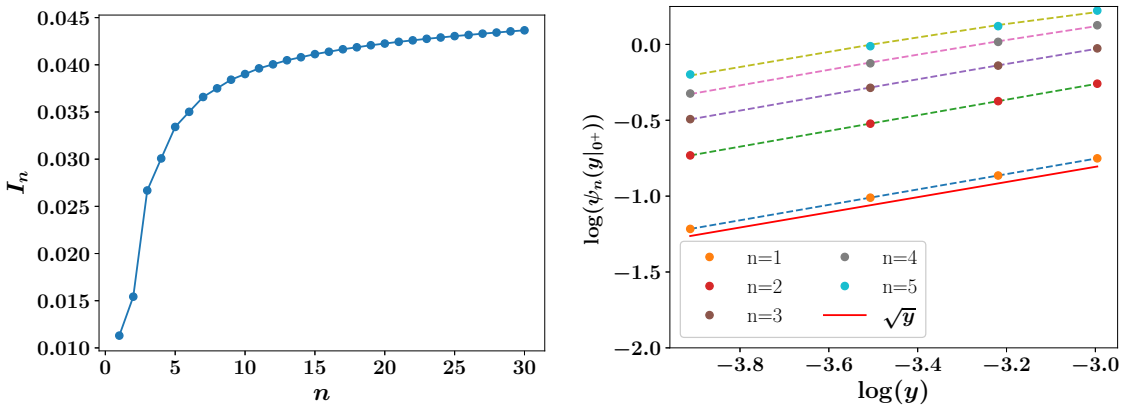

Figure 4.4: (a)(Left) To quantify the similarity between $\psi_n(y)$ and $\sqrt{2}\sin(n\pi y)$, we plot the overlap integral, $I_n = 1 - \int_0^1 \psi_n(y)\sqrt{2}\sin(n\pi y)\,dy$. For large n this seems to be saturating to a finite value, suggesting that the eigenfunctions ψ_n are quite different from $\sin$ functions. (b)(right) Scaling at boundaries of the eigenvectors in log-log scale shows that at the boundaries, the wave-function scales as $\sqrt{y}$.

$\sqrt{2}\sin(n\pi y)$ defined as $I_n = 1 - \int_0^1 \psi_n(y)\sqrt{2}\sin(n\pi y)\,dy$. This increases and saturates to a particular value, suggesting that the wave functions are quite different from $\sin$ functions even for large n. Also the eigenfunctions show a non-analytic behavior at the boundaries, for example near the left boundary one finds $\lim_{y\to 0^+}\psi_n(y) \sim \sqrt{y}$ (see Fig. 4.4b), in contrast to sin-functions for which $\lim_{y\to 0^+}\sin(n\pi y) \sim y$.

The eigenspectrum of fractional operator in bounded domain has been discussed earlier in the literature, using somewhat phenomenological approaches [92, 96, 97, 98]. It is not clear if those approaches can be related to that presented in this chapter.

4.4.2 Comparison of time evolution formula with numerical simulations of the HCME model

We now compare the prediction from Eq. (4.4.2), with $\bar{\kappa} = 1/(2\sqrt{2})$, with results from direct microscopic simulations, described by Eq. (4.2.1) with the additional stochastic exchange dynamics. Initially the system of size N is prepared in a step initial condition, given by

$$\begin{aligned} T_i &= T_L,\ 1 \le i < N/2, \\ &= T_R,\ N/2 \le i \le N+1. \end{aligned} \tag{4.4.13}$$

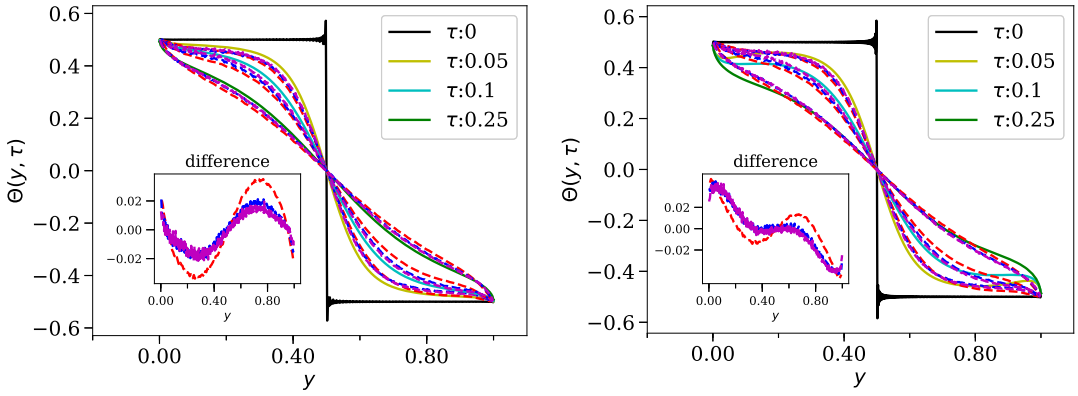

Figure 4.5: The time evolution of temperature starting from an initial step profile. The function $\Theta(y,\tau) = T(y,\tau) - \overline{T} = T_{ss}(y) + f(y,\tau) - \overline{T}$ is plotted and compared with numerical simulations. In the left figure, dashed lines indicate simulation results for the time-evolution, for system sizes $N = 128$ (red), $N = 256$ (blue), $N = 512$ (magenta). The solid lines at different scaled times (τ) are generated from Eq. (4.4.2) by summing over 600 basis states. (right) The same, but now with the theoretical curves computed using the $\sin$-functions instead of the ψ-functions, and eigenvalues $\lambda_n^{3/4}$ instead of μ_n. We notice that they do not match well with simulations, specially the deviations are prominent near the two boundary.

At large times it reaches a steady state described by Eq. (4.3.5). At various intermediate times, we plot the function $\Theta(y,\tau) = T(y,\tau) - \overline{T} = T_{ss}(y) + f(y,\tau) - \overline{T}$, such that $\Theta(0,\tau) = 1/2 = -\Theta(1,\tau)$. In Fig. (4.5) we show the temperature profile at intermediate times from microscopic simulation with scaled space ($y = i/N$) and times ($\tau = t/N^{3/2}$) for various system sizes. We note that with increasing system size, the data converges to the prediction from Eq. (4.4.2). The difference between the numerical profiles and the predicted theoretical profile is shown in the inset. As we increase the system size, this difference systematically decreases. We also demonstrate that using standard Dirichlet $\sin$-functions, instead of the ψ-functions, leads to significant differences, especially near the boundaries.

4.5 Adding noise satisfying fluctuation dissipation to describe equilibrium fluctuations in finite system

In [60], the harmonic chain with random momentum flips (HCMF model) was studied. In the HCMF, the stochastic dynamics flips the momentum of the particle and is embedded in the Hamiltonian dynamics such that the macroscopic dynamics is diffusive. It was shown that the equilibrium energy fluctuations $e(x,t) = E(x,t) - \langle E(x,t)\rangle$, where $E(x,t)$ is the local energy of the system at time t, satisfies the noisy diffusion equation $\partial_t e(x,t) = \partial_x^2 e(x,t) + \partial_x[DT(x,t)\eta(x,t)]$,

with η a space-time mean zero white noise. As a note of caution, from here onwards, we use a different notation than that of the previous sections with $\{x, y\} \in [0, 1]$, and t is, in general, referred to a scaled time. The aim of this section is to establish a fractional fluctuating equation for the HCME model, which has anomalous diffusion properties. Using this equation, we establish a Green-Kubo formula relating the equilibrium current fluctuations to the non-equilibrium current. Next, we discuss the long-range correlations and conjecture a form for the long-range correlations of energy and test it using simulations.

The generalized equation, which we hypothesize in equilibrium at temperature T is

$$\partial_t |\, e_t \,\rangle = -\mathbb{L}_{\bar{\kappa}} |\, e_t \,\rangle + \sqrt{2\bar{\kappa}} \nabla (BT |\, \eta_t \,\rangle), \tag{4.5.1}$$

where $\eta(x, t)$ is a white Gaussian noise with $\langle \eta(x) \rangle = 0$, $\langle \eta(x, t)\eta(y, t') \rangle = \delta(x - y)\delta(t - t')$ and $\mathbb{L}_{\bar{\kappa}}$ is the fractional Laplacian as defined in Eq. (4.2.9). The explicit form for the operator $BB^\dagger$ is established through the requirement that energy fluctuations must respect the fluctuation dissipation (FD) in equilibrium. We define the Green function satisfying

$$\partial_t G_t = -\mathbb{L}_{\bar{\kappa}} G_t, \; \langle x | G_0 | x' \rangle = G_0^{xx'} = \delta(x - x'), \tag{4.5.2}$$

with Dirichlet boundary conditions in $x \in [0, 1]$. This can then be easily expressed in terms of the basis states $\{\psi_n\}_{n\geq 1}$ as $G_t^{xx'} = \sum_{n=1} \psi_n(x)\psi_n(x')e^{-\bar{\kappa}\mu_n t}$. The long-time solution to Eq. (4.5.1) is then given by

$$\begin{aligned} e(x, t) =& \sqrt{2\bar{\kappa}} \int_{-\infty}^{t} ds \langle \; x \mid G_{t-s} \mid \nabla (BT\eta_s) \; \rangle, \\ =& -\sqrt{2\bar{\kappa}} \int_{-\infty}^{t} ds \langle \; x \mid \nabla G_{t-s} \mid (BT\eta_s) \; \rangle. \end{aligned} \tag{4.5.3}$$

The equal time correlation function in equilibrium defined as $C_{\text{eq}}(x, y) = \langle e(x, t)e(y, t) \rangle$ then is

given as

$$\begin{aligned} C_{\rm eq}(x,y) =& 2\kappa \int_{-\infty}^{t} ds \int_{-\infty}^{t} ds' \langle\langle\ x \mid \nabla G_{t-s} \mid BT\eta_s \ \rangle\langle\ \eta_{s'} T B^\dagger \mid \nabla G_{t-s'} \mid\ y\ \rangle\rangle, \\ =& \ 2\bar{\kappa} T^2 \int_{-\infty}^{t} ds \ \langle\ x \mid \nabla G_{t-s} B B^\dagger \nabla G_{t-s} \mid\ y\ \rangle, \\ =& -2\bar{\kappa} T^2 \int_{-\infty}^{t} ds \langle\ x \mid G_{t-s} \nabla B B^\dagger \nabla G_{t-s} \mid\ y\ \rangle, \end{aligned} \tag{4.5.4}$$

where the statistical average is used and we integrate out the space time white noise to give, $\langle\langle x'|B\eta_s\rangle\langle\eta_{s'}B^\dagger|y'\rangle\rangle = \langle B\eta(s)B\eta(s')\rangle = \delta(s-s')BB^\dagger(x',y')$ followed by an integration by parts. Here, the big angles, $\langle \ldots \rangle$ denote average over space-time white noise profiles whereas $\langle ..|$ and $|..\rangle$ denote the bra-ket notation, *e.g.* $\langle x|e\rangle = e(x,t)$. If we identify $-\bar{\kappa}\nabla BB^\dagger\nabla = \mathbb{L}_{\bar{\kappa}}$, and using Eq. (4.5.2) we recover FD relation in equilibrium

$$\begin{aligned} C_{\rm eq}(x,y) =& T^2 \int_{-\infty}^{t} ds \ \left(\langle\ x \mid G_{t-s}\mathbb{L}_{\bar{\kappa}} G_{t-s} \mid\ y\ \rangle + \langle\ y \mid G_{t-s}\mathbb{L}_{\bar{\kappa}} G_{t-s} \mid\ x\ \rangle\right), \\ =& T^2 \int_{-\infty}^{t} ds\ \partial_s \langle\ x \mid G_{t-s} G_{t-s} \mid\ y\ \rangle = \ T^2 \delta(x-y), \end{aligned} \tag{4.5.5}$$

where we used the fact that changing $x \leftrightarrow y$ would not change the correlation function due to time reversal symmetry of the microscopic dynamics. The operator $BB^\dagger$ can consistently be defined on a function $g(x)$, expanded in $\{\alpha_n\}_{n\geq 1}$ basis, as $g(x) = \sum_n \hat{g}_n \alpha_n(x)$. Again, using the definition of $\mathbb{L}_{\bar{\kappa}} = -\bar{\kappa}\nabla BB^\dagger\nabla$ in Eq. (4.2.8), we define the symmetric operator $BB^\dagger$ as,

$$\int_0^1 dx' BB^\dagger(x,x') g(x') = \sum_{n=1}^{\infty} \frac{1}{(\lambda_n)^{1/4}} \hat{g}_n \alpha_n(x). \tag{4.5.6}$$

Note that we do not assume anything about the form of the operator B, which would be important if we were to study non-equilibrium phenomena where temperature is not constant in space.

The connection between the $\mathbb{L}$ operator with the $BB^\dagger$ allows one to identify the current (through continuity equation) as

$$j(x,t) = -\bar{\kappa} \int_0^1 dx' \ BB^\dagger(x,x') \partial_{x'} e(x',t). \tag{4.5.7}$$

Note that the above equation is a linear response relation, but in contrast to the diffusive case, this relation is non-local. Such non-local linear response relation have recently been reported in [94], where an alternate series representation of the kernel $BB^\dagger(x,x')$ has been provided for HCME model with general boundary conditions. In 4.8.4, we show that the spectral representation in Eq. (4.5.6) is completely consistent with the series representation in [94] for fixed boundary condition.

4.5.1 Spatio-temporal equilibrium energy correlations

We compute the two time spatio-temporal energy correlations in equilibrium defined as $C_{\rm eq}(x,t,y,t') = \langle e(x,t)e(y,t')\rangle$ and show that at large times it is given in terms of the Green functions. The two time correlations can be analogously written down as,

$$C_{\rm eq}(x,t,y,t') = 2\bar{\kappa}\int_{-\infty}^{t} ds \int_{-\infty}^{t'} ds' \langle\langle\ x\ |\ \nabla G_{t-s}\ |\ BT\eta_s\ \rangle\langle\ \eta_{s'} TB^\dagger\ |\ \nabla G_{t'-s'}\ |\ y\ \rangle\rangle, \quad (4.5.8)$$

Taking $t > t'$, and performing the t integral we have,

$$C_{\rm eq}(x,t,y,t') = -2\bar{\kappa}T^2\int_{-\infty}^{t'} ds\ \langle\ x\ |\ G_{t-s}\nabla BB^\dagger\nabla G_{t'-s}\ |\ y\ \rangle\theta(t-t'),$$

where $\theta(t)$ is the Heaviside theta function. Proceeding as before and identifying $-\bar{\kappa}\nabla BB^\dagger\nabla = \mathbb{L}_{\bar{\kappa}}$ and interchanging x, y

$$\begin{aligned} C_{\rm eq}(x,t,y,t') &= T^2\int_{-\infty}^{t'} ds\ (\langle\ x\ |\ G_{t-s}\mathbb{L}_{\bar{\kappa}}G_{t'-s}\ |\ y\ \rangle + \langle\ y\ |\ G_{t-s}\mathbb{L}_{\bar{\kappa}}G_{t'-s}\ |\ x\ \rangle)\,, \\ &= T^2\int_{-\infty}^{t'} ds\partial_s\langle\ x\ |\ G_{t-s}G_{t'-s}\ |\ y\ \rangle = T^2 G^{xy}_{t-t'}\theta(t-t'). \end{aligned} \quad (4.5.9)$$

Along with a similar term for $t < t'$, we can write the two time correlations as,

$$C_{\rm eq}(x,t,y,t') = \langle\ x\ |T^2 G_{t-t'}\theta(t-t') + T^2 G_{t'-t}\theta(t'-t)|\ y\ \rangle. \quad (4.5.10)$$

4.5.2 Current fluctuations in equilibrium

Here we define the fluctuating current in the system and then establish Green-Kubo relation for the system connecting the equilibrium current fluctuations and non-equilibrium current in the system. We expect that since the total energy in the isolated system is conserved, the energy flow across the system must be in continuity form $\partial_t e(x,t) + \partial_x j(x,t) = 0$. Along with the definition of current in Eq. (4.3.6), the fluctuating current operator is defined as,

$$| \, j_t \, \rangle = \bar{\kappa}\mathbb{A}| \, e_t \, \rangle - \sqrt{2\bar{\kappa}}| \, BT\eta_t \, \rangle. \tag{4.5.11}$$

From previous section, it follows that the definition of current operator as $\mathbb{A} = -BB^\dagger\nabla$. We also note that since the current operator is odd in derivatives, the adjoint current operator has the property, $\mathbb{A}^\dagger = -\mathbb{A}$. Now we expect that [99] the second moment of equilibrium total current fluctuations is related to the current in NESS through the Green-Kubo formula. A precise statement is:

$$\lim_{\tau\to\infty} \frac{\langle q^2\rangle_{\delta T=0}}{2\tau T^2} = \lim_{\delta T\to 0} \frac{j}{\delta T}, \tag{4.5.12}$$

where $q(\tau) = \int_0^\tau dt \int_0^1 dx j(x,t)$. In order to verify this relation, we first express $\langle q^2\rangle$, in terms of the integrals of the unequal time current correlations:

$$\frac{\langle q^2\rangle_{\delta T=0}}{\tau} = \frac{1}{\tau}\int_0^\tau dt \int_0^\tau dt' \int_0^1 dx \int_0^1 dy \langle j(x,t)j(y,t')\rangle. \tag{4.5.13}$$

Using Eq. (4.5.11) the current correlations can be split into four parts:

$$\begin{aligned}\langle j(x,t)j(y,t')\rangle =& \underbrace{\bar{\kappa}^2\langle\langle \, x \, |\mathbb{A}| \, e_t \, \rangle\langle \, e_{t'} \, |\mathbb{A}^\dagger| \, y \, \rangle\rangle}_{\text{I}} + \underbrace{2\bar{\kappa}T^2\langle \, x \mid BB^\dagger \mid y \, \rangle}_{\text{II}}\delta(t-t') \\ &- \underbrace{\sqrt{2}\bar{\kappa}^{3/2}\langle\langle \, x \mid \mathbb{A} \mid e_t \, \rangle\langle \eta_{t'}TB^\dagger|y\rangle\rangle}_{\text{III}} - \underbrace{\sqrt{2}\bar{\kappa}^{3/2}\langle\langle x|BT\eta_t\rangle\langle \, e_{t'} \mid \mathbb{A}^\dagger \mid y \, \rangle\rangle}_{\text{IV}}.\end{aligned} \tag{4.5.14}$$

Part III in the above equation can be simplified to

$$\begin{aligned}\sqrt{2}\bar{\kappa}^{3/2}\langle\langle\ x\mid\mathbb{A}\mid e_t\ \rangle\langle\eta_{t'}TB^\dagger|y\rangle\rangle &= 2\bar{\kappa}^2\int_{-\infty}^{t}ds\langle\langle\ x\mid\mathbb{A}G_{t-s}\mid\nabla(BT\eta_s)\ \rangle\langle\eta_{t'}TB^\dagger|y\rangle\rangle,\\ &= -\ T^2 2\bar{\kappa}^2\langle\ x\mid(\mathbb{A}\nabla G_{t-t'})BB^\dagger\mid y\ \rangle\theta(t-t'),\\ &= T^2 2\bar{\kappa}^2\langle\ x\mid\mathbb{A}G_{t-t'}\mathbb{A}^\dagger\mid y\ \rangle\theta(t-t'). \end{aligned}\tag{4.5.15}$$

Similarly part IV is given by

$$\begin{aligned}\sqrt{2}\bar{\kappa}^{3/2}\langle\langle x|BT\eta_t\rangle\langle\ e_{t'}\mid\mathbb{A}^\dagger\mid y\ \rangle\rangle &= 2\bar{\kappa}^2T^2\int_{-\infty}^{t'}ds\langle\langle x|B\eta_t\rangle\langle\ \eta_s(\nabla B)^\dagger\mid G_{t'-s}\mathbb{A}^\dagger\mid y\ \rangle\rangle,\\ &= -\ T^2 2\bar{\kappa}^2\langle\ x\mid BB^\dagger\nabla G_{t'-t}\mathbb{A}^\dagger\mid y\ \rangle\theta(t'-t),\\ &= T^2 2\bar{\kappa}^2\langle\ x\mid\mathbb{A}G_{t'-t}\mathbb{A}^\dagger\mid y\ \rangle\theta(t'-t),\end{aligned}$$

while part I, on using (4.5.10), gives

$$\bar{\kappa}^2\langle\langle\ x\ |\mathbb{A}|\ e_t\ \rangle\langle\ e_{t'}\ |\mathbb{A}^\dagger|\ y\ \rangle\rangle = T^2\bar{\kappa}^2\left[\langle\ x\ |\mathbb{A}G_{t-t'}\mathbb{A}^\dagger\theta(t-t')+\mathbb{A}G_{t'-t}\mathbb{A}^\dagger\theta(t'-t)|\ y\ \rangle\right].\tag{4.5.16}$$

We see that III + IV = 2I. The first term explicitly gives,

$$\begin{aligned}\mathrm{I} =&\bar{\kappa}^2\int_0^1dx'\int_0^1dy'\mathbb{A}(x,x')\langle e_t(x')e_{t'}(y')\rangle\mathbb{A}^\dagger(y',y),\\ =&\bar{\kappa}^2T^2\int_0^1dx'\int_0^1dy'\mathbb{A}(x,x')\mathbb{A}(y,y')G_{|t-t'|}(x',y'),\\ =&\bar{\kappa}^2T^2\sum_{n,l,l'}\hat{\zeta}_{nl}\hat{\zeta}_{nl'}(\lambda_l\lambda_{l'})^{1/4}e^{-\bar{\kappa}\mu_n|t-t'|}\alpha_l(x)\alpha_{l'}(y).\end{aligned}\tag{4.5.17}$$

Therefore, the contribution of the parts I − III − IV = −I in (4.5.13) gives, after doing the space and time integrals:

$$\int_0^\tau dt'\int_0^\tau dt\int_0^1dx\int_0^1dy\,(-\mathrm{I}) = -16\bar{\kappa}^2T^2\sum_n\sum_{ll'\ odd}\frac{1}{\bar{\kappa}\mu_n}\left[\tau+\frac{(e^{-\mu_n\tau}-1)}{\mu_n}\right]\hat{\zeta}_{nl}\hat{\zeta}_{nl'}(\lambda_l\lambda_{l'})^{-1/4}.\tag{4.5.18}$$

On using (4.5.6), the contribution of part II in (4.5.13) gives

$$\begin{aligned}\int_0^\tau dt' \int_0^\tau dt \int_0^1 dx \int_0^1 dy(\mathrm{II}) =& 2\bar{\kappa}T^2 \int_0^\tau dt' \int_0^\tau dt \int_0^1 dx \int_0^1 dy BB^\dagger(x,y)\delta(t-t'),\\ =& 2\bar{\kappa}T^2\tau \int_0^1 dx \int_0^1 dy \sum_n \frac{\alpha_n(x)\alpha_n(y)}{\lambda_n^{1/4}},\\ =& 16\bar{\kappa}T^2\tau \sum_{n\ odd} \frac{1}{\lambda_n^{5/4}}. \end{aligned} \tag{4.5.19}$$

Combining the above results we finally have

$$\lim_{\tau\to\infty} \frac{\langle q^2\rangle_{\delta T=0}}{2\tau T^2} = \bar{\kappa}\left(8\sum_{n\ odd}\frac{1}{\lambda_n^{5/4}} - \sum_n \sum_{ll'\ odd} \frac{8}{\mu_n}\frac{\hat{\zeta}_{nl}\hat{\zeta}_{nl'}}{(\lambda_l\lambda_{l'})^{1/4}}\right). \tag{4.5.20}$$

The first summation yields $0.5050\ldots$ and the second yields ≈ 0.0931, hence we get

$$\lim_{\tau\to\infty} \frac{\langle q^2\rangle_{\delta T=0}}{2T^2\tau} \approx 0.4119\bar{\kappa}, \tag{4.5.21}$$

which, up to numerical accuracy is consistent with the numerical value of steady state current ($j/\delta T = 0.4124\bar{\kappa}$) we found in (4.3.7), thus validating the Green-Kubo formula in (4.5.12).

Note that in order to get the expected scaling in system size N, we need to put in the appropriate length scaling of the eigenvalues and eigenfunctions, for example $\lambda_n \to \lambda_n/N^2$ and $\mu_n \to \mu_n/N^{3/2}$). We also need to consider the integrated current $Q(\tau) = \int_0^\tau dt \int_0^N dx j(x,t)$ and then one gets $\lim_{\tau\to\infty} \frac{\langle Q^2\rangle_{\delta T=0}}{2T^2\tau} \approx \frac{0.4119\bar{\kappa}}{\sqrt{N}}$ and $\frac{J}{\delta T} = \frac{j}{\sqrt{N}\delta T} \approx \frac{0.4124\bar{\kappa}}{\sqrt{N}}$.

The above verification of the Green-Kubo identity was obtained using the fluctuating fractional diffusion equation, which is valid in the limit of large system size. A natural question is as to whether the identity is true even for a small chain with the microscopic dynamics (HCME), as would be expected from the fluctuation theorem. In Fig. (4.6), we present a numerical comparison of the equilibrium current fluctuations, with the non-equilibrium current, both computed from the microscopic model for finite systems. We see clear evidence that for small N, the Green-Kubo relation is violated in the HCME model. We also find that the difference between the fluctuation and response parts decreases with system size as $\sim 1/N$. Somewhat surprisingly, the numerically obtained fluctuations (from HCME simulations) are very close to the response computed from the

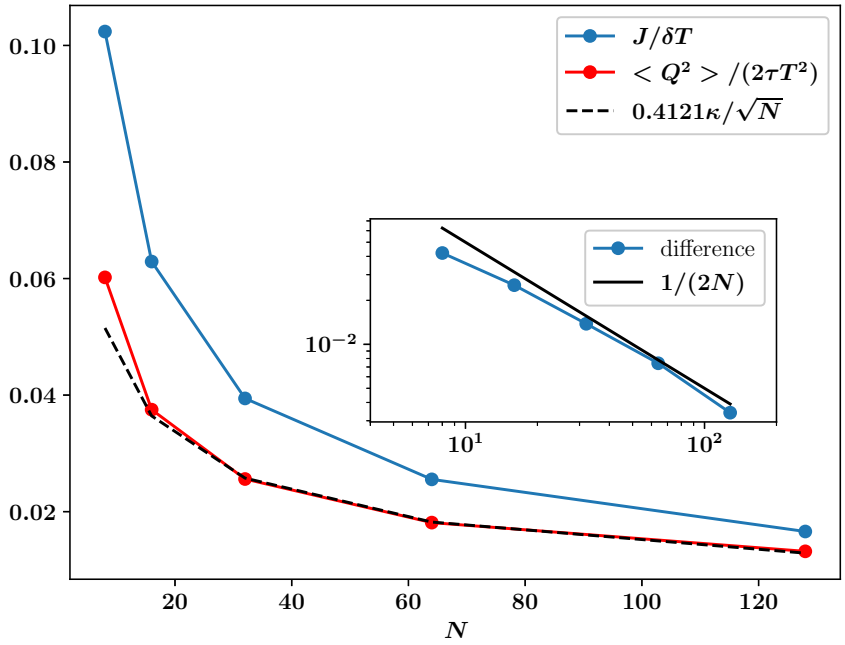

Figure 4.6: For the microscopic HCME model, we compute the two quantities, $J/\delta T$ computed from non-equilibrium simulations connected to heat baths and $< Q^2 > /(2\tau T^2)$ computed from equilibrium simulations, are plotted as a function of N. The black dashed curve is for the theoretical current with appropriate scaling as given in Eq. (4.3.7). We find that for small N, these two do not match, and the difference between the two decays as $1/N$ (inset), which is due to the contribution of current from the stochastic part. This signifies that at large N, Green-Kubo holds while for small N, it fails.

fractional diffusion equation description. A possible reason for the failure of the fluctuation theorem for small systems could be that in this model, the Hamiltonian part of the current (which goes as $1/\sqrt{N}$), and the stochastic part of the current ($\sim 1/N$) have different time-reversal symmetries.

General fractional power

In this section, we discuss a possible generalization of the results of the previous section for the Green-Kubo identity to the case of arbitrary fractional power β of the Laplacian. There is currently no known microscopic model in which heat transfer can be described by a fractional equation with arbitrary β — nevertheless it is an interesting exercise as it leads to some general mathematical identities involving Riemann-zeta functions. Using the definition of fractional Laplacian in Eq. 4.4.12, namely through the operation $\mathbb{L}^{(\beta)}\phi_n(x) = \lambda_n^\beta \phi_n(x)$, we can proceed in a similar way as for the $\beta = 3/4$ case and compute steady state properties in NESS as well as equilibrium current fluctuations.

Corresponding to Eq. (4.3.7) we then get

$$\frac{j}{\delta T} = \frac{1}{8\left(2^{2\beta}-1\right)(2\pi)^{-2\beta}\zeta(2\beta)}, \tag{4.5.22}$$

and corresponding to Eq. (4.5.20) we get

$$\lim_{\tau\to\infty}\frac{\langle q^2\rangle_{\delta T=0}}{2\tau T^2} = 8\left(1-2^{2\beta-4}\right)\pi^{2\beta-4}\zeta(4-2\beta) - \sum_{n\ even}\sum_{ll'\ odd}\frac{8}{\mu_n^{(\beta)}}\frac{\hat{\zeta}_{nl}^{(\beta)}\hat{\zeta}_{nl'}^{(\beta)}}{(\lambda_l\lambda_{l'})^{1-\beta}}, \tag{4.5.23}$$

where due to structure of $\hat{\zeta}_{n,l}^{(\beta)}$, only the terms with even n survives for odd l. This is computed as before but now with power β and is explicitly given as

$$\hat{\zeta}_{2k+2,2m+1}^{(\beta)} = \frac{D_{2k+2}^{(\beta)}}{\lambda_{2m+1}^{\beta}-\mu_{2k+2}^{(\beta)}}, \quad k,m\geq 0\,, \tag{4.5.24}$$

$$\text{where } D_{2k+2}^{(\beta)} = \left[\sum_{m\geq 0}\frac{1}{(\lambda_{2m+1}^{\beta}-\mu_{2k+2}^{(\beta)})^2}\right]^{-1/2}, \tag{4.5.25}$$

and $\{\mu_{2n}^{(\beta)}\}_{n\geq 1}$ are the ordered roots of the equation

$$\sum_{k\geq 0}\frac{1}{\lambda_{2k+1}^{\beta}-\mu^{(\beta)}} = 0\,. \tag{4.5.26}$$

All the coefficients in the above expressions are explicit and we have evaluated numerically the right hand sides of Eqs. (4.5.22, 4.5.23) for values of $\beta\in(0.5,1.5)$. In Fig. (4.7), we plot these quantities and find that they are very close to each other, hence verifying the Green-Kubo formula Eq. (4.5.12) for general β. The differences arise from numerical error due to truncation of series and also use of a finite number of basis functions. For $\beta = 1$, this leads to diffusive results for which the double summation can be computed explicitly. Conversely, on the basis of the validity of the Green-Kubo formula we are then led to conjecture a mathematical identity between the right hand sides of Eqs. (4.5.22, 4.5.23). For $\beta < 1/2$, one has a non-convergent series summation in Eq. (4.5.23), which leads to a breakdown of the identity in this form. This corresponds to defining zeta function for power less than 1, and possibly analytic continuation could extend the definition to other values of β. We believe that the relation holds true at least in the open interval $\beta\in(1/2,3/2)$. However,

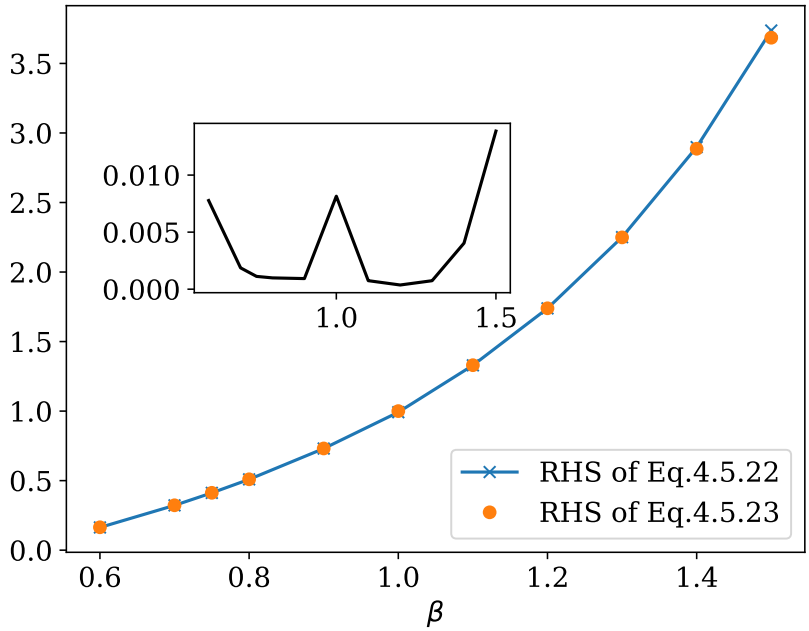

Figure 4.7: The numerically evaluated expressions in Eq. (4.5.22) and Eq. (4.5.23) are plotted as a function of general fractional power β. The two quantities match numerically to a very good precision. The relative error between the two is plotted in the inset.

proving it remains an open problem.

4.6 Long range correlations in NESS

For a noneqlibrium current carrying steady state, it is expected that fluctuations across the system will develop non-zero long-range correlations. These long-range correlations is a distinguishing feature of non-equilibrium systems with conservative dynamics [100]. In some diffusive lattice gas as well as some Hamiltonian systems, these long-range correlations have been studied [101, 102, 103, 104, 60]. The energy correlation in the velocity flip model (HCMF) in NESS is defined as $C_{NESS}(x,y) = \langle e(x,t)e(y,t)\rangle$, where the average is taken in NESS (as $t \to \infty$). It was shown that $C_{NESS}(x,y) = \delta T^2 \Delta^{-1}(x,y)$, where Δ is the Laplacian operator with Dirichlet boundary conditions. From the definition of fluctuating fractional equation in equilibrium, it is tempting to extend the definition of fluctuating fractional equation to non-equilibrium case, where the temperature is space-dependent:

$$\partial_t |\, e_t \,\rangle = -\mathbb{L}_{\bar{\kappa}} |\, e_t \,\rangle + \sqrt{2\bar{\kappa}} \nabla (B T_{NESS} |\, \eta_t \,\rangle), \tag{4.6.1}$$

We note that there is an ambiguity regarding the relative position of the operator B and T_{NESS}, and also with the definition for operator B and $B^\dagger$ separately. If we anyway proceed with a naive replacement of T by $T_{NESS}(x)$ in Eq. (4.5.1), to get (4.6.1), we can perform the computation of $C_{NESS}(x,y)$ and find that this does not agree with the results from direct simulations. However, in analogy to the HCMF model, we conjecture that the NESS energy correlations $C_{NESS}(x,y)$ are given (upto a constant factor ν) by the inverse of the fractional Laplacian (in Dirichlet basis):

$$\delta T^2 \mathbb{C}(x,y) = \frac{\delta T^2}{\nu}\mathbb{L}^{-1} = \frac{\delta T^2}{\nu}\sum_{n\geq 1}\frac{\psi_n(x)\psi_n(y)}{\mu_n}, \tag{4.6.2}$$

where we have defined $\delta T^2 \mathbb{C}(x,y) = C_{NESS}(x,y) - T_{NESS}(x)^2\delta(x-y)$, with the local same-site correlation $T_{NESS}(x)^2\delta(x-y)$ subtracted from correlations.

Numerical verification of Eq. (4.8): We simulate the microscopic system in non-equilibrium with two Langevian heat baths kept at different temperature. After the system is in the steady state, we compute $\mathbb{C}(x,y) = N\langle e(i/N)e(j/N)\rangle$ where $e(i/N) = E(i/N) - \langle E(i/N)\rangle$. In Fig. (4.8) we compare our conjectured form from Eq. (4.6.2) with the results from microscopic simulations. We see that with the constant $\nu \approx 3.77$, the two numerical curves (for $y = 1/4$ and $y = 1/2$) match well with the inverse of fractional Laplacian. The constant ν is related to the total energy fluctuations in the system at NESS as

$$\int_0^1 dx \int_0^1 dy \frac{\delta T^2}{\nu}\mathbb{L}^{-1}(x,y) + \int_0^1 dx T_{NESS}^2(x) = \int_0^1 dx \int_0^1 dy\, C_{NESS}(x,y) = \langle \Delta E_{tot}^2\rangle_{NESS}.$$

By evaluating the integrals on the LHS and finding the RHS from numerical simulations in the NESS, we can use the above equation to independently evaluate ν. We find that the fluctuations $\langle \Delta E_{tot}^2\rangle_{NESS}$, obtained from simulations in NESS, converges very slowly and with the final accessed simulation time (2×10^9 time with 10^8 samples) we estimate $3.51 \leq \nu \leq 4.2$. The value $\nu \approx 3.77$, obtained by fitting the long range correlations data from simulation, is well within the limits of the above estimate. We have tested (see 4.8.6) that the constant ν does not change substantially with δT and $\bar{T}$, within the numerical accuracy and finite size effects. We note in 4.8.6, that if we did the same computation with $\sin(n\pi x)$ basis, then the results would differ significantly. We close this section by making a comment that proving our conjecture on the equality between the

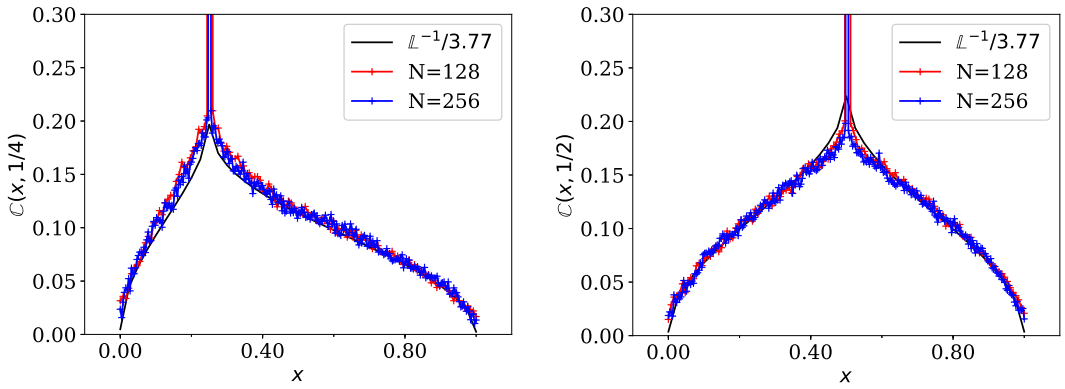

Figure 4.8: Non-equilibrium energy correlation function $\mathbb{C}(x, y)$ in steady state of Harmonic chain momentum exchange model for $y = 1/4$ (left figure) and $y = 1/2$ (right figure). The system size considered here are for $N = 128, 256$ with $T_L = 2, T_R = 1$. The inverse of the fractional Laplacian (summed up to 600 basis states) and with an arbitrary constant factor ($\nu = 3.77$), is plotted (black solid) along with the simulation results.

long-range correlations and the inverse fractional operator is an open question.

4.7 Conclusions

We have shown that in a particular analytically tractable model of heat conduction in one dimension, the macroscopic evolution of energy in an open system is governed by the fractional diffusion equation. This gives us a definition of the fractional operator in a finite domain and also gives a meaning to the fractional operator in terms of linear PDE's (similar to the harmonic extension of a fractional operator [105, 106]). We describe an efficient procedure to numerically construct the eigenspectrum of this operator. In terms of this operator, we compute the steady state and time evolution of temperature field, which we compare with microscopic simulations of the system. We defined the fluctuating fractional equation and used it to verify the Green-Kubo relation in the system. We also generalize the Green-Kubo for general fractional power which leads to some general mathematical identity involving zeta functions. This identity is verified numerically. We also conjecture that the long-range correlations are given by the inverse of a fractional operator. Another very interesting aspect is to study the usefulness of the eigensystem of the fractional operators in studying other applications where the underlying dynamics can be modeled as Levy flights or Levy walks.

4.8 Appendix

4.8.1 Connection coefficients between sine and cosine

We can expand sin in the complete basis of cos as, $\alpha_n(y) = \sum_l \mathcal{T}_{nl}\phi_l(y)$, with explicit coefficients $\mathcal{T}_{nl} = \int_0^1 dy \alpha_n(y)\phi_l(y)$. The coefficients are given as,

$$\mathcal{T}_{nl} = \begin{cases} 0 \text{ if l=o, n is even,} \\ \frac{2\sqrt{2}}{\pi n} \text{ if l=o, n is odd,} \\ \frac{2}{\pi}\left[\frac{\delta_{(n+l),\text{odd}}}{n+l} + \frac{\delta_{(n-l),\text{odd}}}{n-l}\right], \text{ if } l > 0. \end{cases} \tag{4.8.1}$$

4.8.2 Derivation of matrix equations of Fractional operator

Here we enumerate the steps involved in going from the set of PDE's to the matrix representation of $\mathbb{L}$ as stated in the main text. The correlation and temperature fields are expanded as, $C(x,y,\tau) - C_{ss}(x,y) = \sum_{n=1}^{\infty} \hat{C}_n(x,\tau)\alpha_n(y)$ and $T(y,\tau) - T_{ss}(y) = f(y,\tau) = \sum_{n=1}^{\infty} \hat{f}_n(\tau)\alpha_n(y)$. Following [58], the first of the equations in (4.2.2) implies $\partial_x^4 \hat{C}_n(x) = -4\delta_n^4 \hat{C}_n(x)$, where $\delta_n = \sqrt{n\pi\omega/(2\gamma)}$. Solving these equations with the appropriate boundary conditions one eventually gets,

$$\hat{C}_n(x,\tau) = \hat{A}_n(\tau)e^{-\delta_n x}\left[\sin(\delta_n x) - \cos(\delta_n x)\right]. \tag{4.8.2}$$

using the PDE's one gets

$$\begin{aligned}
\hat{A}_n(\tau) &= -\frac{1}{4\gamma\delta_n}\sum_{k=1}\mathcal{T}^{\dagger}_{kn}\sqrt{\lambda_k}f_k \\
\dot{\hat{f}}_m &= \omega^2\sum_{n=1}\mathcal{T}_{mn}\sqrt{\lambda_n}\hat{A}_n(\tau) \\
&= -\frac{\omega^2}{4\gamma}\sum_{n,k=1}\mathcal{T}_{mn}\sqrt{\lambda_n}\frac{1}{\delta_n}\mathcal{T}^{\dagger}_{kn}\sqrt{\lambda_k}f_k \\
&= -\frac{\omega^2}{4\gamma}\sum_{n,k=1}\mathcal{T}_{mn}\frac{\lambda_n}{\delta_n}\mathcal{T}^{\dagger}_{nk}f_k \\
&= -\bar{\kappa}\left[\mathcal{T}\Lambda^{3/4}\mathcal{T}^{\dagger}\right]_{mk}f_k
\end{aligned} \tag{4.8.3}$$

where we used the property of transformation element, $\mathcal{T}^{\dagger}_{kn}\sqrt{\lambda_k} = \mathcal{T}_{kn}\sqrt{\lambda_n}$. with $\mathcal{T}_{nl} = \langle\alpha_n|\phi_l\rangle = \int_0^1 dy\alpha_n(y)\phi_l(y)$ and the constant $\bar{\kappa}$.

4.8.3 Formal identities

Consider the two Fourier cosine series on $[0,1]$,

$$\begin{aligned}
q &= \frac{1}{2} + \sum_{m\ odd}\frac{-2\sqrt{2}}{\pi^2m^2}\sqrt{2}\cos(\pi mq), \\
q^2 - q &= -\frac{1}{6} + \sum_{m\in even}\frac{2\sqrt{2}}{\pi^2m^2}\sqrt{2}\cos(\pi mq), \\
q^2 - q &= \sum_{m\in odd} -\frac{4\sqrt{2}}{(n\pi)^3}\sqrt{2}\sin(\pi mq).
\end{aligned} \tag{4.8.4}$$

Formally differentiating these two equations with respect to q on both sides we get two formal identities (which needs to be interpreted as distributional sense):

$$\sum_{m\ odd} cos(\pi m q) = 0 \tag{4.8.5}$$

$$\sum_{\substack{m\ even,\\ m>1}} \sqrt{2} cos(\pi m q) = -\frac{1}{\sqrt{2}}, \tag{4.8.6}$$

$$\sum_{m\ odd} \frac{\sqrt{2}\sin(m\pi q)}{\sqrt{\lambda_n}} = \frac{1}{2\sqrt{2}}. \tag{4.8.7}$$

4.8.4 Alternate series representation of $BB^\dagger$ and connection with Eq. (4.5.6)

As mentioned in the main text the kernel operator $BB^\dagger$ has appeared earlier in the context of heat conduction through HCME model [94]. Using non-linear hydrodynamics theory in [94], the non-local linear response relation has been established for general boundary conditions characterized by a reflection coefficient $R = \left(\frac{\lambda-\omega}{\lambda+\omega}\right)^2$ which vary from 0 to 1. For given R, the expression for the kernel is given as [94]

$$BB^\dagger(x,x') = \frac{1}{\sqrt{2\pi}} \sum_{n=-\infty}^{\infty} \left[\frac{R^{|2n|}}{\sqrt{|2n+x-x'|}} - \frac{R^{|2n+1|}}{\sqrt{|2n+x+x'|}} \right]. \tag{4.8.8}$$

The value $R = 0$ corresponds to the resonance condition $\omega = \lambda$ for free boundary condition *i.e.* $q_0 = q_1$ and $q_N = q_{N+1}$. On the other hand, $R = 1$ corresponds to fixed boundary condition. For $R = 1$, one can explicitly check with the above representation that

$$\int_0^1 dx'\, BB^\dagger(x,x')\alpha_m(x') = \frac{1}{\lambda_n^{1/4}}\alpha_m(x), \tag{4.8.9}$$

which is same as Eq. (4.5.6). The proof is as follows. The LHS of Eq. (4.8.9) can be written as,

$$L.H.S = \frac{1}{\sqrt{\pi}} \int_0^1 dy \left[\frac{1}{\sqrt{|x-y|}} + \sum_{n=1}^{\infty} \frac{1}{\sqrt{2n+x-y}} + \frac{1}{\sqrt{2n-x+y}} - \frac{1}{\sqrt{2n-2+x+y}} - \frac{1}{\sqrt{2n-x-y}} \right] \sin(m\pi y) \tag{4.8.10}$$

Using change of variables and separating the part in absolute value we have,

$$L.H.S = \frac{1}{\sqrt{\pi}}\Bigg[\int_0^x dz\frac{\sin(m\pi(x-z))}{\sqrt{z}} + \int_0^{1-x} dz\frac{\sin(m\pi(x+z))}{\sqrt{z}} + \sum_{n=1}^{\infty}\Bigg(\int_{2n-1+x}^{2n+x} dz\frac{\sin(m\pi(2n+x-z))}{\sqrt{z}} + \int_{2n-x}^{2n+1-x} dz\frac{\sin(m\pi(z-2n+x))}{\sqrt{z}} - \int_{2n-2+x}^{2n-1+x} dz\frac{\sin(m\pi(z-2n+2-x))}{\sqrt{z}} - \int_{2n-1-x}^{2n-x} dz\frac{\sin(m\pi(2n-x-z))}{\sqrt{z}}\Bigg)\Bigg]$$

Upon using trigonometric identities this can be reduced to,

$$L.H.S. = \frac{1}{\sqrt{\pi}}\Bigg[\Bigg(\int_0^x dz + \sum_{n=1}^{\infty}\Big(\int_{2n-2+x}^{2n-1+x} dz + \int_{2n-1+x}^{2n+x}\Big)\Bigg)\frac{\sin(m\pi(x-z))}{\sqrt{z}} + \Bigg(\int_0^{1-x} dz + \sum_{n=1}^{\infty}\Big(\int_{2n-1-x}^{2n-x} dz + \int_{2n-x}^{2n+1-x}\Big)\Bigg)\frac{\sin(m\pi(x+z))}{\sqrt{z}}\Bigg] \tag{4.8.11}$$

which, upon simplifying further provides the R.H.S. of Eq. (4.8.9),

$$\frac{1}{\sqrt{\pi}}\int_0^{\infty} dz\left[\frac{\sin(m\pi(x-z))}{\sqrt{z}} + \frac{\sin(m\pi(x+z))}{\sqrt{z}}\right] = \frac{1}{\sqrt{m\pi}}\sqrt{2}\sin(m\pi x) \tag{4.8.12}$$

4.8.5 Explicit expressions of some equations mentioned earlier

The total fractional equation (4.5.1) can be written explicitly as,

$$\partial_t e(x,t) = \nabla_x \int dx' \left[\mathbb{A}(x',t)e(x',t) - B(x',t)T\eta(x',t)\right] \tag{4.8.13}$$

The equation for the two time equilibrium spatio-temporal correlation (Eq. (4.5.10))can be written as,

$$C_{\text{eq}}(x,t,y,t') = 2\bar{\kappa}\int_{-\infty}^{t} ds \int_{-\infty}^{t'} ds' \int dx' \int dy' \nabla_{x'} G_{t-s}^{xx'} \langle (BT\eta)(x',s)(BT\eta)(y',s')\rangle \nabla_{y'} G_{t'-s'}^{yy'} \tag{4.8.14}$$

The spatio-temporal current correlations in Eq. (4.5.14) can be explicitly written as,

$$\langle j(x,t)j(y,t')\rangle = \int dx' \int dy' \bar{\kappa}^2 \mathbb{A}(x,x')\mathbb{A}(y,y')\langle e(x',t)e(y',t')\rangle \tag{4.8.15}$$

$$+2\bar{\kappa}T^2 B(x,x')B(y,y')\langle \eta(x',t)\eta(y',t')\rangle \tag{4.8.16}$$

$$-\sqrt{2}\bar{\kappa}^{3/2}T\mathbb{A}(x,x')B(y,y')\langle e(x',t)\eta(y',t')\rangle \tag{4.8.17}$$

$$-\sqrt{2}\bar{\kappa}^{3/2}TB(x,x')\mathbb{A}(y,y')\langle \eta(x',t)e(y',t')\rangle \tag{4.8.18}$$

Since it might be a bit confusing using the symbolic vector notation for the operations in the main text, here we show explicitly the expressions for individual terms and show the 2nd and 3rd terms give a similar term to 1st. Eq. (4.8.15) gives,

$$\begin{aligned}\bar{\kappa}^2 \int dx' \int dy' \mathbb{A}(x,x')\mathbb{A}(y,y')G^{x'y'}_{|t-t'|} &= \bar{\kappa}^2 \int dx' \int dy' BB^\dagger(x,x')\partial_{x'}BB^\dagger(y,y')\partial_{y'}G^{x'y'}_{|t-t'|} \\ &= \bar{\kappa}^2 \int dx' \int dy' \mathbb{A}(x,x')G^{x'y'}_{|t-t'|}\mathbb{A}^\dagger(y',y) \end{aligned} \tag{4.8.19}$$

where we used the adjoint representation for $\mathbb{A}^\dagger(y,y') = \mathbb{A}(y',y)$. Eq. (4.8.17) gives,

$$\begin{aligned}\text{III} &= \int dx' \int dy' \sqrt{2}\bar{\kappa}^{3/2}T\mathbb{A}(x,x')B(y,y')\langle e(x',t)\eta(y',t')\rangle \\ &= -2\bar{\kappa}T^2 \int dx' \int dy' \int dx'' \int dy'' \int_{-\infty}^{t} ds BB^\dagger(x,x')\partial_{x'}B(y,y')G^{x'x''}_{t-s}\partial_{x''}B(x'',y'')\langle \eta(y'',s)\eta(y',t')\rangle \\ &= 2\bar{\kappa}T^2 \int dx' \int dy' \int dx'' BB^\dagger(x,x')\partial_{x'}B(y,y')\partial_{x''}(G^{x'x''}_{t-t'})B(x'',y')\theta(t-t') \\ &= 2\bar{\kappa}T^2 \int dx' \int dy' \int dx'' \mathbb{A}(x,x')G^{x'x''}_{t-t'}\mathbb{A}^\dagger(x'',y)\theta(t-t'). \end{aligned} \tag{4.8.20}$$

Eq. (4.8.18) gives,

$$\begin{aligned}\text{IV} &= \int dx' \int dy' \sqrt{2}\bar{\kappa}^{3/2}TB(x,x')\mathbb{A}(y,y')\langle \eta(x',t)e(y',t')\rangle \\ &= -2\bar{\kappa}T^2 \int dx' \int dy' \int dx'' \int dy'' \int_{-\infty}^{t} ds B(x,x')\mathbb{A}(y,y')G^{y'x''}_{t'-s}\partial_{x''}B(x'',y'')\langle \eta(x',t)\eta(y'',s)\rangle \\ &= 2\bar{\kappa}T^2 \int dx' \int dy' \int dx'' B(x,x')\mathbb{A}(y,y')\partial_{x''}(G^{y'x''}_{t'-t})B(x'',x')\theta(t'-t) \\ &= 2\bar{\kappa}T^2 \int dx' \int dy' \int dx'' \mathbb{A}(y,y')G^{y'x''}_{t'-t}\mathbb{A}^\dagger(x'',x)\theta(t'-t). \end{aligned} \tag{4.8.21}$$

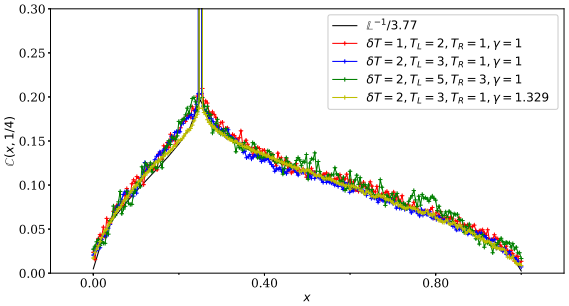

Figure 4.9: Simulation results for $N = 256$, with 4 different temperature and exchange rate parameters mentioned in the graph. The black curve is theoretically computed curve with $\nu = 3.77$, we see the results from the simulation are very close to predicted theoretical curve for the different parameters. This suggests that the parameter ν is independent of absolute value of the applied boundary temperature, the temperature gradient of the system and the long range correlations do not depend on the details like the stochastic exchange rate etc. The slight differences are again, hopefully a result of finite size effect.

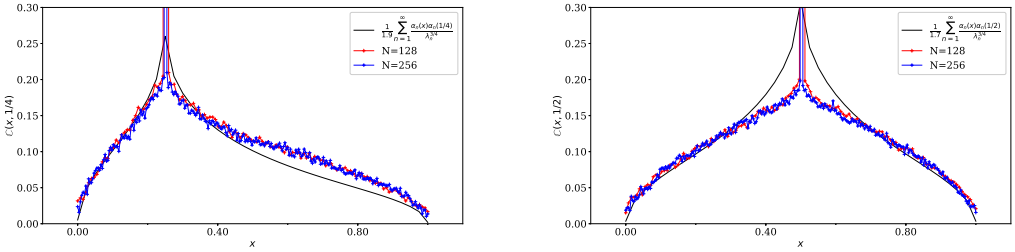

Figure 4.10: Here we show that instead of using ψ_n and μ_n if we use $\sin$ and $\lambda_n^{3/4}$ for construction of inverse of the fractional operator, there are significant difference between the simulations with the formula $\mathbb{C}(x, y) = \sum_{n=1}^{\infty} \frac{\alpha_n(x)\alpha_n(y)}{\lambda_n^{3/4}}$

The second term is explicit in the main-text.

4.8.6 Some tests on Long-range correlations

In Fig. (4.9) we do microscopic simulations for different temperature differences, and absolute temperatures to show, to good accuracy, the constant ν does not depend on these factors. In Fig. (4.10) we test the use of $\alpha(\sin)$ basis instead of the ψ basis for theoretical prediction for the nature of long-range correlations, and show it performs badly.

5

Harmonic chain with volume exchange

5.1 Introduction

In the previous chapter we have seen that the anomalous transport in a stochastically perturbed Harmonic chain is governed by a fractional diffusion equation. In this chapter, we look at a simpler model of anomalous transport in one dimension where we derive the corresponding fractional evolution equation for the temperature profile inside a finite domain and show explicitly how this evolution approaches to the appropriate fractional diffusion operator in the infinite domain.

This chapter is organized as follows:

In Sec. 5.2 we define the model explicitely and then summarize our main results. Next, in Sec. 5.3 we show that the microscopic dynamics implies that in the scaling limit, the system can be described by a coupled set of PDEs for the temperature and correlations. We solve these set of coupled PDEs in Sec. 5.4 to obtain the steady state temperature profile as well as the correlations in the system. In Sec. 5.5 we show that the relaxation dynamics of the temperature field is governed by a integro-differential operator. We find the spectrum of this fractional operator and then describe the temperature evolution using this fractional operator. In Sec. 5.6 we show that in the infinite domain limit, this integro-differential operator reduces to a skew fractional operator. Finally we conclude in Sec. 5.7.

5.2 Definition of the model and summary of results

This model consists of a finite one dimensional lattice of L sites where each site carries a 'stretch' variable $\eta_i,\ i = 1, 2, ..., L$ under an onsite external potential $V(\eta_i) = \eta_i^2/2$. The lattice is attached

to two thermal reservoirs at temperatures T_ℓ and T_r on the left and right ends, respectively and subjected to a volume conserving stochastic noise. The dynamics of this model has two parts: (a) the usual deterministic part plus the Langevin terms coming from the baths and (b) a stochastic exchange part where ηs from any two neighboring sites, chosen at random, are exchanged at constant rate γ. The dynamics is given by

$$\begin{aligned}\frac{d\eta_i}{dt} &= V'(\eta_{i+1}) - V'(\eta_{i-1}) + \delta_{i,1}\left(-\lambda V'(\eta_1) + \sqrt{2\lambda T_\ell}\zeta_\ell(t)\right) \\ &\quad + \delta_{i,L}\left(-\lambda V'(\eta_L) + \sqrt{2\lambda T_r}\zeta_r(t)\right) + \text{stochastic exchange at rate } \gamma,\end{aligned} \tag{5.2.1}$$

with fixed boundary conditions (BCs) $\eta_0 = \eta_{L+1} = 0$. Here $\zeta_{\ell,r}(t)$ are mean zero and unit variance, independent Gaussian white noises. Note that, in contrast to the HCME case, this dynamics has two conserved quantities: the 'volume' η_i and the energy $V(\eta_i)$. This model was first introduced by Bernardin and Stoltz in the closed system setup [52] where starting from the harmonic chain with Hamiltonian given earlier, they have treated the positions q_is and the momenta p_is on the same footing. Note that for harmonic chain, the dynamics of the 'stretch' variable $r_i = q_{i+1} - q_i$ and the momentum variable are similar: $\dot{r}_i = p_{i+1} - p_i$ and $\dot{p}_i = r_{i+1} - r_i$ for $i = 1, 2, ..., N$. Hence for $N = L/2$, defining $\eta_{2j-1} = r_j$ and $\eta_{2j} = p_j$, one finds that both the above equations can be expressed in a single equation: $\dot{\eta}_m = \eta_{m+1} - \eta_{m-1}$ for $m = 1, 2, ..., L$. The system can also be interpreted as a fluctuating interface where the algebraic volume of the interface at site m is given by η_m and the energy $V(\eta) = \eta^2/2$ [52]. Hence, the stochastic exchange part in Eq. (5.2.1) can be thought of as a volume-energy conserving noise. We call this model as 'harmonic chain with volume exchange' (HCVE).

It has been shown that the HCVE model defined on an isolated infinite one dimensional lattice (*i.e.* $\lambda = 0$ in Eq. (5.2.1) with $i = -\infty, .., -1, 0, 1, .., \infty$) exhibits super diffusion of energy [90]:

$$\begin{aligned}&\partial_t e(x,t) = -\mathbb{L}_\infty[e(x,t)], \\ &\mathbb{L}_\infty = \frac{1}{\sqrt{2\gamma}}[(-\Delta)^{3/4} - \nabla(-\Delta)^{1/4}],\end{aligned} \tag{5.2.2}$$

where the skew-fractional operator $\mathbb{L}_\infty$ has the Fourier representation $|q|^{3/2}(1 - i\ \mathrm{sgn}(q))$ with $i = \sqrt{-1}$ and sgn(q) is the Signum function. Note that the spectrum is different from that in the

infinite HCME model. In this chapter, however, we consider the HCVE model on a finite lattice of size L in open set up *i.e.* connected to heat baths at the two ends as described in Eq. (5.2.1). It is known that in this case also, as in HCME, the stationary current scales as $j \sim L^{-1/2}$ [90].

Results - We explicitly find that in the large L limit the average energy current $j = -2\langle \eta_i \eta_{i+1} \rangle - \gamma(\langle \eta_{i+1}^2 \rangle - \langle \eta_i^2 \rangle)$ in the stationary state is given by

$$j_{ss} = \frac{1}{2}\sqrt{\frac{\pi}{\gamma}}\frac{(T_\ell - T_r)}{\sqrt{L}} + \mathcal{O}\left(\frac{1}{L}\right). \tag{5.2.3}$$

In the non-stationary regime, we numerically find that the temperature profile $T_i(t) = \langle \eta_i^2(t) \rangle$ and the two-point correlations $C_{i,j}(t) = \langle \eta_i(t)\eta_j(t) \rangle$ for $i \neq j$ have the following scaling forms

$$\begin{aligned} T_i(t) &= \mathcal{T}\left(\frac{i}{L}, \frac{t}{L^{3/2}}\right) \\ C_{i,j}(t) &= \frac{1}{\sqrt{L}}\mathcal{C}\left(\frac{|i-j|}{\sqrt{L}}, \frac{i+j}{2L}, \frac{t}{L^{3/2}}\right), \end{aligned} \tag{5.2.4}$$

in the leading order for large L. The scaling functions $\mathcal{T}(y,\tau)$ and $\mathcal{C}(x,y,\tau)$ satisfy the following equations inside the domain $\mathcal{D} = \{0 \leq x \leq \infty\,;\, 0 \leq y \leq 1\}$:

$$\partial_y \mathcal{C}(x,y,\tau) = -\gamma \partial_x^2 \mathcal{C}(x,y,\tau) \tag{5.2.5}$$

$$\partial_y \mathcal{T}(y,\tau) = -2\gamma \left[\partial_x \mathcal{C}(x,y,\tau)\right]_{x=0} \tag{5.2.6}$$

$$\partial_\tau \mathcal{T}(y,\tau) = 2\partial_y \mathcal{C}(0,y,\tau), \tag{5.2.7}$$

with $\mathcal{C}(x,y,0)|_{x\to\infty} = 0$ and $\mathcal{C}(x,y,0) = 0$. We find that the exact solutions of these equations are given by

$$\mathcal{T}(y,\tau) = \mathcal{T}_{ss}(y) + \mathcal{T}_r(z = 1-y, \tau) \tag{5.2.8}$$

$$\mathcal{C}(x,y,\tau) = \mathcal{C}_{ss}(x,y) + \mathcal{C}_r(x, z = 1-y, \tau). \tag{5.2.9}$$

In the above equation, NESS part of the profiles are

$$\begin{aligned}\mathcal{T}_{ss}(y) &= T_r + (T_\ell - T_r)\sqrt{1-y},\\ \mathcal{C}_{ss}(x,y) &= -\frac{T_\ell - T_r}{4}\sqrt{\frac{\pi}{\gamma}}\,\mathrm{erfc}\left(\frac{x}{\sqrt{4\gamma(1-y)}}\right).\end{aligned} \tag{5.2.10}$$

The relaxation parts to the above steady states is given as

$$\mathcal{C}_r(x,z,\tau) = -\int_0^z \frac{\exp\left(-\frac{x^2}{4\gamma(z-z')}\right)}{\sqrt{4\pi\gamma(z-z')}}\,\frac{\partial \mathcal{T}_r(z',\tau)}{\partial z'}dz', \tag{5.2.11}$$

where $\mathcal{T}_r(z,\tau)$ satisfies the following continuity equation:

$$\partial_\tau \mathcal{T}_r(z,\tau) = \frac{1}{\sqrt{\pi\gamma}}\partial_z\left[\int_0^z dz'\,\frac{\partial_{z'}\mathcal{T}_r(z',\tau)}{\sqrt{z-z'}}\right], \tag{5.2.12}$$

inside the domain $0 \le z \le 1$ with BCs $\mathcal{T}_r(0,\tau) = \mathcal{T}_r(1,\tau) = 0$. The relaxation parts $\mathcal{T}_r(z,\tau)$ and $\mathcal{C}_r(x,z,\tau)$ describe the approach towards the NESS solutions in the $\tau \to \infty$ limit. Note that Eq. (5.2.12), can formally be written in terms of the Riemann-Liouville operator. The equations Eq. (5.2.3), Eq. (5.2.10), Eq. (5.2.11) and Eq. (5.2.12), comprise our main results. The evolution of the temperature in Eq. (5.2.12) is indeed given by a linear but non-local equation defined inside a finite domain $0 \le z \le 1$. However, following a similar calculation for infinite system we later show that Eq. (5.2.12) reduces to Eq. (5.2.2) in Sec. 5.3. This establishes, without ambiguity, that the non-local operator in Eq. (5.2.12) is the correct finite domain representation of the fractional operator $\mathbb{L}_\infty$ in Eq. (5.2.2). Another point to note that the temperature profile in SS, $\mathcal{T}_{ss}(y)$, is asymmetric under space reversal as the microscopic model itself does not have such symmetry. As a result, any locally created perturbation splits into one traveling sound mode and one non-moving heat mode. This is in contrast to the HCME model where one observes two sound modes moving in opposite directions in addition to a non-moving heat mode [52, 107]. Consequently, in this case there is singularity in $\partial_y \mathcal{T}_{ss}(y)$ only at one boundary and we find that the meniscus exponent [108] is again $1/2$ as in the HCME model with fixed boundary conditions. Interestingly, it turns out that for this boundary condition, both the temperature and the correlation become independent of the strength of coupling λ with the heat baths in the large L limit.

5.3 Derivation of the continuum equations for temperature and correlations:

5.3.1 The Fokker-Planck operator and discrete equations for correlation functions:

We start with the Fokker-Planck (FP) equation associated to the dynamics Eq. (5.2.1), which describes the evolution of the joint distribution $P(\vec{\eta}, t)$ of $\vec{\eta} = (\eta_1, \eta_2, \cdots, \eta_L)$ at time t :

$$\partial_t P(\vec{\eta}, t) = [\mathcal{L}_\ell + \mathcal{L}_b + \mathcal{L}_{ex}]\, P(\vec{\eta}, t), \tag{5.3.1}$$

where, $\mathcal{L}_\ell$ is the Liouvillian part, $\mathcal{L}_b$ contains the effects of the Langevin baths at the boundaries and $\mathcal{L}_{ex}$ represents the contribution from the exchange noise. The explicit expressions of the deterministic and Langevin parts of the Fokker Planck (FP) equation given by the operators $\mathcal{L}_l$, $\mathcal{L}_b$ are

$$\mathcal{L}_l = \sum_{i=2}^{L-1} (V'(\eta_{i-1}) - V'(\eta_{i+1}))\partial_{\eta_i} + V'(\eta_{L-1})\partial_{\eta_L} - V'(\eta_2)\partial_{\eta_1}$$

$$\mathcal{L}_b = \lambda T_\ell\, \partial^2_{\eta_1} + \lambda \partial_{\eta_1} V'(\eta_1) + \lambda T_r\, \partial^2_{\eta_L} + \lambda \partial_{\eta_L} V'(\eta_L),$$

where T_ℓ and T_r are the temperatures of the reservoirs on the left and right, respectively. The stochastic part $\mathcal{L}_{ex}$ is given as

$$\mathcal{L}_{ex} P = \gamma \sum_{i=1}^{L-1} \left[P(\vec{\eta}_{i,i+1}) - P(\vec{\eta}) \right], \tag{5.3.2}$$

where $\vec{\eta}_{i,i+1}$ denote the configuration after the exchange of variable i with $i+1$. Starting from the FP equation in Eq. (5.3.1), we obtain the dynamical equations satisfied by $T_i = \langle \eta_i^2(t) \rangle$ and

$C_{i,j} = \langle \eta_i(t)\eta_j(t)\rangle$ for $i \neq j$ in the bulk:

$$\begin{aligned}
\dot{C}_{ij} &= C_{i+1,j} - C_{i-1,j} + C_{i,j+1} - C_{i,j-1} + \gamma[C_{i-1,j} + C_{i+1,j} + C_{i,j-1} + C_{i,j+1} - 4C_{i,j}],\\
\dot{C}_{i,i+1} &= T_{i+1} - C_{i-1,i+1} + C_{i,i+2} - T_i + \gamma[C_{i-1,i+1} + C_{i,i+2} - 2C_{i,i+1}],\\
\dot{T}_i &= 2[C_{i,i+1} - C_{i-1,i}] + \gamma[T_{i+1} + T_{i-1} - 2T_i].
\end{aligned} \tag{5.3.3}$$

Rest of the equations at the boundaries are given in Appendix. (5.8). Fortunately the equations for two point correlations do not involve higher order correlations, which allows us to solve these equations analytically, in the $L \to \infty$ limit.

5.3.2 Derivation of continuum equations for the temperature and correlation fields from the discrete equations

In this section, we outline the steps to obtain the continuum set of PDEs Eqs. (5.2.5)-(5.2.7). We first solve the discrete equations numerically to observe that, for large L the solutions have the scaling properties as given in Eq. (5.2.4) where we have two length scales of $\mathcal{O}(L)$ along the diagonal ($i + j$ =constant) and of $\mathcal{O}(\sqrt{L})$ along perpendicular to the diagonal ($|i - j|$=constant) direction, and a time scale of $\mathcal{O}(L^{3/2})$. This time scale can be anticipated from the propagator $e^{-|q|^{3/2}[1-i\mathrm{sgn}(q)]t}$ of the Eq. (5.2.2) in Fourier space. The two length scales are understood by looking at the orders of the $C_{i,j}$ and T_i, and their derivatives numerically. Interestingly, the scaled correlation function $\mathcal{C}$ relaxes very fast over much shorter time scale [$\mathcal{O}(L)$] compared to the evolution time scale [$\mathcal{O}(L^{3/2})$] of the temperature field $\mathcal{T}$. Due to this fact, Eq. (5.2.5) and Eq. (5.2.6) do not involve the time derivative. As a result the correlation function $\mathcal{C}$ evolves adiabatically obeying the (anti-)diffusion Eq. (5.2.5), with a drive at the boundary by the time dependent temperature field through Eq. (5.2.6). The equation for the temperature profile given in Eq. (5.2.7) is in the expected continuity equation.

These observations suggest that we look for solutions of Eq. (5.3.3) in the scaling form Eq. (5.2.4). In the non-stationary regime, we numerically find that the temperature profile $T_i(t) = \langle \eta_i(t)^2\rangle$ and

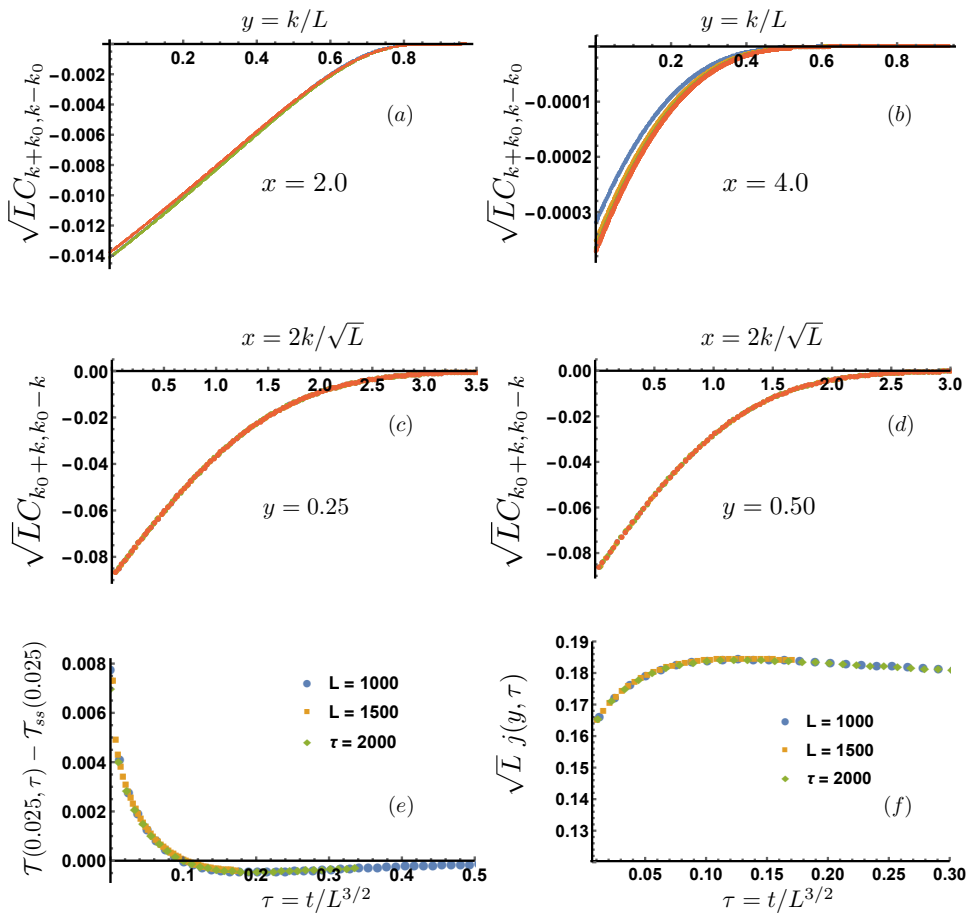

Figure 5.1: Data collapse of the correlation functions and temperature profile confirming the scaling behaviors in Eqs. (5.3.4) and (5.3.5). Figures (a) and (b) show the data collapse as a function of the scaling variable $y = (i+j)/2L$ with four systems sizes $L = 1000$ (Blue, dark gray), $L = 2000$ (Orange, deep gray), $L = 3000$ (Green, light gray) and $L = 4000$ (Red, bottom dark gray), for two fixed values of $x = |j-i|/\sqrt{L}$. Figures (c) and (d), show the data collapse as a function of the scaling variable x with the above four system sizes for two fixed values of y. The collapse are so good that other colors/shades not visible. Figure (e) describes the scaling behavior for the evolution of the temperature $\mathcal{T}(y,\tau) = T_{\lfloor yL \rfloor}(\tau L^{3/2})$ at a fixed position $y = 0.025$ for different system sizes as a function of the scaled time $\tau = t/L^{3/2}$. Note that, the temperatures are of $\mathcal{O}(1)$ whereas the correlations are of $\mathcal{O}(1/\sqrt{L})$. Also note from figures (c) and (b) that $\mathcal{C}_{ss}(x \to \infty, z) = 0$. Last figure (f) establishes that the current in the system is of order $1/\sqrt{L}$ and also evolves in scaled time $\tau = t/L^{3/2}$. The other parameters in the simulation are $\gamma = \Lambda = 1, T_\ell = 1.1,\ T_r = 0.9$.

the two-point correlations $C_{i,j}(t) = \langle \eta_i(t)\eta_j(t)\rangle$ for $i \neq j$ have the following scaling forms

$$C_{i,j}(t) = \frac{1}{\sqrt{L}}\mathcal{C}\left(\frac{|i-j|}{\sqrt{L}}, \frac{i+j}{2L}, \frac{t}{L^{3/2}}\right), \tag{5.3.4}$$

$$T_i(t) = \mathcal{T}\left(\frac{i}{L}, \frac{t}{L^{3/2}}\right), \tag{5.3.5}$$

in the leading order for large L which are also supported by numerical evidence shown in Fig 5.1. In Figs. (5.1a), (5.1b), (5.1c) and (5.1d), we verify the scaling behaviors of the correlations in Eq. (5.3.4). Figs. (5.1c) and (5.1d), describes scaling behavior with respect to time. Using these, we define contin-

uum ordinates as, $\frac{|i-j|}{\sqrt{L}} = x$, $\frac{|i+j|}{2L} = y$, $\frac{t}{L^{3/2}} = \tau$ and $\frac{1}{\sqrt{L}} = \epsilon$, where $x \in (0, \infty)$ and $y \in (0, 1)$. In the following, we insert this scaling form and Taylor expand in $\epsilon = 1/\sqrt{L}$. Keeping terms to leading order in ϵ we obtain the continuum equations.

1. Bulk Equations, $|i - j| \geq 2$

   The discrete equation in bulk:

$$\dot{C}_{i,j} = -\left(C_{i-1,j} - C_{i+1,j} + C_{i,j-1} - C_{i,j+1} - \gamma[C_{i,j-1} + C_{i,j+1} + C_{i+1,j} + C_{i-1,j} - 4C_{i,j}]\right), \tag{5.3.6}$$

   using above scaling definitions, we can write the above mentioned discrete equation as,

$$\begin{aligned}\epsilon^4 \partial_\tau \mathcal{C}(x, y, \tau) = -\epsilon \Bigg[& \mathcal{C}(x - \epsilon, y - \frac{\epsilon^2}{2}) - \mathcal{C}(x + \epsilon, y + \frac{\epsilon^2}{2}) + \mathcal{C}(x + \epsilon, y - \frac{\epsilon^2}{2}) - \mathcal{C}(x - \epsilon, y + \frac{\epsilon^2}{2}) \\ & -\gamma(\mathcal{C}(x + \epsilon, y - \frac{\epsilon^2}{2}) + \mathcal{C}(x - \epsilon, y + \frac{\epsilon^2}{2}) + \mathcal{C}(x + \epsilon, y + \frac{\epsilon^2}{2}) \\ & +\mathcal{C}(x - \epsilon, y - \frac{\epsilon^2}{2}) - 4\mathcal{C}(x, y)) \Bigg],\end{aligned} \tag{5.3.7}$$

   which by Taylor expansion of each terms in $x,\ y$ and τ, we obtain the leading order terms for continuum dynamical equation as

$$\epsilon^4 \partial_\tau \mathcal{C}(x, y, \tau) = 2\epsilon^3 \partial_y \mathcal{C}(x, y, \tau) + 2\gamma\epsilon^3 \partial_x^2 \mathcal{C}(x, y, \tau). \tag{5.3.8}$$

   At the dominant order ($\mathcal{O}(\epsilon^3)$), we find,

$$\partial_y \mathcal{C}(x, y, \tau) + \gamma \partial_x^2 \mathcal{C}(x, y, \tau) = 0. \tag{5.3.9}$$

2. Nearest neighbor term, $j = i + 1$

   The off-diagonal term:

$$\dot{C}_{i,i+1} = T_{i+1} - C_{i-1,i+1} + C_{i,i+2} - T_i + \gamma\left[C_{i-1,i+1} + C_{i,i+2} - 2C_{i,i+1}\right], \tag{5.3.10}$$

after proper scaling, we get,

$$\epsilon^4\partial_\tau\mathcal{C}(\epsilon, y+\frac{\epsilon^2}{2},\tau) = \mathcal{T}(y+\epsilon^2)-\mathcal{T}(y) \quad +\epsilon\mathcal{C}(2\epsilon, y+\epsilon^2)-\epsilon\mathcal{C}(2\epsilon,y)+\gamma\epsilon\left[\mathcal{C}(2\epsilon,y)+\mathcal{C}(2\epsilon,y+\epsilon^2)\right.$$
$$\left.-2\mathcal{C}(\epsilon,y+\epsilon^2/2)\right].$$

Expanding above equation in x and y, and keeping the relevant order terms in ϵ we get the continuum equation as

$$\epsilon^4\partial_\tau\mathcal{C}(0,y,\tau) = \epsilon^2\left(\partial_y\mathcal{T}(y,\tau)+2\gamma\partial_x\mathcal{C}(0,y,\tau)\right)+\mathcal{O}(\epsilon^3), \tag{5.3.11}$$

and hence to the dominating order, the governing continuum equation is

$$\partial_y\mathcal{T}(y,\tau)+2\gamma\partial_x\mathcal{C}(0,y,\tau)=0. \tag{5.3.12}$$

3. Diagonal term $i=j$

   Next is the diagonal term where $i=j$,

$$\dot{T}_i = 2[C_{i,i+1}-C_{i-1,i}]+\gamma[T_{i+1}+T_{i-1}-2T_i]. \tag{5.3.13}$$

which in continuum limit given as

$$\epsilon^3\partial_\tau\mathcal{T}(y,\tau) = 2\epsilon\left[\mathcal{C}(\epsilon,y+\frac{\epsilon^2}{2})-\mathcal{C}(\epsilon,y-\frac{\epsilon^2}{2})\right]+\gamma\left[\mathcal{T}(y+\epsilon^2)+\mathcal{T}(y-\epsilon^2)-2\mathcal{T}(y)\right].$$

After expansion, we arrive at

$$\epsilon^3\partial_\tau\mathcal{T}(y,\tau) = 2\epsilon\left[\epsilon^2\partial_y\mathcal{C}(0,y,\tau)+\epsilon^3\frac{\gamma}{2}\partial_y^2\mathcal{T}(y,\tau)\right]+\mathcal{O}(\epsilon^4). \tag{5.3.14}$$

Hence, the leading order term is

$$\partial_\tau\mathcal{T}(y,\tau) = 2\partial_y\mathcal{C}(0,y,\tau). \tag{5.3.15}$$

4. Current

   The microscopic energy current in the system is defined through

$$\partial_t \langle \eta_i^2 \rangle = -[j_{i\to i+1} - j_{i-1\to i}], \tag{5.3.16}$$

   where $j_{i\to i+1} = -2C_{i,i+1} - \gamma(T_{i+1} - T_i)$. The stochastic part of the current decays as $\mathcal{O}(1/L)$ and in the macroscopic limit goes to zero. In the continuum limit, the deterministic part contributes in the leading order to provide, $j = -2\mathcal{C}(0, y, \tau)/\sqrt{L}$.

The above analysis gives us the bulk equations for the system as given in Eqs. (5.2.5),(5.2.6),(5.2.7). Solutions of these equations for $\mathcal{C}(x, y, \tau)$ and $\mathcal{T}(y, \tau)$ have two parts Eq. (5.2.9). It is easier to deal with these equation the transformation of $z = 1 - y$, which satisfies,

$$\partial_z \mathcal{C}(x, z, \tau) = \gamma \partial_x^2 \mathcal{C}(x, z, \tau)\,, \tag{5.3.17}$$

$$\partial_z \mathcal{T}(z, \tau) = 2\gamma \partial_x \mathcal{C}(x, z, \tau)_{x=0}\,, \tag{5.3.18}$$

$$\partial_\tau \mathcal{T}(y, \tau) = -2\partial_z \mathcal{C}(0, z, \tau). \tag{5.3.19}$$

These equations have to be solved with appropriate boundary conditions which will be discussed in the next few sections, where we discuss the solution of these equations in steady state and the approach to it.

5.4 Stationary state solution of $\mathcal{T}(z)$ and $\mathcal{C}(x, z)$

In the NESS the equations Eqs. (5.3.17)-(5.3.19) become simpler since $\partial_\tau \mathcal{T} \to 0$ as $\tau \to \infty$ implying $\mathcal{C}_{ss}(0, y) = d$. Now making the variable transformation $z = (1 - y)$, the problem of finding $\mathcal{C}_{ss}$ reduces to solving a diffusion equation with its value at $x = 0$ held fixed for all y. We need to solve these equations along with the boundary conditions

$$\begin{aligned} &(i)\, \mathcal{C}_{ss}(x, z \to 0) = 0,\ (ii)\, \mathcal{C}_{ss}(x \to \infty, z) = 0, \\ &(iii)\, \mathcal{C}_{ss}(x = 0, z) = d. \end{aligned} \tag{5.4.1}$$

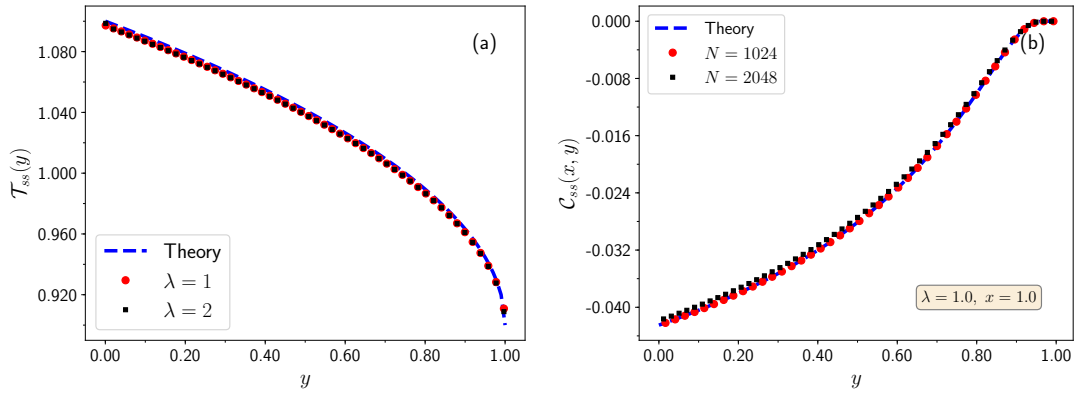

Figure 5.2: Numerical verification of the analytical NESS predictions for (a) $\mathcal{T}_{ss}(y)$ and (b) $\mathcal{C}_{ss}(x, y)$ in Eq. (5.2.10). Symbols denote corrosponding quantities that are obtained from simulations with $\omega = \gamma = 1$, $T_\ell = 1.1$, $T_r = 0.9$ and $N = 1024$, whereas the dashed lines are from theory.

The boundary conditions (i) and (ii) follow from our numerical observations shown in Figs. 5.1(a,b) and Figs. 5.1(c,d) respectively. The last boundary condition (iii) is obtained by observing that the LHS of (5.3.19) is zero in the steady state; hence $(\partial_z \mathcal{C}_{ss}(0, z) = 0)$. The unknown constant d will be fixed by the temperatures at the boundary. The first equation is easy to solve by taking Laplace transform in z along with boundary conditions. Finally, after inverting the Laplace transform, we find the solution is given by

$$\mathcal{C}_{ss}(x, z) = d\ \text{erfc}\left[\frac{x}{\sqrt{4\gamma z}}\right], \tag{5.4.2}$$

where, erfc is the complimentary error function defined as $\text{erfc}(x) = 1 - \frac{2}{\sqrt{\pi}} \int_0^x dt e^{-t^2}$. Now, using this solution in Eq. (5.3.18), we get $\partial_z \mathcal{T}_{ss}(z) = -d\sqrt{4\gamma/\pi z}$, whose solution is

$$\mathcal{T}_{ss}(z) = \mathcal{T}_{ss}(0) - 2d\sqrt{\frac{4\gamma z}{\pi}}. \tag{5.4.3}$$

The constants $\mathcal{T}_{ss}(0)$ and d will now be determined from the boundary conditions of temperature field, $\mathcal{T}(z = 0) = T_r$ and $\mathcal{T}(z = 1) = T_\ell$. We finally have

$$T_\ell - T_r = -2d\sqrt{\frac{4\gamma}{\pi}},\ d = -\frac{\Delta T}{4}\sqrt{\frac{\pi}{\gamma}}, \tag{5.4.4}$$

where $\Delta T = (T_\ell - T_r)$ is the temperature difference between the left and right heat baths. Reverting now back to y variables using $z = 1 - y$, the exact expressions for the steady state temperature

profile and correlations are

$$\mathcal{T}_{ss}(y) = T_r + \Delta T\sqrt{1-y}, \tag{5.4.5}$$

$$\mathcal{C}_{ss}(x,y) = -\frac{\Delta T}{4}\sqrt{\frac{\pi}{\gamma}}\text{erfc}\left[\frac{x}{\sqrt{4\gamma(1-y)}}\right]. \tag{5.4.6}$$

Hence the current in the system is given by $j_{ss} = \frac{\mathcal{J}_{ss}}{\sqrt{L}}$, where,

$$j_{ss} = -\frac{2\mathcal{C}_{ss}(0,y)}{\sqrt{L}} = \frac{\Delta T}{2}\sqrt{\frac{\pi}{\gamma}}\frac{1}{\sqrt{L}}. \tag{5.4.7}$$

In Fig. 5.2 we verify the analytical results for $\mathcal{T}_{ss}$ and $\mathcal{C}_{ss}$ numerically, where we observe nice agreement. Next, we study the solution in the relaxation regime.

5.5 Relaxation to steady state

We now focus on the relaxation to the NESS. It is often convenient to separate the relaxation part as done in Eq. (5.2.8) and Eq. (5.2.9) where $\mathcal{T}_r(z,\tau)$ and $\mathcal{C}_r(x,z,\tau)$ describes the approach towards the NESS solutions in Eq. (5.2.10). It is easy to see that $\mathcal{C}_r(x,z,\tau)$ and $\mathcal{T}_r(z,\tau)$ satisfies the following equations

$$\partial_z\mathcal{C}_r(x,z,\tau) = \gamma\partial_x^2\mathcal{C}_r(x,z,\tau), \tag{5.5.1}$$

$$\partial_z\mathcal{T}_r(z,\tau) = 2\gamma\left[\partial_x\mathcal{C}_r(x,z,\tau)\right]_{x=0}, \tag{5.5.2}$$

$$\partial_\tau\mathcal{T}_r(z,\tau) = -2\partial_z\mathcal{C}_r(0,z,\tau), \tag{5.5.3}$$

with initial condition $\mathcal{C}_r(x,z,0) = 0$ and BC $\mathcal{C}_r(x,z,\tau)|_{x\to\infty} = 0$. The above equations are obtained from Eq. (5.2.5)-(5.2.7) after subtracting the steady state part and then making the variable transformation $z = (1-y)$. Note that the BC in Eq. (5.5.2) acts like a current source, at $x = 0$ boundary, to the diffusion Eq. (5.5.1). The Greens function $g(x,z)$ of this equation with above BC's satisfies, $\partial_z g(x,z) = \frac{\gamma}{2}\partial_x^2 g(x,z)$, where, $g(x,z)$ is given by $g(x,z) = \sqrt{4\gamma z}h(x/\sqrt{4\gamma z})$ where,

$h(w) = \frac{e^{-w^2}}{\pi} - w\text{erfc}(w)$, hence, the general time dependent solution is written as

$$\begin{aligned}\mathcal{C}_r(x,z,\tau) =& 2\int_0^z dx' \frac{e^{-(x-x')^2/(4\gamma z)}}{\sqrt{4\pi\gamma z}} \mathcal{C}_r(x',0,\tau) \\ &-\frac{1}{2\gamma}\left(\int_0^z dz'(g(x,z-z')\partial_{z'}^2\mathcal{T}_r(z',\tau))\right) \\ &-\frac{1}{2\gamma}\,\partial_{z'}\mathcal{T}_r(z',\tau)g(x,z)|_{z'\to 0}. \end{aligned} \tag{5.5.4}$$

With the initial condition $\mathcal{C}_r(x,0,\tau) = 0$ the first term drops out. It is easy to check that the remaining part satisfies (5.5.1) with boundary condition (5.5.2) as follows

$$\begin{aligned}\partial_x\mathcal{C}_r(x,z,\tau)|_{x\to 0} =& \frac{1}{2\gamma}\left(\int_0^z dz'\partial_{z'}^2\mathcal{T}_r(z',\tau) + \partial_{z'}\mathcal{T}_r(z',\tau)|_{z'\to 0}\right) \\ =& \frac{1}{2\gamma}\partial_z\mathcal{T}_r(z,\tau), \end{aligned} \tag{5.5.5}$$

where we have used $\partial_x g(x,z)|_{x\to 0} = -1$. Further using the fact that $g(x,z-z')\partial_{z'}T_r(z')|_{z'\to z} \to 0$ we can simplify (5.5.4) as

$$\begin{aligned}\mathcal{C}_r(x,z,\tau) &= \frac{1}{2\gamma}\left(\int_0^z dz'\partial_{z'}(g(x,z-z'))\partial_{z'}\mathcal{T}_r(z',\tau)\right) \\ &= -\frac{1}{\sqrt{\gamma}}\int_0^z dz' \frac{e^{-x^2/(4\gamma(z-z'))}}{\sqrt{4\pi(z-z')}}\partial_{z'}\mathcal{T}_r(z',\tau),\end{aligned}$$

which gives the relaxation of the correlation fields. The evolution of temperature field is obtained from (5.5.3) by putting $x \to 0$ in the above expression for $\mathcal{C}_r(x,z,\tau)$, we immediately have,

$$\partial_\tau\mathcal{T}_r(z,\tau) = \kappa\,\partial_z\int_0^z \frac{\partial_{z'}\mathcal{T}_r(z',\tau)}{\sqrt{z-z'}}dz',\ \ 0 \le z \le 1, \tag{5.5.6}$$

where, $\kappa = \frac{1}{\sqrt{\pi\gamma}}$. The infinite system generalization of this equation will be discussed later (see Sec. 5.6).

Series solution of the fractional PDE Eq. (5.5.6) in the finite domain

The evolution of the relaxation part of the temperature profile *i.e.* $\mathcal{T}_r(1-y,\tau) = \mathcal{T}(y,\tau) - \mathcal{T}_{ss}(y)$ is given by Eq. (5.5.6). Note that, $\mathcal{T}_r(z,\tau)$ is zero at both the boundaries: $z = 0$ and $z = 1$. As a

result it is natural to expand this function in $\alpha_n(z) = \sqrt{2}\sin(n\pi z),\ n = 1, 2, 3...$ complete basis defined in $z \in (0, 1)$, as $\mathcal{T}_r(z, \tau) = \sum_n \hat{\mathcal{T}}_n(\tau)\alpha_n(z)$. Substituting this form in Eq. (5.5.6), we have,

$$\sum_n \dot{\hat{\mathcal{T}}}_n \alpha_n(z) = \kappa \sum_n \hat{\mathcal{T}}_n(\tau)(n\pi)\partial_z \int_0^z \frac{\phi_n(z')}{\sqrt{z - z'}} dz'. \tag{5.5.7}$$

Now let us expand the function $f_n(z) = \partial_z \int_0^z \frac{\phi_n(z')}{\sqrt{z-z'}} dz'$ also in orthogonal basis $\alpha_n(y),\ n = 1, 2.....$ Let the expansion is given as $f_n(z) = \sum_{l=1} \zeta_{nl}\alpha_l(z)$ where $\zeta_{nl} = \int_0^1 dz\ f_n(z)\ \alpha_l(z)$. As a result we have,

$$\sum_{n=1} \dot{\hat{\mathcal{T}}}_n \alpha_n(z) = \kappa \sum_{n,l=1} \hat{\mathcal{T}}_n(\tau)(n\pi)\zeta_{nl}\alpha_l(z). \tag{5.5.8}$$

Using orthogonality, this can be written in vector notation as ($\hat{\mathcal{T}}_n = \langle n|\hat{\mathcal{T}}\rangle$),

$$|\ \dot{\hat{\mathcal{T}}}\ \rangle = \kappa\, \mathbf{B}|\ \hat{\mathcal{T}}\ \rangle, \tag{5.5.9}$$

where $B_{nk} = (n\pi)\zeta_{nk}$ and $|\ \dots\ \rangle$ denotes a column vector. If R is the matrix which diagonalizes $\mathbf{B}$ as $R^{-1}\mathbf{B}R = \Lambda$, then the time dependent solution is given as $|\ \hat{\mathcal{T}}(\tau)\ \rangle = Re^{\kappa\Lambda\tau}R^{-1}|\ \hat{\mathcal{T}}(0)\ \rangle$ and temperature at time τ is given as $\mathcal{T}(y, \tau) = \mathcal{T}_{ss}(y) + \sum_n \alpha_n(1-y)\hat{\mathcal{T}}_n(\tau)$. As the temperature field evolves at much faster timescales compared to the correlation field, the time dependent solution for correlations $\mathcal{C}_r(x, 1 - y, \tau)$ is governed by the evolution of the temperature field. The solution for evolution of correlations is written as, $\mathcal{C}(x, y, \tau) = \mathcal{C}_r(x, 1 - y, \tau) + \mathcal{C}_{ss}(x, y)$, where

$$\begin{aligned}\mathcal{C}(x, z, \tau) &= -\int_0^z dz' \frac{e^{-x^2/(4\gamma(z-z'))}}{\sqrt{4\pi\gamma(z - z')}} \partial_{z'} T_r(z', \tau), \\ &= \sum_{n=1} \hat{\mathcal{T}}_n(\tau)(n\pi) \int_0^z dz' \frac{e^{-x^2/(4\gamma(z-z'))}}{\sqrt{4\pi\gamma(z - z')}} \phi_n(z'),\end{aligned} \tag{5.5.10}$$

where, $\phi_n(y) = \sqrt{2}\cos(n\pi y),\ n \geq 1$ and $\phi_0(y) = 1$. The integral can be evaluated explicitly and doing the summations gives the evolution of the correlation fields.

Eigensystem: The eigenvalues (μ_n) of the bounded skew-fractional laplacian, $\mathbf{B}$ have interesting behavior, the first four of them are real and distinct. The higher eigenvalues all come in complex conjugate pairs. For large n, $\mu_n \sim \sqrt{\frac{\pi}{2}}|n\pi|^{3/2}(1 \pm i\ sgn(n))$, but for smaller n there is a system-

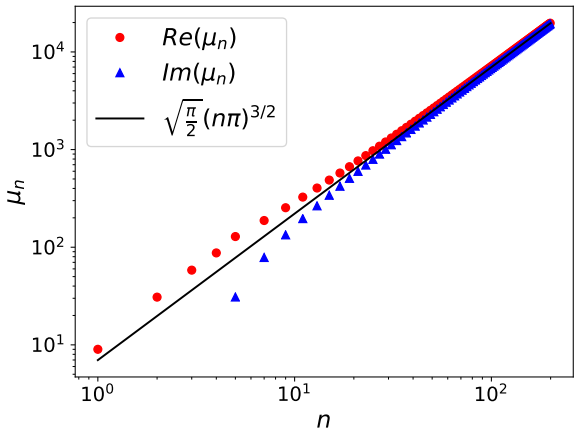

Figure 5.3: The real and imaginary part of the alternate eigenvalues for the matrix $\mathbf{B}$. The first 4 eigenvalues are completely real and distinct. The higher eigenvalue comes in pairs of $\mu_n(1 \pm i)$. For large n, the eigenvalues are close to $\sqrt{\frac{\pi}{2}}(n\pi)^{3/2}(1 \pm i)$. For smaller n, there is a deviation from asymptomatic scaling due to finite definition of the operator.

atic deviation due to the effect of finite domain. In Fig. 5.3, the real and imaginary part of alternate eigenvalues are plotted as a function of n, where the asymptotic scaling with $\sqrt{\frac{\pi}{2}}(n\pi)^{3/2}$ is seen clearly for large n. We note that this is not due to the the truncation of the matrix but an artefact of the finiteness of the system. Note that the large n behavior of μ_n is similar to the Fourier spectrum of the non-local operator $\mathbb{L}_\infty$ in Eq. (5.2.2) describing the evolution in infinite system. Hence it is interesting to see if one recovers the evolution Eq. (5.2.2) in the infinite system limit Sec. (5.6). The eigenvectors of the operator is defined as $\psi_n(y) = \sum_{l=1} R^{-1}_{nl}\alpha_l(y)$. Numerically computing this gives, the first six eigenvectors to be completely real. The eigenvectors corresponding to higher eigenvalues are complex and and comes in pairs. The real and imaginary parts of the first few eigenvectors are shown in Fig.5.5 un both real space and also in a polar representation. For plane wave solutions these would have been circles of length 1, here the polar plot shows a spiral decay to origin owing to the skewness of the operator.

Comparison with numerics: While it is difficult to solve this infinite order matrix equation analytically, we solve it numerically by truncating it at some finite order. In Fig. 5.4, we compare the evolution from this numerical solution with the same obtained from direct numerical simulation of Eq. (5.2.1) and observe nice agreement. Using this solution in Eq. (5.2.11) we obtain $C(x, z, \tau)$ in Eq. (5.2.9) which we also compare with simulation results in the inset of Fig. 5.4 and again observe good agreement.

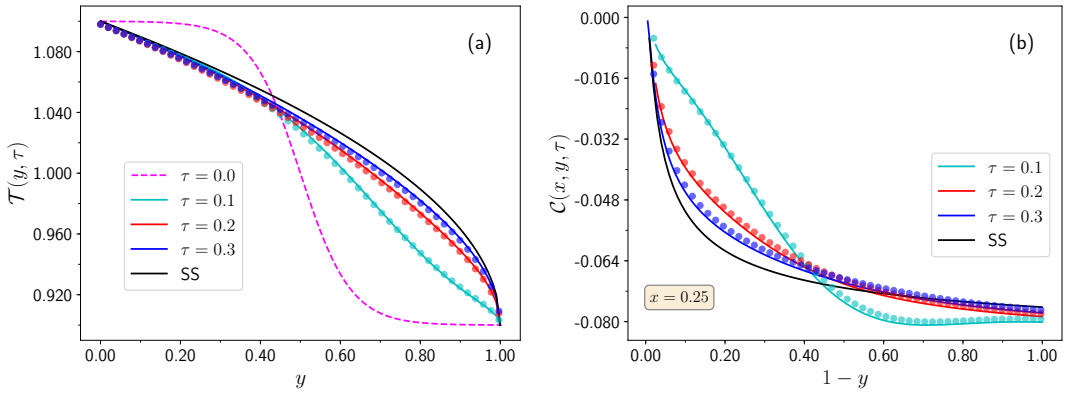

Figure 5.4: Numerical verification of the evolution of (a) the temperature profiles $\mathcal{T}(y,\tau) = \mathcal{T}_{ss}(y) + \mathcal{T}_r(1-y,\tau)$ obtained using the solution of Eq. (5.2.12).(b) the correlation $\mathcal{C}(x,y,\tau) = \mathcal{C}_{ss}(x,y) + \mathcal{C}_r(x,1-y,\tau)$ given in Eq. (5.2.9) where $\mathcal{C}_r$ is computed using the solution in Eq. (5.2.11). The magenta dashed line and the solid black line represent the initial and the NESS temperature profiles, respectively. Symbols are obtained from simulations with $\lambda = \gamma = 1$, $T_\ell = 1.1$, $T_r = 0.9$ and $L = 2048$, and the solid lines are from theory.

5.6 Fractional evolution of temperature in an infinite line

One can extend the calculation for temperature evolution Eq. (5.5.6) in an finite system of length L and obtain the same set of bulk equations which now hold for $y \in [0, L]$. We are interested in the behavior of the evolution of temperature profile in $L \to \infty$ limit, where the effect of boundaries are not important. The evolution equations for the relaxation parts in this case are same as that of Eqs. (5.5.1)-(5.5.3) but now $0 \le x \le \infty$ and $0 \le y \le L$. To proceed, we introduce the orthonormal and complete basis in $y \in [0, L]$, $\phi_n^{\pm}(y) = \frac{1}{\sqrt{L}} e^{\pm i n \pi y/L}$ for $n \ge 1$ and $\phi_0(y) = 1/\sqrt{L}$. Expanding the correlations and temperature in this basis as Fourier series we get,

$$\mathcal{C}_r(x,y,\tau) = \hat{A}_0(x,\tau) + \sum_{n=1} \hat{A}_n^+(x,\tau)\phi_n^+(y) + \hat{A}_n^-(x,\tau)\phi_n^-(y),$$
$$\mathcal{T}(y,\tau) = \hat{T}_0(\tau) + \sum_{n=1} \hat{T}_n^+(\tau)\phi_n^+(y) + \hat{T}_n^-(\tau)\phi_n^-(y), \tag{5.6.1}$$

where $\hat{A}_n^{\pm}(x,\tau) = \int_0^L \mathcal{C}_r(x,y,\tau)\phi_n^{\pm}(y)dy$, $\hat{A}_0(x,\tau) = \int_0^L \mathcal{C}_r(x,y,\tau)\phi_0 dy$, $\hat{T}_n^{\pm}(\tau) = \int_0^L \mathcal{T}_r(y,\tau)\phi_n^{\pm}(y)dy$, $\hat{T}_0(\tau) = \int_0^L \mathcal{T}_r(y,\tau)\phi_0 dy$. Using these expressions in the PDEs [see Appendix. (5.8.2)], we get

$$\dot{\hat{T}}_0 = 0,\ \dot{\hat{T}}_n^{\mp} = -\frac{1}{\sqrt{2\gamma}}(1 \pm i)\lambda_n^{3/4}\hat{T}_n^{\mp},\ \ n = 1, 2, 3... \tag{5.6.2}$$

where $\lambda_n = (n\pi/L)^2$. This can be interpreted in domain $y \in [0, L]$ as,

$$\begin{aligned}\partial_\tau \mathcal{T}_r(y,\tau) &= -\frac{1}{\sqrt{2\gamma}}(|\Delta|^{3/4} - \nabla|\Delta|^{1/4})\mathcal{T}_r(y,\tau),\\ &= -\frac{1}{\sqrt{2\gamma}}\mathbb{L}_\infty \mathcal{T}_r(y,\tau),\end{aligned} \tag{5.6.3}$$

where $\mathbb{L}_\infty$ is an positive operator defined by its action as, $\mathbb{L}_\infty \phi_n^\pm(y) = \lambda_n^{3/4}(1 - i\ \mathrm{sgn}(n))\phi_n^\pm(y)$. With $L \to \infty$ the spectrum becomes continuous as well as the eigenfunctions become plane wave. Thus in infinite system at equilibrium, the evolution of temperature profile is given by a skew-symmetric fractional Laplacian given in Eq. (5.2.2) .

One can alternatively see this equivalence from the integro-differential evolution in infinite space through the action of the operator $\partial_\tau T(y,\tau) = -\frac{1}{\sqrt{2\gamma}}\mathbb{L}_\infty T(y,\tau)$. Where a similar calculation as in Sec. (5.5) gives $\mathbb{L}_\infty f(y) = \frac{1}{\sqrt{\pi\gamma}}\,\partial_y \int_{-\infty}^{y} \frac{\partial_{y'} f(y')}{\sqrt{y-y'}} dy'$, where in contrast to (5.5.6), the lower limit is changed from $-\infty$ to 0. Using the identity

$$\int_{-\infty}^{y} dz \frac{1}{\sqrt{y-z}}\, e^{iqz} = \frac{\sqrt{\pi}}{\sqrt{iq}}\, e^{iqy},$$

one can easily show that

$$\mathbb{L}_\infty\, e^{iqy} = \lambda_q\, e^{iqy},\ \ \lambda_q = \sqrt{\frac{1}{2\gamma}}[1 - i\ \mathrm{sgn}(q)]\ |q|^{3/2},$$

which is same as the Fourier spectrum of the skew-symmetric fractional Laplacian. given in Eq. 5.2.2.

5.7 Conclusion

In this chapter, we have studied anomalous transport in a one-dimensional system with two conserved quantities, in the open system setup. Starting from a microscopic description and acquiring knowledge about scaling properties from numerical studies, we derive exact expressions of the temperature profiles and the two point correlations in the steady state. We also study the evolution of these quantities towards steady state. We explicitly show that the evolution of the temperature pro-

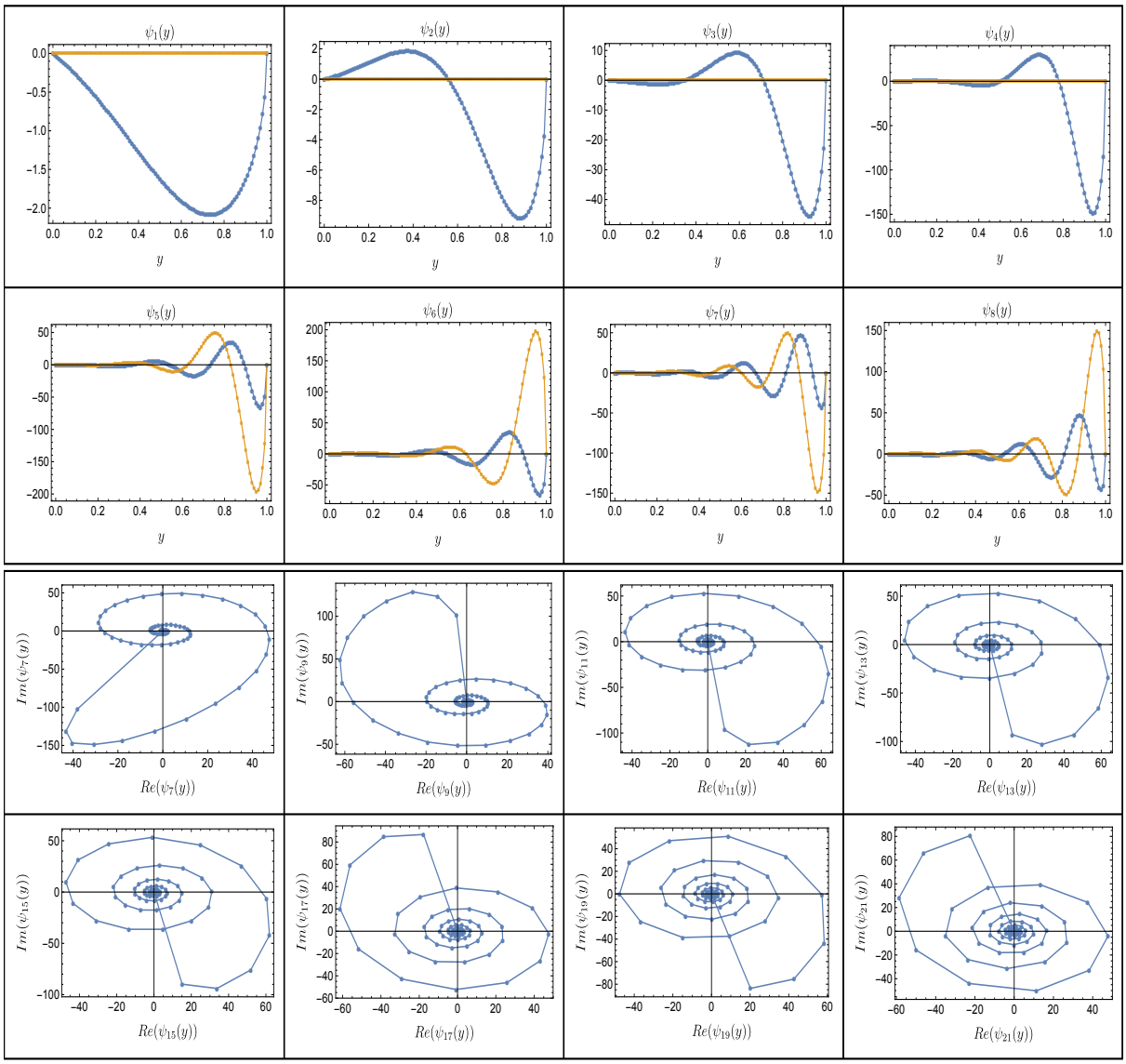

Figure 5.5: The real (Blue, deep gray) and imaginary (Orange, light gray) part of the right eigenvectors for the matrix $\mathbf{B}$ for the first few eigenvalues. The plots for even ordered eigenvectors ($n = 8, 10\ldots$) are related to the eigenvectors of the previous eigenvectors by a reflection around x axis and hence are not plotted. A polar representation is shown as the real and imaginary parts of the eigenvectors for $n \geq 7$. The polar plots are for $n = 7, 9, 11\ldots$.

files in this model is governed by a non-local operator defined inside a finite domain which correctly takes the previously obtained infinite system representation. We provide numerical verifications of the analytical results.

5.8 Appendix

5.8.1 Boundary equations

The dynamical equations at the boundaries are given by

1. for $i = j = 1$

$$\dot{T}_1 = 2\lambda T_\ell + 2C_{1,2} - 2\lambda T_1 + \gamma[T_2 - T_1] \tag{5.8.1}$$

2. for $i = j = L$

$$\dot{T}_L = 2\lambda T_r - 2C_{L-1,L} - 2\lambda T_L + \gamma[T_{L-1} - T_L] \tag{5.8.2}$$

3. $i = 1$ and $2 < j < L$

$$\begin{aligned}\dot{C}_{1,j} =& C_{2,j} - \lambda C_{1,j} + C_{1,j+1} - C_{1,j-1} \\ &+\gamma[C_{1,j-1} + C_{1,j+1} + C_{2,j} - 3C_{1,j}]\end{aligned} \tag{5.8.3}$$

4. $j = L$ and $1 < i < L - 1$

$$\begin{aligned}\dot{C}_{i,L} =& C_{i+1,L} - C_{i-1,L} - C_{i,L-1} - \lambda C_{i,L} \\ &+\gamma[C_{i-1,L} + C_{i+1,L} + C_{i,L-1} - 3C_{i,L}]\end{aligned} \tag{5.8.4}$$

5. $i = 1$ and $j = L$

$$\begin{aligned}\dot{C}_{1,L} =& C_{2,L} - C_{1,L-1} - 2\lambda C_{1,L} \\ &+\gamma[C_{2,L} + C_{1,L-1} - 2C_{1,L}]\end{aligned} \tag{5.8.5}$$

6. $i = 1$ and $j = 2$

$$\dot{C}_{1,2} = T_2 - \lambda C_{1,2} + C_{1,3} - T_1 + \gamma[C_{1,3} - C_{1,2}] \tag{5.8.6}$$

7. $j = L$ and $i = L - 1$

$$\begin{aligned}\dot{C}_{L-1,L} =& T_L - C_{L-2,L} - T_{L-1} - \lambda C_{L-1,L} \\ &+\gamma[C_{L-2,L} - C_{L-1,L}]\end{aligned} \tag{5.8.7}$$

5.8.2 Fractional equation in infinite domain

The expansions in Eq. (5.6.1) along with the set of PDEs Eq. (5.2.5)-(5.2.7) gives the following differential equation for the components,

$$\begin{aligned}&\partial_x^2 \hat{A}_n^{\pm}(x,\tau) = ((1 \mp i)\alpha_n)^2 \hat{A}_n^{\pm}(x,\tau),\ \partial_x^2 \hat{A}_0(x,\tau) = 0 \\ &\pm \frac{in\pi}{L} \hat{T}_n^{\pm}(\tau) = -2\gamma \partial_x \hat{A}_n^{\pm}(x,\tau)_{|x\to 0},\end{aligned} \tag{5.8.8}$$

where $\alpha_n = \sqrt{\frac{n\pi}{2L\gamma}}$. The solution to these equations are in general given as, $\hat{A}_n^{\pm}(x,\tau) = a_n^{\pm}(\tau) e^{\pm\alpha_n(1\mp i)x}$, $\hat{A}_0(x,\tau) = d(\tau)x + e(\tau)$ Choosing solutions which do not blow up at infinity at large x and obey the boundary conditions. We have, $\mathcal{C}_r(x,y,\tau) = e(\tau) + \sum_{n=1}^{\infty} a_n^- e^{-\alpha_n(1+i)x}\phi_n^-(y) + c.c.$ where c.c. stands for complex conjugate. $e(\tau)$ is zero because there is no time-dependent source in the system. Using above equations, we have

$$\hat{T}_n^{\pm} = 2\gamma a_n^{\mp}(\tau)\alpha_n \frac{(1 \mp i)}{(n\pi/L)},\ \dot{\hat{T}}_n^{\mp} = \mp 2i \frac{n\pi}{L} a_n^{\pm}(\tau) \tag{5.8.9}$$

Using these two, we have Eq. (5.6.2).

Part IV

Conclusions

To conclude, in this thesis we have studied some problems in understanding anomalous transport in one-dimensional systems. In the first part of the thesis we studied numerically heat transport in the Toda system, which is a classically integrable system. We found that, both in equilibrium and non-equilibrium setup, the system shows properties of ballistic transport. We computed analytically the equilibrium correlations in the harmonic and the hard particle gas which can be viewed as special limiting cases of the Toda chain. However, we note that there is no rigorous proof that an integrable system should have ballistic transport, and the interesting question of understating non-ballistic transport in integrable systems would be an interesting direction to be explored. We have also done a comparative study of the differences in transport between integrable and non-integrable systems in both the equilibrium and non-equilibrium setups. We found that certain hydrodynamic tools used in transport of non-integrable are useful in understanding transport in integrable systems. An interesting question is the possibility of describe integrable systems using hydrodynamics, and also the questions related to relaxation and thermalization in integrable systems.

In the second part of the thesis, we have explored super-diffusive transport in one-dimensional systems with stochastic dynamics. We approached this problem by studying analytically tractable models which show super-diffusion and studied them in the non-equilibrium setup with different temperatures applied at the boundaries. Starting from the microscopic model, we established a fractional equation description for transport in these systems which can describe equilibrium as well as non-equilibrium properties in the super-diffusive system. These works give a possible hint that a fractional diffusion equation plays a similar role in super-diffusive transport as heat equation (Fourier law) for diffusive transport. However this possibility must be explored by studying other models and needs to be extended to obtain a full characterization of the NESS in super-diffusive systems.

References

[1] Federico Bonetto, Joel L Lebowitz, and Luc Rey-Bellet. Fourier's law: a challenge to theorists. In *Mathematical physics 2000*, pages 128–150. World Scientific, 2000.

[2] Stefano Lepri, Roberto Livi, and Antonio Politi. Thermal conduction in classical low-dimensional lattices. *Physics Reports*, 377(1):1–80, 2003.

[3] Abhishek Dhar. Heat transport in low-dimensional systems. *Advances in Physics*, 57(5):457–537, 2008.

[4] Stefano Lepri. *Thermal Transport in Low Dimensions: From Statistical Physics to Nanoscale Heat Transfer*, volume 921. Springer International Publishing Switzerland 2016, 1 edition, 2016.

[5] Chih-Wei Chang, David Okawa, Henry Garcia, Arunava Majumdar, and Alex Zettl. Breakdown of fourier's law in nanotube thermal conductors. *Physical review letters*, 101(7):075903, 2008.

[6] Victor Lee, Chi Hsun Wu, Zong Xing Lou, Wei Li Lee, and Chih Wei Chang. Divergent and Ultrahigh Thermal Conductivity in Millimeter-Long Nanotubes. *Physical Review Letters*, 118(13), 2017.

[7] G Benettin, S Pasquali, and A Ponno. The fermi–pasta–ulam problem and its underlying integrable dynamics: an approach through lyapunov exponents. *Journal of Statistical Physics*, pages 1–22, 2018.

[8] Herbert Spohn. Interacting and noninteracting integrable systems. *Journal of Mathematical Physics*, 59(9), 2018.

[9] Onuttom Narayan and Sriram Ramaswamy. Anomalous Heat Conduction in One-Dimensional Momentum-Conserving Systems. *Physical Review Letters*, 89(20), 2002.

[10] Henk Van Beijeren. Exact results for anomalous transport in one-dimensional hamiltonian systems. *Physical Review Letters*, 108(18), 2012.

[11] Herbert Spohn. Nonlinear Fluctuating Hydrodynamics for Anharmonic Chains. *Journal of Statistical Physics*, 154(5):1191–1227, 2014.

[12] A Gerschenfeld, B Derrida, and JL Lebowitz. Anomalous fourier's law and long range correlations in a 1d non-momentum conserving mechanical model. *Journal of Statistical Physics*, 141(5):757–766, 2010.

[13] Z. Rieder, J. L. Lebowitz, and E. Lieb. Properties of a harmonic crystal in a stationary nonequilibrium state. *Journal of Mathematical Physics*, 8(5):1073–1078, 1967.

[14] Hiroshi Nakazawa. On the lattice thermal conduction. *Progress of Theoretical Physics Supplement*, 45:231–262, 1970.

[15] Dibyendu Roy and Abhishek Dhar. Heat transport in ordered Harmonic Lattices. *Journal of Statistical Physics*, 131(3):535–541, 2008.

[16] Peter Mazur and Elliott Montroll. Poincaré cycles, ergodicity, and irreversibility in assemblies of coupled harmonic oscillators. *Journal of Mathematical Physics*, 1(1):70–84, 1960.

[17] D. W. Jepsen. Dynamics of a simple many body system of hard rods. *J. Math. Phys.*, 6(3):405, 1965.

[18] B. Sriram Shastry and A. P. Young. Dynamics of energy transport in a Toda ring. *Physical Review B - Condensed Matter and Materials Physics*, 82(10), 2010.

[19] X Zotos. Ballistic transport in classical and quantum integrable systems. *Journal of Low Temperature Physics*, 126(3/4):1185–1194, 2002.

[20] Hirotsugu Matsuda and Kazushige Ishii. Localization of normal modes and energy transport in the disordered harmonic chain. *Progress of Theoretical Physics Supplement*, 45:56–86, 1970.

[21] AJ O'Connor and JL Lebowitz. Heat conduction and sound transmission in isotopically disordered harmonic crystals. *Journal of Mathematical Physics*, 15(6):692–703, 1974.

[22] Robert J Rubin and William L Greer. Abnormal lattice thermal conductivity of a one-dimensional, harmonic, isotopically disordered crystal. *Journal of Mathematical Physics*, 12(8):1686–1701, 1971.

[23] A Casher and JL Lebowitz. Heat flow in regular and disordered harmonic chains. *Journal of Mathematical Physics*, 12(8):1701–1711, 1971.

[24] Oskari Ajanki and François Huveneers. Rigorous scaling law for the heat current in disordered harmonic chain. *Communications in Mathematical Physics*, 301(3):841–883, 2011.

[25] Theo Verheggen. Transmission coefficient and heat conduction of a harmonic chain with random masses: Asymptotic estimates on products of random matrices. *Communications in Mathematical Physics*, 68(1):69–82, 1979.

[26] Abhishek Dhar. Heat conduction in the disordered harmonic chain revisited. *Physical review letters*, 86(26):5882, 2001.

[27] Stefano Lepri, Roberto Livi, and Antonio Politi. Heat conduction in chains of nonlinear oscillators. *Physical review letters*, 78(10):1896, 1997.

[28] S. Lepri, R. Livi, and A. Politi. On the anomalous thermal conductivity of one-dimensional lattices. *Europhysics Letters*, 43(3):271–276, 1998.

[29] Trieu Mai, Abhishek Dhar, and Onuttom Narayan. Equilibration and universal heat conduction in fermi-pasta-ulam chains. *Physical review letters*, 98(18):184301, 2007.

[30] Yi Zhong, Yong Zhang, Jiao Wang, and Hong Zhao. Normal heat conduction in one-dimensional momentum conserving lattices with asymmetric interactions. *Physical Review E*, 85(6):060102, 2012.

[31] Suman G. Das, Abhishek Dhar, and Onuttom Narayan. Heat Conduction in the α-β Fermi-Pasta-Ulam Chain. *Journal of Statistical Physics*, 154(1-2):204–213, 2014.

[32] Lei Wang, Nianbei Li, and Peter Hänggi. Simulation of heat transport in low-dimensional oscillator lattices. In *Thermal Transport in Low Dimensions*, pages 239–274. Springer, 2016.

[33] Giulio Casati. Energy transport and the fourier heat law in classical systems. *Foundations of physics*, 16(1):51–61, 1986.

[34] Pedro L Garrido, Pablo I Hurtado, and Bjoern Nadrowski. Simple one-dimensional model of heat conduction which obeys fourier's law. *Physical review letters*, 86(24):5486, 2001.

[35] Peter Grassberger, Walter Nadler, and Lei Yang. Heat conduction and entropy production in a one-dimensional hard-particle gas. *Physical review letters*, 89(18):180601, 2002.

[36] Abhishek Dhar. Heat conduction in a one-dimensional gas of elastically colliding particles of unequal masses. *Physical Review Letters*, 86(16):3554–3557, 2001.

[37] Pablo I Hurtado and Pedro L Garrido. A violation of universality in anomalous fourier's law. *Scientific reports*, 6:38823, 2016.

[38] Shunda Chen, Jiao Wang, Giulio Casati, and Giuliano Benenti. Nonintegrability and the fourier heat conduction law. *Physical Review E*, 90(3):032134, 2014.

[39] Andrey Pereverzev. Fermi-pasta-ulam β lattice: Peierls equation and anomalous heat conductivity. *Physical Review E*, 68(5):056124, 2003.

[40] Jani Lukkarinen and Herbert Spohn. Anomalous energy transport in the fpu-β chain. *Communications on Pure and Applied Mathematics: A Journal Issued by the Courant Institute of Mathematical Sciences*, 61(12):1753–1786, 2008.

[41] Bernie Nickel. The solution to the 4-phonon boltzmann equation for a 1d chain in a thermal gradient. *Journal of Physics A: Mathematical and Theoretical*, 40(6):1219, 2007.

[42] Santhosh G. and Deepak Kumar. Universality classes for phonon relaxation and thermal conduction in one-dimensional vibrational systems. *Phys. Rev. E*, 84:041119, Oct 2011.

[43] Kenichiro Aoki, Jani Lukkarinen, and Herbert Spohn. Energy transport in weakly anharmonic chains. *Journal of statistical physics*, 124(5):1105–1129, 2006.

[44] Christian B. Mendl and Herbert Spohn. Dynamic correlators of fermi-pasta-ulam chains and nonlinear fluctuating hydrodynamics. *Physical Review Letters*, 111(23), 2013.

[45] Suman G. Das, Abhishek Dhar, Keiji Saito, Christian B. Mendl, and Herbert Spohn. Numerical test of hydrodynamic fluctuation theory in the Fermi-Pasta-Ulam chain. *Physical Review E - Statistical, Nonlinear, and Soft Matter Physics*, 90(1), 2014.

[46] Christian B. Mendl and Herbert Spohn. Equilibrium time-correlation functions for one-dimensional hard-point systems. *Physical Review E - Statistical, Nonlinear, and Soft Matter Physics*, 90(1), 2014.

[47] BJ Alder and TE Wainwright. Velocity autocorrelations for hard spheres. *Physical review letters*, 18(23):988, 1967.

[48] BJ Alder and TE Wainwright. Decay of the velocity autocorrelation function. *Physical review A*, 1(1):18, 1970.

[49] Dieter Forster, David R Nelson, and Michael J Stephen. Large-distance and long-time properties of a randomly stirred fluid. *Physical Review A*, 16(2):732, 1977.

[50] Giada Basile, Cédric Bernardin, and Stefano Olla. Momentum conserving model with anomalous thermal conductivity in low dimensional systems. *Physical Review Letters*, 96(20):1–4, 2006.

[51] Giada Basile, Cédric Bernardin, and Stefano Olla. Thermal conductivity for a momentum conservative model. *Communications in Mathematical Physics*, 287(1):67–98, 2009.

[52] Cédric Bernardin and Gabriel Stoltz. Anomalous diffusion for a class of systems with two conserved quantities. *Nonlinearity*, 25(4):1099–1133, 2012.

[53] C Kipnis, C Marchioro, and E Presutti. Heat flow in an exactly solvable model. *Journal of Statistical Physics*, 27(1):65–74, 1982.

[54] Shang-keng Ma. One-dimensional boltzmann equation with a three-body collision term. *Journal of Statistical Physics*, 31(1):107–114, 1983.

[55] Anatoly Malevanets and Raymond Kapral. Mesoscopic model for solvent dynamics. *The Journal of chemical physics*, 110(17):8605–8613, 1999.

[56] Luca Delfini, Stefano Lepri, Roberto Livi, and Antonio Politi. Nonequilibrium invariant measure under heat flow. *Physical Review Letters*, 101(12), 2008.

[57] S. Lepri, C. Mejía-Monasterio, and A. Politi. A stochastic model of anomalous heat transport: Analytical solution of the steady state. *Journal of Physics A: Mathematical and Theoretical*, 42(2), 2009.

[58] Stefano Lepri, Carlos Mejía-Monasterio, and Antonio Politi. Nonequilibrium dynamics of a stochastic model of anomalous heat transport. *Journal of Physics A: Mathematical and Theoretical*, 43(6), 2010.

[59] L. Delfini, S. Lepri, R. Livi, C. Mejía-Monasterio, and A. Politi. Nonequilibrium dynamics of a stochastic model of anomalous heat transport: Numerical analysis. *Journal of Physics A: Mathematical and Theoretical*, 43(14), 2010.

[60] C. Bernardin, V. Kannan, J. L. Lebowitz, and J. Lukkarinen. Harmonic Systems with Bulk Noises. *Journal of Statistical Physics*, 146(4):800–831, 2012.

[61] Milton Jara, Tomasz Komorowski, and Stefano Olla. Superdiffusion of Energy in a Chain of Harmonic Oscillators with Noise. *Communications in Mathematical Physics*, 339(2):407–453, 2015.

[62] Herbert Spohn and Gabriel Stoltz. Nonlinear Fluctuating Hydrodynamics in One Dimension: The Case of Two Conserved Fields. *Journal of Statistical Physics*, 160(4):861–884, 2015.

[63] Morikazu Toda. *Theory of Nonlinear Lattices; Volume 20 of Springer Series in Solid-State Sciences*. Springer Science & Business Media, 2012, 2, illustr edition, 2012.

[64] H. Flaschka. The Toda lattice. II. Existence of integrals. *Physical Review B*, 9(4):1924–1925, 1974.

[65] M. Henon. Integrals of the Toda lattice. *Physical Review B*, 9(4):1921–1923, 1974.

[66] M Kac and P Moerbeke. A complete solution of the periodic Toda problem. *Proceedings of the National Academy of Sciences of the United States of America*, 72(8):2879–2880, 1975.

[67] Etsuro Date and Shunichi Tanaka. Periodic Multi-Soliton Solutions of Korteweg-de Vries Equation and Toda Lattice. *Progress of Theoretical Physics Supplement*, 59(0):107–125, 1976.

[68] Morikazu Toda and Noriko Saitoh1. The Classical Specific Heat of the Exponential Lattice. *Journal of the Physical Society of Japan*, 52(11):3703–3705, 1983.

[69] H. Büttner and F. G. Mertens. Toda lattice: Statistical mechanics and solitons. *Solid State Communications*, 29(9):663–665, 1979.

[70] P Gruner-Bauer and FG Mertens. Excitation spectrum of the toda lattice for finite temperatures. *Zeitschrift für Physik B Condensed Matter*, 70(4):435–447, 1988.

[71] N Theodorakopoulos and M Peyrard. Solitons and nondissipative diffusion. *Physical Review Letters*, 83(12):2293–2296, 1999.

[72] A Cuccoli, M Spicci, V Tognetti, and R Vaia. Dynamic correlations of the classical and quantum toda lattices. *Physical Review B*, 47(13):7859, 1993.

[73] Martin C. Gutzwiller. The quantum mechanical toda lattice. *Annals of Physics*, 124(2):347–381, 1980.

[74] Bill Sutherland. A brief history of quantum soliton with new results on the quantisation of the Toda lattice. *Rocky Mountain Journal of Mathematics*, 8:413, 1978.

[75] Alessandro Cuccoli, Roberto Livi, Mauro Spicci, Valerio Tognetti, and Ruggero Vaia. Thermodynamics of the Toda Chain. *International Journal of Modern Physics B*, 8(18):2391–2446, 1994.

[76] M Toda. Solitons and heat conduction. *Physica Scripta*, 20:424–430, 1979.

[77] Takahiro Hatano. Heat conduction in the diatomic Toda lattice revisited. *Physical Review E*, 59(1):1–4, 1999.

[78] Alessandra Iacobucci, Frederic Legoll, Stefano Olla, and Gabriel Stoltz. Thermal conductivity of the Toda Lattice with conservative noise. *Journal of Statistical Physics*, 140(2):336–348, 2010.

[79] Cédric Bernardin and Patrícia Gonçalves. Anomalous Fluctuations for a Perturbed Hamiltonian System with Exponential Interactions. *Communications in Mathematical Physics*, 325(1):291–332, 2014.

[80] G Benettin, H Christodoulidi, and A. Ponno. The Fermi – Pasta – Ulam problem and its underlying integrable dynamics. *Journal of Statistical Physics*, 152(2):195–212, 2013.

[81] Lev Vidmar and Marcos Rigol. Generalized Gibbs ensemble in integrable lattice models. *Journal of Statistical Mechanics: Theory and Experiment*, 2016(6), 2016.

[82] Sheldon Goldstein, Joel L. Lebowitz, Roderich Tumulka, and Nino Zanghì. Canonical typicality. *Physical Review Letters*, 96(5), 2006.

[83] Sourav Nandy, Arnab Sen, Arnab Das, and Abhishek Dhar. Eigenstate Gibbs ensemble in integrable quantum systems. *Physical Review B*, 94(24), 2016.

[84] Sanjib Sabhapandit and Abhishek Dhar. Exact probability distribution for the two-tag displacement in single-file motion. *Journal of Statistical Mechanics: Theory and Experiment*, 2015(7):P07024, 2015.

[85] Chaitra Hegde, Sanjib Sabhapandit, and Abhishek Dhar. Universal large deviations for the tagged particle in single-file motion. *Physical Review Letters*, 113(12), 2014.

[86] Sha Liu, Peter Hänggi, Nianbei Li, Jie Ren, and Baowen Li. Anomalous heat diffusion. *Physical Review Letters*, 112(4), 2014.

[87] Yunyun Li, Sha Liu, Nianbei Li, Peter Hanggi, and Baowen Li. 1D momentum-conserving systems: The conundrum of anomalous versus normal heat transport. *New Journal of Physics*, 17, 2015.

[88] Anjan Roy, Abhishek Dhar, Onuttom Narayan, and Sanjib Sabhapandit. Tagged Particle Diffusion in One-Dimensional Systems with Hamiltonian Dynamics-II. *Journal of Statistical Physics*, 160(1):73–88, 2015.

[89] Anjan Roy, Onuttom Narayan, Abhishek Dhar, and Sanjib Sabhapandit. Tagged Particle Diffusion in One-Dimensional Gas with Hamiltonian Dynamics. *Journal of Statistical Physics*, 150(5):851–866, 2013.

[90] Cédric Bernardin, Patrícia Gonçalves, and Milton Jara. 3/4-Fractional Superdiffusion in a System of Harmonic Oscillators Perturbed by a Conservative Noise. *Archive for Rational Mechanics and Analysis*, 220(2):505–542, 2016.

[91] G. M. Viswanathan, V. Afanasyev, Sergey V. Buldyrev, Shlomo Havlin, M. G.E. Da Luz, E. P. Raposo, and H. Eugene Stanley. Levy flights in random searches. *Physica A: Statistical Mechanics and its Applications*, 282(1):1–12, 2000.

[92] A. Zoia, A. Rosso, and M. Kardar. Fractional Laplacian in bounded domains. *Physical Review E - Statistical, Nonlinear, and Soft Matter Physics*, 76(2), 2007.

[93] Giada Basile, Tomasz Komorowski, and Stefano Olla. Private communication.

[94] Julien Cividini, Anupam Kundu, Asaf Miron, and David Mukamel. Temperature profile and boundary conditions in an anomalous heat transport model. *Journal of Statistical Mechanics: Theory and Experiment*, 013203(1), 2017.

[95] Herbert Spohn. *Large scale dynamics of interacting particles*. Springer Science & Business Media, 2012.

[96] S. V. Buldyrev, M. Gitterman, S. Havlin, A. Ya Kazakov, M. G.E. Da Luz, E. P. Raposo, H. E. Stanley, and G. M. Viswanathan. Properties of Lévy flights on an interval with absorbing boundaries. *Physica A: Statistical Mechanics and its Applications*, 302(1-4):148–161, 2001.

[97] S. V. Buldyrev, S. Havlin, A. Ya Kazakov, M. G.E. da Luz, E. P. Raposo, H. E. Stanley, and G. M. Viswanathan. Average time spent by Lévy flights and walks on an interval with absorbing boundaries. *Physical Review E - Statistical Physics, Plasmas, Fluids, and Related Interdisciplinary Topics*, 64(4):11, 2001.

[98] W. Chen and S. Holm. Fractional Laplacian time-space models for linear and nonlinear lossy media exhibiting arbitrary frequency power-law dependency. *The Journal of the Acoustical Society of America*, 115(4):1424–1430, 2004.

[99] Anupam Kundu, Abhishek Dhar, and Onuttom Narayan. The green-kubo formula for heat conduction in open systems. *Journal of Statistical Mechanics: Theory and Experiment*, 03(03):L03001, 2009.

[100] Pedro L Garrido, Joel L Lebowitz, Christian Maes, and Herbert Spohn. Long-range correlations for conservative dynamics. *Physical Review A*, 42(4):1954, 1990.

[101] H. Spohn. Long range correlations for stochastic lattice gases in a non-equilibrium steady state. *Journal of Physics A: General Physics*, 16(18):4275–4291, 1983.

[102] T. Bodineau, B. Derrida, V. Lecomte, and F. Van Wijland. Long range correlations and phase transitions in non-equilibrium diffusive systems. *Journal of Statistical Physics*, 133(6):1013–1031, 2008.

[103] L. Bertini, A. De Sole, D. Gabrielli, G. Jona-Lasinio, and C. Landim. On the long range correlations of thermodynamic systems out of equilibrium. *arXiv preprint arXiv:0705.2996.*, pages 1–4, 2007.

[104] Bernard Derrida. Non-equilibrium steady states: fluctuations and large deviations of the density and of the current. *Journal of Statistical Mechanics: Theory and Experiment*, 2007(07):P07023, 2007.

[105] Mateusz Kwaśnicki. Ten equivalent definitions of the fractional laplace operator. *Fractional Calculus and Applied Analysis*, 20(1):7–51, 2017.

[106] https://www.ma.utexas.edu/mediawiki/index.php/Fractional_Laplacian, 2018.

[107] Herbert Spohn. Fluctuating hydrodynamics approach to equilibrium time correlations for anharmonic chains. *Lecture Notes in Physics*, 921:107–158, 2016.

[108] Stefano Lepri and Antonio Politi. Density profiles in open superdiffusive systems. *Physical Review E - Statistical, Nonlinear, and Soft Matter Physics*, 83(3), 2011.